



Norwegian University of
Science and Technology

Buckling and Load Shedding in Redundant Plated Ship Structures

Astrid Maria Palm

Marine Technology

Submission date: January 2016

Supervisor: Jørgen Amdahl, IMT

Co-supervisor: Eivind Steen, DNV GL

Norwegian University of Science and Technology
Department of Marine Technology

MASTER THESIS 2015

for

Stud. Techn. Astrid Maria Palm

Buckling and load shedding in redundant plated ship structures

Knekking og omfordeling av laster i redundante platekonstruksjoner i skip

Background

Present Rules given by Classification Societies gives rational criteria for dimensioning the hull for safe operations. However, the ship designers/yards are in fierce competition and reducing weight and thus fuel is high on the agenda. This leads to more optimal and thinner structures and the structural failure limits are being challenged. In particular, the future Rules will be based on modern Ultimate Limit State (ULS) principles. This implies that the classical elastic buckling limit is no longer defined as a failure mode; it will be exceeded some times during the lifetime of the ship. What are the consequences of this and how to account for such effects in a Rule approval procedure?

The technical challenges are linked to the structural response in local areas, which enters the (geometrically) non-linear region when the compressive stresses exceed the elastic buckling limit. Moreover, the production and welding procedures induce geometrical imperfections/out-of-straightness of main load carrying members; these deviations do also have an impact on the structural response and need to be considered.

DNV has some years ago developed a linear FE approach, which applies a set of fictitious anisotropic material parameters (C_{ij}) in order to mimic the real non-linear buckling response (first published PRADS 2001, Ref.1). The purpose was to modify/reduce the membrane stiffness in regions where the elastic buckling limit is exceeded so as to cope with load shedding (stress redistributions) using essentially a “linear” approach.

Objective

The task of the master thesis work is to test and evaluate if this anisotropic “linear” FE approach is suited as a Rule procedure for assessing and dimensioning redundant plated structures, which locally are subjected to compressive stresses exceeding the elastic buckling limit. Both load-independent (imperfections) and load-dependent anisotropic stiffness corrections should be assessed in the perspective of the former being a reasonable conservative approach in a “linear” design approach or not.

Method

Compare linear and non-linear FE model results and tune the “linear” approach in order to simulate the real “non-linear” load shedding in a typical ship double bottom design (or other type of structures). The FE program ABAQUS will be the main tool.

The work is proposed being carried out in the following steps:

1. Local buckling behavior of plates/stiffened panels:
 - a. Single-bay plates: Perform analyses of the compressive strength and stiffness of unstiffened plates for uni-axial and bi-axial in-plane loading. Study and explain the overall Poisson effect of the plates as function of geometry, plate aspect ratio and imperfection amplitudes.
 - b. Validate a simple stiffness model for load-independent anisotropic stiffness corrections developed by DNV GL.
 - c. Multi-bayed panels: Simulate the effect of large integrated panels as typical for ships and assess the effect of imperfection shapes (“Hungry-Horse”/Eigenmodes) and lateral pressure on the in-plane stiffness response (initial and non-linear).
 - d. Multi-bayed stiffened panels: Study the initial and non-linear behavior of a selected plate panel (regular stiffeners in one direction) and identify possible effects affecting the structural response not covered by the models analyzed under a) and b).

2. Benchmark a larger slender car-deck type of structure, considering the following features:
 - a. Compare fine-mesh non-linear ABAQUS model with coarse rule ABAQUS model.
 - b. Evaluate the load-independent stiffness correction in relation to the standard linear isotropic and present anisotropic model using the non-linear results as basis (ABAQUS).
 - c. Tune the stiffness coefficients (C_{ij}) in the anisotropic model to mimic load-dependent non-linear ABAQUS results.
 - d. Optimize the deck structure with respect to plate thickness and document potential steel savings using the linear anisotropic approach as compared to the standard isotropic approach.

3. Conclusions and recommendations for further work

Literature studies of specific topics relevant to the thesis work may be included.

The work scope may prove to be larger than initially anticipated. Subject to approval from the supervisors, topics may be deleted from the list above or reduced in extent.

In the thesis the candidate shall present her personal contribution to the resolution of problems within the scope of the thesis work.

Theories and conclusions should be based on mathematical derivations and/or logic reasoning identifying the various steps in the deduction.

The candidate should utilise the existing possibilities for obtaining relevant literature.



Thesis format

The thesis should be organised in a rational manner to give a clear exposition of results, assessments, and conclusions. The text should be brief and to the point, with a clear language. Telegraphic language should be avoided.

The thesis shall contain the following elements: A text defining the scope, preface, list of contents, summary, main body of thesis, conclusions with recommendations for further work, list of symbols and acronyms, references and (optional) appendices. All figures, tables and equations shall be numerated.

The supervisors may require that the candidate, in an early stage of the work, presents a written plan for the completion of the work. The plan should include a budget for the use of computer and laboratory resources which will be charged to the department. Overruns shall be reported to the supervisors.

The original contribution of the candidate and material taken from other sources shall be clearly defined. Work from other sources shall be properly referenced using an acknowledged referencing system.

The report shall be submitted in two copies:

- Signed by the candidate
- The text defining the scope included
- In bound volume(s)
- Drawings and/or computer prints which cannot be bound should be organised in a separate folder.
- The report shall also be submitted in pdf format along with essential input files for computer analysis, spreadsheets, MATLAB files etc. in digital format.

Ownership

NTNU has according to the present rules the ownership of the thesis. Any use of the thesis has to be approved by NTNU (or external partner when this applies). The department has the right to use the thesis as if the work was carried out by a NTNU employee, if nothing else has been agreed in advance.

Thesis supervisor

Prof. Jørgen Amdahl

Thesis co-supervisor:

Eivind Steen; DNV GL Maritime – Technical Advisory/Structures MANNO367

Lars Brubak; DNV GL Maritime – Technical Advisory/Structures MANNO367

Ole Jakob Hareide; DNV GL Maritime – Technical Advisory/Structures MANNO367

Kristoffer Lofthaug; DNV GL Maritime – Technical Advisory/Structures MANNO367

Åge Bøe; DNV GL Maritime - Ship Structures, Stability & Load Line MCANO870

Deadline: January 19, 2016

Trondheim, August 25, 2015


Jørgen Amdahl

Preface

This master thesis is the concluding work of the Master of Science degree in Marine Technology. The thesis was written during the Autumn of 2015 in cooperation with DNV GL. Most of the work was done at the DNV GL offices at Høvik.

The process of writing this thesis has been very educational, from sitting buried in plate buckling theory to familiarizing with Abaqus and programming in Python for efficient parametric studies. I have worked consistently since August, with regular meetings with my supervisors at DNV GL. I have had some challenges along the way, resulting in many rearrangements and repetitions of analyses. The greatest challenge has been to grasp the aspects of rule development and the consequences of using simplified methods to obtain conservative design procedures.

Acknowledgements

First of all I am truly grateful to the problem owner of this thesis, Eivind Steen (DNV GL), for giving me the opportunity to write at the DNV GL offices at Høvik and for valuable advise throughout the semester. This also includes my supervisor at NTNU, Jørgen Amdahl, who has been involved in some of the previous work on the field. My co-supervisors Åge Bøe (DNV GL) and Lars Brubak (DNV GL) deserve an appreciation for help with outlining the problem text and for providing relevant Abaqus models. A special thank goes to Ole Jakob Hareide (DNV GL) and Kristoffer Lofthaug (DNV GL) for operating as my personal support center the past months. I also wish to thank my parents for good support. Finally, I am truly grateful to Eirik Samnøy for persevering with me the past semester.

Kolsås, 2016-01-18



Astrid Maria Palm

Abstract

A linear Finite Element (FE) procedure developed by DNV GL as an alternative to standard design procedures for redundant plated panels has been tested and evaluated. The method is based on modifying the so-called macro material input in an anisotropic FE-model, so as to cope with structural non-linearities by essentially using a linear approach. In the studies performed in this thesis, both the initial loss of stiffness at the presence of imperfections and the load-dependent behaviour of compressed plates are addressed. The evaluations are performed in light of a number of parametric studies on the elastic buckling behaviour and imperfection sensitivity of unstiffened plates and larger multi-bayed panels. The Non-linear Finite Element software Abaqus is used as main tool.

As an introductory to the elastic buckling problem, a study of the compressive strength of biaxially loaded unstiffened plates was performed. The results showed that a significant stiffness reduction takes place in the vicinity of the elastic buckling limit, followed by a nearly constant post-buckling stiffness. This implies an extensive load-shedding to adjacent supporting elements that is not captured by standard linear procedures. Subsequent studies including an initial geometry equal to that of the transverse eigenmode documented the effects of initial imperfections on the initial stiffness. The transverse and the coupled stiffness were seen to be highly affected by the imperfection amplitude, the latter even taking on a negative value for major imperfections. The immediate deflection mode after onset of compression proved to have a considerable impact on the initial stiffness. Large imperfection amplitudes, $w_0 > t_{plate}$, imposed an advanced deflection mode in the form of a flattened buckle along the mid-plate, which displayed a lower stiffness than the applied imperfection mode.

Based on a number of parametric studies including variations of the plate aspect ratio, slenderness and imperfection level, the explicit formulations for initial stiffness developed by DNV GL were compared with numerical results. High agreement was found for small imperfections, $w_0 < t_{plate}$, and moderate aspect and slenderness ratios. Considerable deviations were seen for larger imperfections, $w_0 > t_{plate}$, with the numerical results being on the lower side. The deviating trend was more pronounced for large aspect ratios, $\alpha > 3$, and slender plates. The knock-down of numerical results was found to be due to the altered deflection mode imposed by large initial distortions. This behaviour is not captured by the analytical formulations, which presumes a constant deflection mode equal to the initial im-

perfection.

A study on the effects of various imperfection geometries and lateral pressure was performed on a multi-bayed model similar to a typical stiffened panel. The imperfections were defined as weighed combinations of the unfavourable eigenmode and the more realistic "Hungry-Horse"(HH) geometry. The HH-mode was found to be stiffer than the geometries with eigenmode contributions, and even coincided with the linear elastic stiffness for small imperfection amplitudes. The emergence of buckling modes was not considerably affected by neither the initial imperfection nor lateral pressure, considering that the eigenmode grew quite rapidly for most conditions.

The practical application of the macro material model was evaluated for a card-deck configuration. A coarsely meshed linear anisotropic model with modified initial stiffness properties was compared to a non-linear isotropic model with geometrical imperfections. The anisotropic approximation showed high agreement with the non-linear model, given moderate imperfection levels. The membrane stresses in the plating, stresses in supporting frames and so the overall stiffness of the panel were successfully mimicked for strain ranges in the proximity of the elastic buckling limit of individual plates. A study on embedding load-dependent effects in the macro material input was found to give accurate estimates of the plate membrane stresses and the stress redistribution to transverse frames at target load-states. Thickness iterations with the macro material model documented a theoretical potential for steel savings for the considered car-deck. The latter however requires an evaluation of all relevant load-conditions and safety limits to be confirmed as a conservative approach.

The main conclusion include two convenient applications of the macro material model in design. Firstly, the imitation of initial stiffness may enable steel savings, depending on the configuration and operation of the considered panel. Secondly, the load-dependent macro material input may serve as a convenient alternative to non-linear procedures in the prediction of the stress redistribution accompanying elastic buckling. However, such a utilization requires more confident assumptions regarding modelling of initial imperfections and a generalization with respect to model configuration and load-conditions to be truly applicable and conservative as a design procedure.

Sammendrag

En alternativ lineær regelprosedyre for redundante platekonstruksjoner utviklet av DNV GL er testet og evaluert. Metoden går ut på å etterligne relevante ikke-lineære effekter ved å modifisere materialparametrene i en lineær anisotrop elementanalyse. Studiene gjennomført i denne oppgaven omfatter testing og validering av eksplisitte uttrykk for den initielle stivheten til plater med imperfeksjoner, samt en videreføring av dette der den last-avhengige responsen er forsøkt etterlignet. Til slutt er potensialet for å spare stål i en spesifikk bildekkkonfigurasjon evaluert. De endelige analysene er basert på et antall parameterstudier av både enkle plater og større platefelt typisk for marine konstruksjoner, med fokus på initiell stivhet og oppførsel ved elastisk buling. Det ikke-lineære elementmetodeprogrammet Abaqus er brukt som hovedverktøy.

En studie av oppførselen til rektangulære plater ved bi-aksiell forskyvning ble gjennomført for å få grunnleggende erfaring med elastisk buling. Resultatene viste en betraktelig reduksjon av membranstivheten, samt en tilnærmet konstant stivhet etter buling. Dette innebærer en vesentlig grad av redistribusjon av spenninger til nærliggende bærende elementer som ikke er tatt høyde for ved standard lineære prosedyrer. Påfølgende studier ble gjennomført med en initiell geometri tilsvarende egenmoden ved tverrgående forskyvning. Den tverrgående og koblede stivheten var svært sensitive for den initielle amplituden, da den sistnevnte til og med var negativ for store imperfeksjoner. Det umiddelbare defleksjonsmønsteret viste seg å ha stor innflytelse på den initielle stivheten. De større imperfeksjonene, $w_0 > t_{plate}$, resulterte i en avansert defleksjonsmode i form av en avflatet halvbue over platens lengde med to initierte topper mot endene. Denne viste lavere stivhet enn den initielle geometrien.

Den eksplisitte løsningen for initiell stivhet utviklet av DNV GL ble undersøkt på grunnlag av parameterstudier med variasjoner av platens aspektforhold, slankhet og imperfeksjonsamplitude. Høy overensstemmelse ble funnet for mindre imperfeksjoner, $w_0 < t_{plate}$, imens større amplituder ga numeriske resultater i underkant av de analytiske. Dette viste seg å være på grunn av den avanserte defleksjonsmoden sett ved større initielle amplituder. Den analytiske løsningen forutsetter et konstant defleksjonsmønster, og gir derfor høyere initiell stivhet enn numeriske resultater dersom dette ikke er oppfylt.

En studie av ulike imperfeksjonsmønstre og lateralt trykk ble gjennomført på et større platefelt. Imperfeksjonene ble definert av en vektet kombinasjon av egenmoden og den mer realistiske "Hungry-Horse" (HH)-geometrien. Det ble funnet at HH-moden var initiell stive-

re enn imperfeksjonene med bidrag fra egenmoden, og var for små imperfeksjoner tilnærmet lik den lineære elastiske stivheten. Både den initielle imperfeksjonen og lateralt trykk ble funnet å ha liten påvirkning på fremveksten av defleksjonsmønsteret, da egenmoden vokste frem på et tidlig stadie for de fleste betingelsene.

Den praktiske bruken av den alternative lineære prosedyren ble evaluert ved å inkludere de eksplisitt bestemte stivhetskoeffisientene i den anisotrope materialmodellen til en grovt meshet modell av et spesifikt bildekk. Den anisotrope tilnærmingen viste høy overensstemmelse med den initielle oppførselen til en identisk ikke-lineær isotrop modell med fint mesh. Membranspenninger i platene, samt spenninger i bærende rammer var nøyaktig etterlignet for tøyingsnivåer i nærheten av knekking av integrerte plater. Et forsøk på å etterligne last-avhengige spenninger ble gjennomført ved å justere de anisotrope koeffisientene på grunnlag av oppførselen til en enkel platemodell. Metoden ga presise estimater av den faktiske spenningen i både plater og rammer ved utvalgte tøyingsnivåer. Potensialet for å spare stål i den vurderte bildekk-modellen ble evaluert ved iterasjoner av platetykkelsen i den anisotrope modellen. Analysene viste et teoretisk potensiale for å redusere platetykkelsen. Om dette faktisk er mulig avhenger av om alle relevante last-tilfeller og sikkerhetskriterier tillater det.

Hovedkonklusjonen peker på to praktiske bruksområder for den alternative anisotrope prosedyren i design. For det første gir etterlikningen av stivhetsreduksjon ved imperfeksjoner rom for en potensiell stålbesparing som resultat av en lavere utnyttelse av platene i avstivede platefelt. For det andre kan den last-avhengige modifikasjonen være et alternativ til ikke-lineære metoder ved etterlikning av redistribusjon av spenninger ved elastisk buling. For å fungere som en anvendelig og konservativ prosedyre vil imidlertid en slik anvendelse kreve tryggere antakelser ved modellering av imperfeksjoner, samt en generalisering med hensyn på konfigurasjon og lasttilfeller.

Contents

- Preface** **v**

- Abstract** **vii**

- Sammendrag** **ix**

- 1 Introduction** **1**
 - 1.1 Background and motivation 1
 - 1.2 Previous work 2
 - 1.3 Scope 3

- 2 Redundant Plated Structures** **5**
 - 2.1 Elastic plate buckling 7
 - 2.1.1 Slenderness parameter 9
 - 2.1.2 Stress redistribution 9
 - 2.1.3 Load-shortening relation 10
 - 2.2 Initial imperfections 11
 - 2.2.1 Imperfections in design and rule formulations 11
 - 2.2.2 DNV GL tolerance levels 13
 - 2.2.3 Faulkner’s imperfection model 13

- 3 Modern Design** **15**
 - 3.1 ULS Design principles 15
 - 3.1.1 Capacity definitions 15
 - 3.2 Nonlinear Finite Element Methods 17
 - 3.2.1 Non-linear geometrical behaviour 17
 - 3.2.2 Nonlinear material behaviour 18
 - 3.2.3 Geometrical imperfections 18
 - 3.2.4 Element meshing 18
 - 3.2.5 Load history 19
 - 3.2.6 Boundary conditions and extent of model 19

- 4 Macro Material Modelling** **21**
 - 4.1 Macro material concepts 21

4.2	Closed-form stiffness solution	22
4.3	Macro material model embedded in FE-software	26
5	Compressive Strength of Unstiffened Plates	27
5.1	Model description	27
5.1.1	Boundary conditions	27
5.1.2	Mesh	28
5.1.3	Initial imperfections	28
5.2	Analysis methodology	30
5.3	Results	31
5.3.1	Biaxial Stress-paths	31
5.3.2	$d = -22.5^\circ$	32
5.3.3	$d = 0^\circ$	33
5.3.4	$d = 45^\circ$	34
5.3.5	$d = 90^\circ$	34
5.3.6	$d = 112^\circ$	35
5.4	Effect of plate aspect ratio	37
6	Unstiffened Rectangular Plates with Initial Imperfections	41
6.1	Model description	41
6.2	Results	41
6.3	Discussion of negative Poisson effect	43
6.4	Validation of closed-form solution	45
6.4.1	Extraction of initial stiffness coefficients	45
6.4.2	Initial stiffness vs. plate aspect ratio	46
6.4.3	Initial stiffness vs. plate slenderness	47
7	Multi-bayed Panel with Initial Imperfections	51
7.1	Model description	51
7.1.1	Boundary conditions	51
7.1.2	Mesh	53
7.2	Initial imperfections	53
7.3	Results	55
7.3.1	Longitudinal compression	56

7.3.2	Transverse compression	58
8	Multi-bayed Panel Subjected to Lateral Pressure	61
8.1	Analysis methodology	61
8.2	Results	61
8.2.1	Longitudinal compression	62
8.2.2	Transverse compression	64
9	Stiffened Multi-bayed Panel	67
9.1	Model description	67
9.2	Results	68
9.2.1	Longitudinal compression	68
9.2.2	Transverse compression	69
10	Car-deck	73
10.1	Model description	73
10.1.1	Non-linear isotropic model	74
10.1.2	Initial imperfection	75
10.1.3	Linear anisotropic model	76
10.1.4	Linear isotropic (Rule) model	76
10.2	Study of initial stiffness	77
10.2.1	Applicability of macro material model under lateral pressure	81
10.3	Load-dependent stiffness correction	84
10.3.1	Anisotropic approximation of single plate model	84
10.3.2	Anisotropic approximation of car-deck using integrated plate	85
10.3.3	Anisotropic approximation of car-deck using single plate model	86
10.4	Optimization of deck structure	90
11	Concluding Remarks	95
11.1	Conclusion	95
11.2	Further work	97
	Bibliography	99
	Appendices	I

A Load-dependent stiffness reduction	III
B Python Imperfection Script	V
C Stiffened multi-bayed panel under lateral pressure	XI
D Car-deck model	XIII
E Calculation Sheet - Initial stiffness	XV
F Load-dependent Macro Material Input	XVII

List of Figures

1	Plate panel configuration	5
2	Bending of ship girder	6
3	Relevant load-condition for stiffened panel	6
4	Plate load-carrying characteristics	7
5	Plate-induced global buckling (Ventsel and Krauthammer (2001))	8
6	Stiffener-induced global buckling (Ventsel and Krauthammer (2001))	8
7	Plate buckling (Ventsel and Krauthammer (2001))	8
8	Stiffener tripping (Ventsel and Krauthammer (2001))	8
9	Load-shortening relation	10
10	"Hungry-Horse" imperfection	12
11	Ultimate capacity characteristics	16
12	Plate model	28
13	Eigenmode $m = 1$	29
14	Eigenmode $m = 2$	29
15	Eigenmode $m = 3$	29
16	Proportional prescribed strain paths, \odot : $d = -22.5^\circ, 0^\circ, 45^\circ, 90^\circ, 112.5^\circ$	30
17	Biaxial membrane stresses	31
18	Biaxial stress-paths	31
19	Stress-paths w. eigenvalue limits	31
20	Load-shortening relation $d = -22.5^\circ$	32
21	Load-shortening relation $d = 0^\circ$	33
22	Load-shortening relation $d = 45^\circ$	34
23	Load-shortening relation $d = 90^\circ$	35
24	Load-shortening relation $d = 112.5^\circ$	36
25	Biaxial stress-path, model A1	37
26	Biaxial stress-path, model A2	37
27	Biaxial stress-path, model A3	37
28	Biaxial stress-path, model A4	37
29	Reduction of coefficient C_{22}	38
30	Reduction of coefficient C_{12}	38
31	Transverse load-shortening relation, model A3	42

32	Coupled stiffness model A3	42
33	Knock-down of initial stiffness	42
34	Deflection mode $x = 0.025/0.5$	43
35	Deflection mode $x = 0.1$	43
36	Deflection mode $x = 0.3$	43
37	Poisson effect caused by membrane stretching	44
38	CF vs. Abaqus, $w_0 = 3mm, t = 12.5mm$	46
39	CF vs. Abaqus, $w_0 = 6mm, t = 12.5mm$	46
40	CF vs. Abaqus, $w_0 = 12mm, t = 12.5mm$	47
41	CF vs. Abaqus, $w_0 = 37mm, t = 12.5mm$	47
42	CF vs. Abaqus, $w_0 = 3mm, \alpha = 4$	48
43	CF vs. Abaqus, $w_0 = 6mm, \alpha = 4$	48
44	CF vs. Abaqus, $w_0 = 12mm, \alpha = 4$	48
45	CF vs. Abaqus, $w_0 = 37mm, \alpha = 4$	48
46	Multi-bayed model	52
47	Load-shortening relation, 15 elem. vs. 8 elem.	53
48	Longitudinal load-shortening relation, $w_0 = 2mm$	56
49	Longitudinal load-shortening relation, $w_0 = 5mm$	56
50	Longitudinal load-shortening relation, $w_0 = 9mm$	56
51	Longitudinal load-shortening relation, $w_0 = 28mm$	56
52	Longitudinal deflection mode, $w_0 = 2mm$ HH, scale=30	57
53	Transverse load-shortening relation, $w_0 = 2mm$	58
54	Transverse load-shortening relation, $w_0 = 5mm$	58
55	Transverse load-shortening relation, $w_0 = 9mm$	58
56	Transverse load-shortening relation, $w_0 = 28mm$	58
57	Transverse deflection mode, $w_0 = 2mm$ HH, scale=30	59
58	Transverse deflection mode, $w_0 = 28mm$ HH, scale=30	59
59	Deflection mode, $P = 0.2MPa, w_0 = 9mm$ EM, scale=30	62
60	Longitudinal load-shortening relation, $w_0 = 9mm$ EM	63
61	Longitudinal load-shortening relation, $w_0 = 9mm$ HH	63
62	Longitudinal deflection mode, $P = 0.2MPa, w_0 = 9mm$ HH, scale=30	64
63	Deflection mode, $P = 0.2MPa, w_0 = 9mm$ EM, scale=30	64

64	Transverse load-shortening relation, $w_0 = 9mm$ EM	65
65	Transverse load-shortening relation, $w_0 = 9mm$ HH	65
66	Transverse deflection mode, $P = 0.2MPa$, $w_0 = 9mm$ HH, scale=30	66
67	Stiffened multi-bayed model	68
68	Longitudinal load-shortening relation, $w_0 = 9mm$ EM	69
69	Longitudinal load-shortening relation, $w_0 = 9mm$ HH	69
70	Longitudinal load-shortening relation, $w_0 = 2mm$ HH	69
71	Transverse load-shortening relation, $w_0 = 9mm$ EM	70
72	Transverse load-shortening relation, $w_0 = 9mm$ HH	70
73	Transverse load-shortening relation, $w_0 = 2mm$ HH	70
74	Car-deck model	74
75	Non-linear isotropic model, fine mesh	75
76	Initial imperfection	75
77	Linear anisotropic model, coarse mesh	76
78	Longitudinal load-shortening relation, $w_0 = 3mm$	77
79	Longitudinal load-shortening relation, $w_0 = 5mm$	77
80	Longitudinal load-shortening relation, $w_0 = 11mm$	78
81	Longitudinal load-shortening relation, $w_0 = 32mm$	78
82	Transverse load-shortening relation, $w_0 = 3mm$	78
83	Transverse load-shortening relation, $w_0 = 5mm$	78
84	Transverse load-shortening relation, $w_0 = 11mm$	79
85	Transverse load-shortening relation, $w_0 = 32mm$	79
86	Axial stresses in middle frame, $w_0 = 3mm$	79
87	Axial stresses in middle frame, $w_0 = 5mm$	79
88	Axial stresses in middle frame, $w_0 = 11mm$	80
89	Axial stresses in middle frame, $w_0 = 32mm$	80
90	Global transverse stiffness, $w_0 = 3mm$	80
91	Global transverse stiffness, $w_0 = 5mm$	80
92	Deflection caused by lateral pressure, scale=50	82
93	Local stiffness	82
94	Global stiffness	82
95	Anisotropic prediction of transverse stresses	85

96	Anisotropic prediction of longitudinal stresses	85
97	Anisotropic prediction of transverse stresses, integrated plate	86
98	Anisotropic prediction of longitudinal stresses, integrated plate	86
99	Anisotropic prediction of transverse stresses, single plate	87
100	Anisotropic prediction of longitudinal stresses, single plate	87
101	Anisotropic prediction of transverse stresses, tuned coefficients	88
102	Anisotropic prediction of longitudinal stresses, tuned coefficients	88
103	Membrane stresses in frame	88
104	Global stiffness	89
105	Transverse membrane stresses in plate	91
106	Transverse membrane stresses in frame	91
107	Stress accumulation in mid-frame flange	92
108	Variation of C_{11} , $d = -22.5^\circ$	III
109	Variation of C_{11} and C_{21} , $d = 0^\circ$	III
110	Variation of C_{11} and C_{21} , $d = 45^\circ$	III
111	Variation of C_{22} and C_{12} , $d = 90^\circ$	III
112	Variation of C_{22} , $d = 112.5^\circ$	III
113	Longitudinal load-shortening relation, $w_0 = 9mm$ EM	XI
114	Longitudinal load-shortening relation, $w_0 = 9mm$ HH	XI
115	Transverse load-shortening relation, $w_0 = 9mm$ EM	XI
116	Transverse load-shortening relation, $w_0 = 9mm$ HH	XI
117	Load-dependent macro material input, single plate model	XVII
118	Load-dependent macro material input, integrated plate	XVII

List of Tables

1	Boundary conditions, unstiffened plate	28
2	Comparison of C_{11} [$\times 10^5 MPa$]	45
3	Comparison of C_{21} [$\times 10^5 MPa$]	45
4	Comparison of C_{12} [$\times 10^5 MPa$]	46
5	Comparison of C_{22} [$\times 10^5 MPa$]	46
6	Boundary conditions, multi-bayed model	52
7	Weighed imperfection modes, longitudinal shortening, scale = 100	54
8	Weighed imperfection modes, transverse shortening, scale = 100	55
9	Boundary conditions, stiffened multi-bayed model	67
10	Boundary conditions, Car-deck model	74
11	Tuning of E_2	87
12	Tuning of ν_{12}	87

Abbreviations

HH	Hungry-Horse
EM	Eigenmode
ULS	Ultimate Limit State
PULS	Panel Ultimate Limit State
FE	Finite Element
NLFEM	Non-linear Finite Element Methods
RP	Recommended Practice
LPF	Load Proportionality Factor
IACS	International Association of Classification Societies
DOF	Degree of freedom
S4R	Square 4-node reduced integration element

Symbols

General comment: Frequently used symbols are defined below. Symbols not defined here are explained in the text. A symbol may have more than one meaning.

σ_1	Longitudinal membrane stress
σ_2	Transverse membrane stress
ϵ_1	Longitudinal overall nominal strain
ϵ_2	Transverse overall nominal strain
λ	Slenderness parameter
σ_y	Yield strength
σ_E	Euler buckling stress
E	Young's Modulus
ν	Poisson ratio
s	Stiffener spacing
η	Usage factor
w_{max}	Faulkner imperfection amplitude
x	Faulkner imperfection scale factor
l	Plate length
b	Plate width
t	Plate thickness
C_{11}	Longitudinal stiffness coefficient
C_{22}	Transverse stiffness coefficient
C_{12}, C_{21}	Coupled stiffness coefficient
w	Load-dependent deflection

w_0	Initial out-of-plane distortion
m	Number of half-waves across plate length
n	Number of half-waves across plate width
U	Translational degree of freedom
UR	Rotational degree of freedom
d	Angle of proportional strain history
P	Lateral pressure
E_1	Anisotropic longitudinal stiffness
E_2	Anisotropic transverse stiffness
ν_{12}	Anisotropic Poisson coefficient
F_2	Prescribed transverse force

1 Introduction

Combining light weight with high strength is an important aspect of the design process of marine structures. Light and energy efficient ships enable reduced fuel consumption and shipowners are always aiming to push the costs down. This puts a great pressure on designers and classification societies in the process of meeting both the customer expectations and established safety limits. Potential steel savings comes with a prize and must not compromise the fundamental strength of the structure.

Stiffened plate panels are the main structural component in most marine structures, such as the ship hull and deck panels. The design criteria for such configurations have generally been based on the elastic buckling limit. However, due to the strength reserves that plates possess beyond elastic buckling, local buckling of individual panels are no longer considered critical. From this arises the need for more sophisticated design procedures that cope with all relevant non-linear effects, however simple enough to compete with established methods.

1.1 Background and motivation

Standard design formulations for redundant plated structures have been developed based on linear plate buckling theory, as found in the DNV GL specifications for ultimate and buckling strength of stiffened and unstiffened plates (DNVGL (2010b)). Initial imperfections, residual stresses and plasticity are traditionally accounted for by empirical corrections. Besides having the asset of providing simple and effective strength predictions, these formulations do not document the effects of various imperfection shapes and sizes nor the deflection geometry. Also, the structural response in excess of the elastic buckling limit is not considered. This becomes an issue when faced with modern Ultimate Limit State(ULS) design principles where the structural strength is defined by the ultimate capacity, rather than the onset of elastic buckling.

While hand-calculations and explicit formulations have been highly appreciated in the shipbuilding industry, computerized tools become more and more accepted. Of these, Non-linear Finite Element Methods (NLFEM) provide the most realistic simulation of the structural behaviour. However, considering the large amount of stiffened panels in ship structures, the applicability of NLFEM in design is limited. This forms the motive of developing a

compromise between sophisticated non-linear methods and the simple linear procedures. Semi-analytical tools, such as the DNV GL software PULS, short for Panel Ultimate Limit State, has proved to meet some of these requirements. Some of the features embedded in this buckling tool enable an approximation of relevant non-linear effects in the form of a set of fictitious macro material coefficients (Steen et al. (2001)). These form the basis for a modified linear Finite Element approach which may serve as an alternative to standard design procedures.

1.2 Previous work

This thesis is based on previous work in the research area of semi-analytical tools used in design of redundant plated panels prone to buckling. This field has proved to be important to enable efficient and accurate methods for ultimate strength predictions (Paik et al. (2008a), Paik et al. (2008b)).

The semi-analytical computer program PULS is accepted as part of the DNV GL specifications for ultimate and buckling strength of unstiffened and stiffened plates (DNVGL (2010b)). The implementation was performed by Eivind Steen and Tom Østvold (Steen and Østvold (2000)), partially based on computational models developed in the doctoral thesis due to dr. Eirik Byklum (Byklum (2002)). A number of studies in addition to the latter provide a sound basis of comparison with non-linear finite element analyses (Steen et al. (2004a), Steen et al. (2004b)). Numerous additional articles and reports have been used as support in the discussions and analyses performed in this thesis (Brubak and Helleland (2007), Byklum et al. (2004), Byklum and Amdahl (2002) to mention a few). Most important is the article *Elastic Postbuckling Stiffness of Biaxially Compressed Rectangular Plates* (Steen et al. (2008)), where an explicit solution for the initial stiffness of imperfect plates is derived. The plate buckling theories presented in *Buckling of Bars, Plates and Shells* (Brush and Almroth (1975)) forms the foundation for the theoretical background adopted in this thesis.

A literature study on plate buckling theory and modern design procedures was performed by the author during the fall of 2014 (Palm (2014)). This included an introduction to the main principles and theories behind PULS. Some of the theoretical background presented in this master thesis is directly retrieved from the preceding project thesis.

1.3 Scope

The objective of this master thesis is to test and evaluate if the modified linear Finite Element approach developed by DNV GL is suited as a design procedure for dimensioning of redundant plated structures. Both the initial loss of stiffness at the presence of imperfections and the load-dependent behaviour of compressed plates are addressed. The work includes the following steps:

1. Local buckling behaviour of plates/stiffened panels:
 - (a) Single-bay plates: Perform analyses of the compressive strength and stiffness of unstiffened plates for uni-axial and bi-axial in-plane loading. Study and explain the overall Poisson effect of the plates as function of geometry, plate aspect ratio and imperfection amplitudes.
 - (b) Validate a simple stiffness model for load-independent anisotropic stiffness corrections developed by DNV GL.
 - (c) Multi-bayed panels: Simulate the effect of large integrated panels as typical for ships and assess the effect of imperfection shapes (“Hungry-Horse”/Eigenmodes) and lateral pressure on the in-plane stiffness response (initial and non-linear).
 - (d) Multi-bayed stiffened panels: Study the initial and non-linear behavior of a selected plate panel (regular stiffeners in one direction) and identify possible effects affecting the structural response not covered by the models analyzed under a) and b).
2. Benchmark a larger slender car-deck type of structure, considering the following features:
 - (a) Compare fine-mesh non-linear ABAQUS model with coarse rule ABAQUS model.
 - (b) Evaluate the load-independent stiffness correction in relation to the standard linear isotropic and present anisotropic model using the non-linear results as basis (ABAQUS).
 - (c) Tune the stiffness coefficients (C_{ij}) in the anisotropic model to mimic load-dependent non-linear ABAQUS results.

- (d) Optimize the deck structure with respect to plate thickness and document potential steel savings using the linear anisotropic approach as compared to the standard isotropic approach.

The theoretical background considered relevant for the current topics is collected in Chapter 1 to 4. Computerized parametric studies and experimental work performed by the author are found in Chapter 5 to 10. Some of the analyses and results presented herein are not directly connected to the study of the macro material design procedure. They are, however, essential for the understanding of the elastic buckling problem and the effects of initial imperfections and thus form the basis for subsequent discussions and conclusions. Some chapters include a discussion of the results found in the preceding analyses, while a summarized conclusion is given in Chapter 11.

2 Redundant Plated Structures

Marine structures are to a large extent assembled of stiffened panels, supported by heavier longitudinal and transverse girders. The conventional configuration of such panels is shown in Figure 1. Typical structures of this kind are the ship hull and superstructure as well as the decks on offshore platforms (Amdahl (2013)). In general, a structural component may fail due to buckling, local yielding, rupture or fatigue due to cyclic on- and off-loading. The structure as a whole should contain enough strength to prevent total collapse, even if individual panels or plates were to fail. This is ensured by a high degree of redundancy. However, the plate field should be designed in such a way that individual components never are exposed to loads exceeding the safety limits regarding the ultimate capacity(DNVGL (2015)).

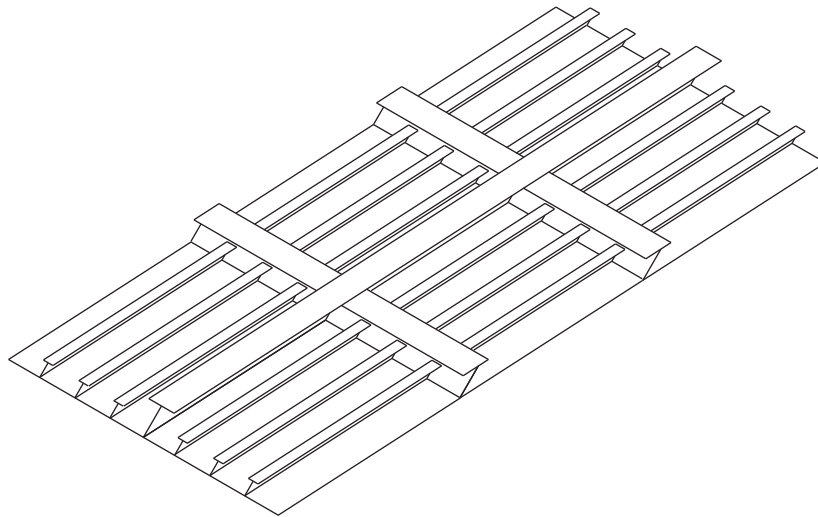


Figure 1: Plate panel configuration

Stiffened panels constituting the ship hull are often subjected to large in-plane stresses as a result of the longitudinal bending of the hull girder. The two most relevant ship motions are shown in Figure 2. The first example displays the wave trough positioned amidships with the crests at the perpendiculars. This results in sagging and compression in deck panels. In the latter condition the ship is hogging with the wave crest positioned amidships, which causes compression in bottom and double bottom plating.

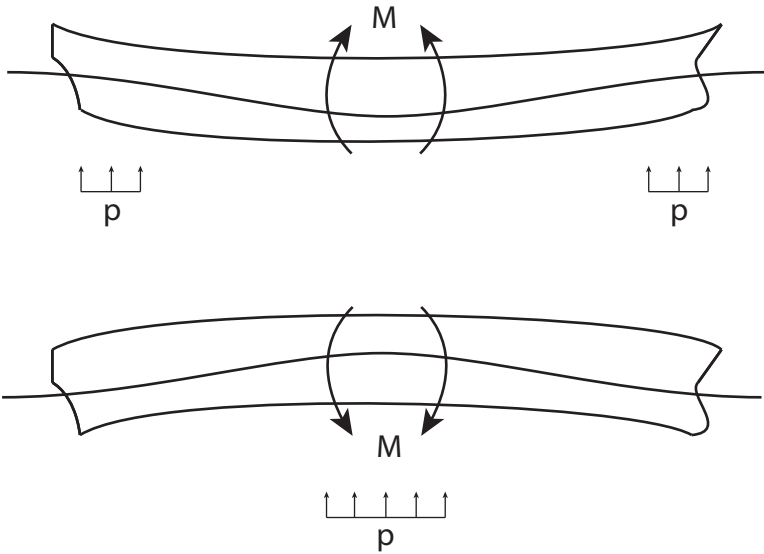


Figure 2: Bending of ship girder

The typical load condition for a stiffened plate field in a bottom or deck structure is depicted in Figure 3. The high biaxial membrane stresses combined with the slender configuration of individual plates result in a particularly high vulnerability to buckling.

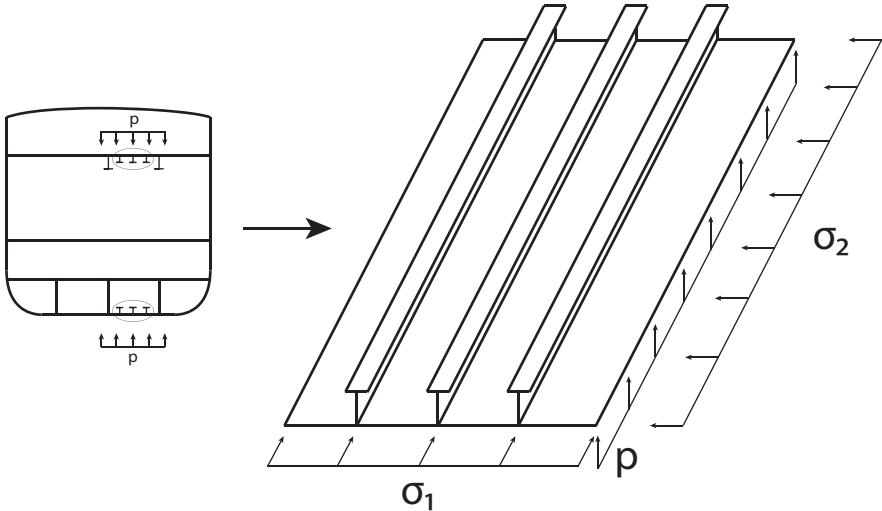


Figure 3: Relevant load-condition for stiffened panel

2.1 Elastic plate buckling

Elastic plate buckling is defined by the minimum eigenvalue and recognized by a sudden loss of stability followed by rapid development of deflections. Buckling of plates that are properly supported is generally referred to as stable as they exhibit a positive stiffness in the post-buckling region, commonly visualized as in Figure 4 (Brush and Almroth (1975)). This entails a significant load-carrying capacity even in excess of the elastic buckling limit.

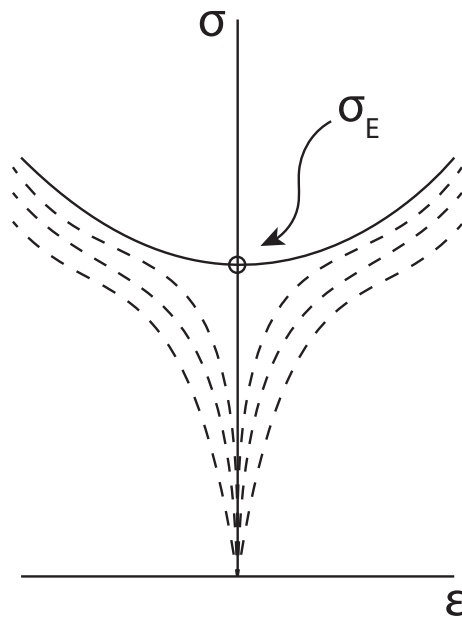
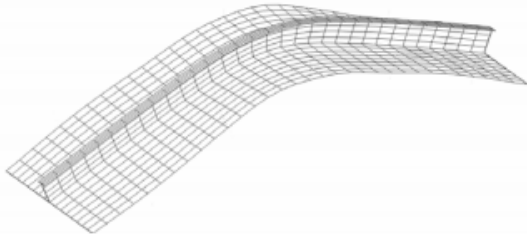
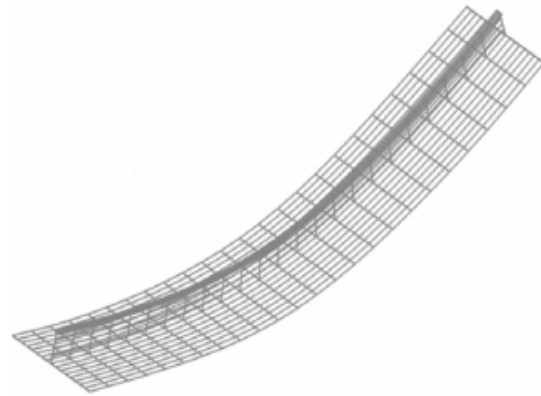


Figure 4: Plate load-carrying characteristics

A stiffened plate panel may undergo several modes of deflection under uni-axial or biaxial compression. The failure modes are generally sorted into four forms of instability, each of them representing either global or local buckling, illustrated by the subsequent figures.



*Figure 5: Plate-induced global buckling
(Ventsel and Krauthammer (2001))*



*Figure 6: Stiffener-induced global buckling
(Ventsel and Krauthammer (2001))*

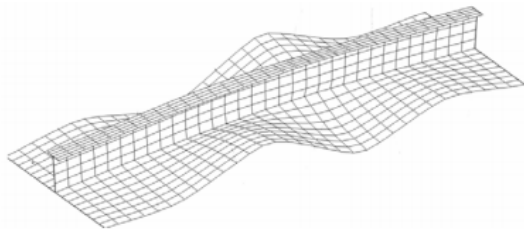


*Figure 7: Plate buckling
(Ventsel and Krauthammer (2001))*

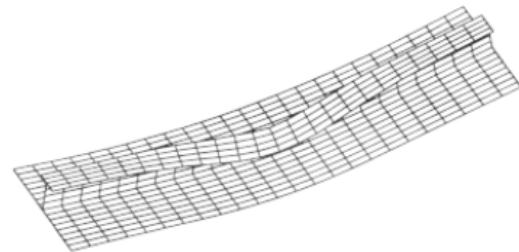


*Figure 8: Stiffener tripping
(Ventsel and Krauthammer (2001))*

The first two modes represent global buckling, also referred to as overall grillage buckling (Paik and Thayamballi (2003)). This failure mode is characterized by bending of longitudinal stiffeners and may take the form of plate-induced or stiffener-induced deflection, Figure 5 and 6 respectively. Local buckling corresponds to plate buckling between stiffeners or torsional buckling of stiffeners, depicted in Figure 7 and Figure 8 respectively. In this thesis focus will be on local plate buckling as this failure mode becomes highly relevant when adopting modern rule formulations.

Analysing the strength and stiffness of structures prone to buckling involves examining all relevant deflection modes as well as potential interactions between these. So-called mode-snapping effects may be detrimental even though the overall buckling resistance is high. Such phenomena are especially pertinent if the eigenvalues of the relevant buckling modes are clustered together. This is also important to be aware of when embedding initial imperfections in modelling. Interaction effects may be relevant both on a local and global level. In the case of heavy stiffeners, the global eigenvalues will generally lie far in excess of the local limits. For a panel with slender stiffeners, interaction effects between local and

global buckling modes may be more of an issue.

2.1.1 Slenderness parameter

A convenient and widely used parameter in the context of elastic buckling is the slenderness parameter, defined by DNV GL as (DNVGL (2015)):

$$\lambda = \sqrt{\frac{\sigma_y}{\sigma_E}} \quad (1)$$

where σ_y is the material yield strength and σ_E is the Euler buckling stress for plates, written as:

$$\sigma_E = \frac{k\pi^2 E}{12(1-\nu^2)(\frac{b}{t})^2} \quad (2)$$

ν is recognized as the Poisson ratio, E is the Young's Modulus and the parameter k is determined by the plate supports. The slenderness parameter disclose whether the structural response is governed by buckling or material yield. In general, $\lambda > 1.4$ defines a slender structure while $\lambda < 0.6$ denotes a stocky structure (DNVGL (2015)). Included in the function for the critical buckling stress is the width-thickness ratio $\frac{b}{t}$ (generally denoted $\frac{s}{t}$ in this thesis, where s = stiffener spacing). It is observed that a larger width or a lower thickness results in a lower elastic buckling limit.

2.1.2 Stress redistribution

Elastic buckling is accompanied by progressive growth of 2^{nd} -order membrane stresses that comes in addition to the direct applied loads or prescribed displacements. These stresses accumulate in intersections between individual plates and the supporting structure such as stiffeners or girders. When the total stress (direct + 2^{nd} -order) approaches the material yield strength the structure is considered close to the collapse limit. This load-shedding to supporting structure is referred to as stress redistribution and must be accounted for in design formulations when elastic plate buckling is accepted. Consequently, adopting ULS-principles in design codes implies that stresses are free to wander between plating, stiffeners and frames, which is a non-linear problem.

2.1.3 Load-shortening relation

The linear membrane stiffness is determined by Hooke's law (Young's modulus E). Any deviation from this value is due to the combined action of elastic buckling and the presence of initial imperfections. The loss of stiffness imposed by either of the two is conveniently illustrated by so-called load-shortening curves, which display in-plane stresses against the corresponding shortening of the panel. The tangent to the curve represent the incremental stiffness at any point in the response-history. An example of such a relation is given in Figure 9, which is a replica of an illustration by DNV GL (DNVGL (2015)).

For a nearly perfect plate the load-shortening curve will coincide with the linear slope until the elastic buckling limit is reached (continuous line Figure 9). From this point on the plate experiences a significant loss of membrane stiffness, whereafter the stiffness approaches a constant value in the post-buckling range. In the case of initial imperfections the incremental membrane stiffness will deviate from the linear value from before onset of loads and more so the larger the amplitude of the imperfection (dashed line Figure 9).

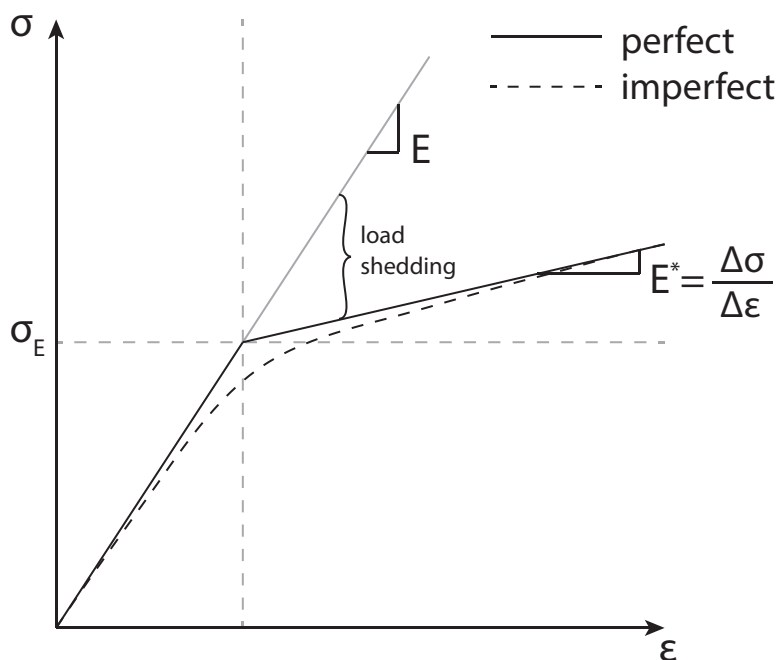


Figure 9: Load-shortening relation

E^* denotes the reduced incremental membrane stiffness of the buckled plate. The stress redistribution to supporting structure at a given shortening ϵ is dictated by the deviation

from the linear stress level (DNVGL (2015)):

$$\sigma_{shed} = (E - E^*)(\epsilon - \epsilon_E) \quad (3)$$

In this thesis, the elastic buckling behaviour and the corresponding loss of stiffness and redistribution of stresses will generally be demonstrated by load-shortening curves, supplemented by load-paths mapped into the biaxial stress-space. The load-paths conveniently dictate the stress redistribution that takes place in the vicinity of the elastic buckling limit.

2.2 Initial imperfections

The fabrication of typical stiffened plate panels in marine structures involves heating arising from welding and cutting. These processes result in distortions, characterized by a deflected shape and an amplitude and are the major reason for deviations in the buckling strength of seemingly identical plates (Singer et al. (1998)). The effects of initial imperfections depend on numerous factors and may not always be predicted intuitively. Primarily the severity is determined by the shape and size of the distortions, which again are results of the slenderness and aspect ratio of individual plates. Also, the configuration and redundancy level of the structure in addition to the nature of relevant load conditions (biaxial compression and lateral loads) are decisive for how detrimental the initial imperfections turn out to be.

Stiffened plate panels possess an extensive degree of redundancy in the ability to transfer induced membrane stresses to neighbouring frames and girders. A certain degree of initial out-of-flatness is not critical regarding the ultimate capacity. Normal production levels will typically give a scatter of capacity in the range 5 – 15% (DNVGL (2015)). However, the sensitivity and instability must be mapped in order to identify critical combinations of loading- and boundary conditions and imperfection geometry.

2.2.1 Imperfections in design and rule formulations

The application of initial imperfections in design is characterized by great uncertainty. Thus, imperfection sensitivity is a hot topic. Typical imperfection patterns seen in fabrication of stiffened plate panels are quite randomly distributed. Such geometries are inconvenient to model and exact data are not available. A simplified imperfection model is required concerning an efficient application and realistic strength predictions. However, some knowl-

edge about relevant fabrication shapes should be retrieved in order to balance the modelled deflection according to the expected imperfection. Considering the buckling strength, imperfection modes that coincide with the structure's own preferred deflection shapes (eigenmodes) are most unfavourable. A common and conservative approach is to set off the minimum eigenmode, which generally results in a reduced ultimate capacity. An eigenvalue analysis is conducted prior to the strength analysis in order to obtain both elastic buckling stresses (eigenvalues) and eigenmodes. If the eigenvalues corresponding to the lower eigenmodes are clustered together, the structure will be prone to mode snapping. In this case a measured imperfection shape may be obtained by combining the corresponding eigenmodes.

The fabrication processes of stiffened panels generally impose a cylindrical deflection shape of plates between stiffeners known as the "Hungry-Horse" (HH), depicted in Figure 10. This imperfection mode will in most cases introduce stiffening effects and add on to the strength of the structure (Amdahl (2013)). It may, however, also entail mode-snapping effects due to the out-of-mode configuration for longitudinal compression. An alternative to the conventional implementation of imperfections is a weighted combination of the eigenmode and the HH-deflection. This may give a more realistic deflection pattern and less conservative strength estimates.

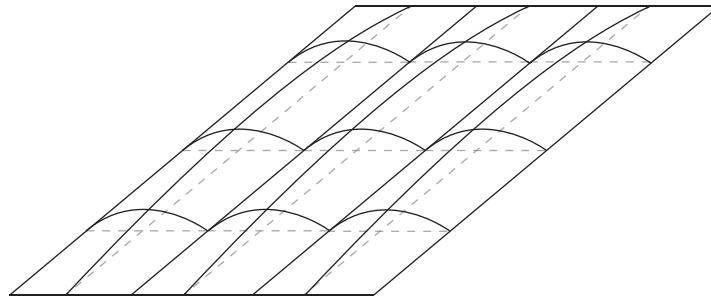


Figure 10: "Hungry-Horse" imperfection

The modelling procedures used in this thesis applies an imperfection geometry with equal amplitude for all integrated plates. Whether the applied geometry resembles the eigenmode or the "Hungry-Horse" imperfection, there is a considerable difference between this simplified approach and actual randomly distributed imperfection patterns. One should have this in mind when evaluating the results.

2.2.2 DNV GL tolerance levels

The procedures in the DNV GL Recommended Practice (RP) for buckling strength of plated structures (DNVGL (2010b)) presumes that the structure is built according to DNV-OS-C401 *Fabrication and Testing of Offshore Structures* (DNVGL (2010a)) or general ship classification standards such as the *IACS Shipbuilding and Repair Quality Standard* (IACS (2013)). In the former, the fabrication tolerances for initial out-of-straightness for plates between stiffeners is defined by:

$$\delta = 0.005 \times s \quad (4)$$

where s is the stiffener spacing. This is a generalized tolerance level and may, depending on the considered configuration, differ from the levels given by IACS (International Association of Classification Societies). The RP is however considered relevant for ships under normal operation and the given tolerance level is often used as imperfection amplitude in modelling. It is worth pointing out that there is a great difference between this model imperfection and real-life distortions. The former is primarily applied to trigger the desired buckling mode, so as to provide conservative strength estimates, and may to a varying degree correspond to the actual imperfection.

2.2.3 Faulkner's imperfection model

There exist numerous philosophies for prediction of the imperfection amplitude (e.g. Carlsen and Czujko (1978)). One of these is due to Faulkner (Faulkner (1975)), who's model captures imperfection sizes in the range from slight to severe distortions. The model is based on actual measurements of imperfections in ship plating and so include typical fabrication level imperfections. The maximum initial amplitude w_{max} is related to the panel geometry (slenderness) and material properties in the following manner:

$$\frac{w_{max}}{t} = x\beta^2 \quad \beta = \frac{s}{t} \sqrt{\frac{\sigma_y}{E}} \quad (5)$$

where the relation between yield strength and the Euler stress is recognized as the slenderness parameter defined in Section 2.1. The imperfection scale factor x is taken as:

- $x = 0.01$ - Slight imperfection
- $x = 0.05$ - Representative imperfection
- $x = 0.1$ - Average imperfection
- $x = 0.3$ - Severe imperfection (damage)

Using Faulkner's prediction of imperfection amplitudes in modelling will for slender plates give considerable initial distortions, even in excess of established tolerance levels. The latter condition, $x = 0.3$, will in most cases give imperfection amplitudes way in excess of the plate thickness. Such distortions would never be tolerated in design but may give a measure of the residual strength of a damaged plate or panel.

3 Modern Design

Former design codes have been based on the elastic buckling criteria. Strength estimates have thereof been determined with adequate accuracy using linear analyses. In modern specifications, Ultimate Limit State (ULS) principles are introduced, which are based on the ultimate structural strength rather than the onset of elastic buckling. The ultimate strength is understood as the structure's load-bearing capacity without major damages in the form of permanent plastic buckles. First yield in certain "hard corners" is defined as the failure criteria (DNVGL (2015)). The main motive for introducing ULS principles in design is the highly redundant nature of stiffened steel panels and the corresponding positive post-buckling stiffness of supported plates. Using the elastic buckling limit as failure criteria has simply been proved too conservative and fails to describe the structural behaviour at larger deflections.

3.1 ULS Design principles

The ULS design principles may be summarized by the following, taken from the DNV GL Classification Guideline for buckling (DNVGL (2015)):

- Elastic buckling of plates between stiffeners is accepted as long as the stress redistribution to supporting structure is accounted for.
- Elastic global buckling of stiffeners is not accepted. Stiffeners should possess adequate strength to provide support to plating.
- To prevent permanent plastic sets, the ultimate capacity shall not be exceeded by a safety margin defined in the Rules.

Accepting elastic buckling not only allows for higher stresses but puts greater demands on the numerical tools used in buckling and ultimate strength assessments. The buckling procedure must mimic the non-linear behaviour resulting from large deflections and initial imperfections to give a more accurate strength estimate than current linear formulations.

3.1.1 Capacity definitions

Due to the various motions of the ship girder the relevant load history for hull panels is characterized by a continuous on- and off-loading of the directional load components. The prob-

lem is simplified by assuming a proportional load history in the 2-D or 3-D load space. The applied loads are scaled up until the structure collapses(ultimate capacity, $\begin{bmatrix} \sigma_{1u} \\ \sigma_{2u} \\ \sigma_{3u} \end{bmatrix}$) and the load history is ensured to go through the point in space which corresponds to the Rule design load (reference load, $\begin{bmatrix} \sigma_{10} \\ \sigma_{20} \\ \sigma_{30} \end{bmatrix}$). The relation between applied loads, the design load and the ultimate capacity is conveniently visualized in stress-space by adopting the ULS capacity surface and the usage factor η , as depicted in Figure 11, a replica of a DNV GL illustration (DNVGL (2015)). The usage factor is defined as the ratio between applied loads and the ultimate capacity:

$$\eta_{act} = \frac{\text{applied load}}{\text{ultimate capacity}} = \frac{\sqrt{\sigma_{10}^2 + \sigma_{20}^2 + \sigma_{30}^2}}{\sqrt{\sigma_{1u}^2 + \sigma_{2u}^2 + \sigma_{3u}^2}} \quad (6)$$

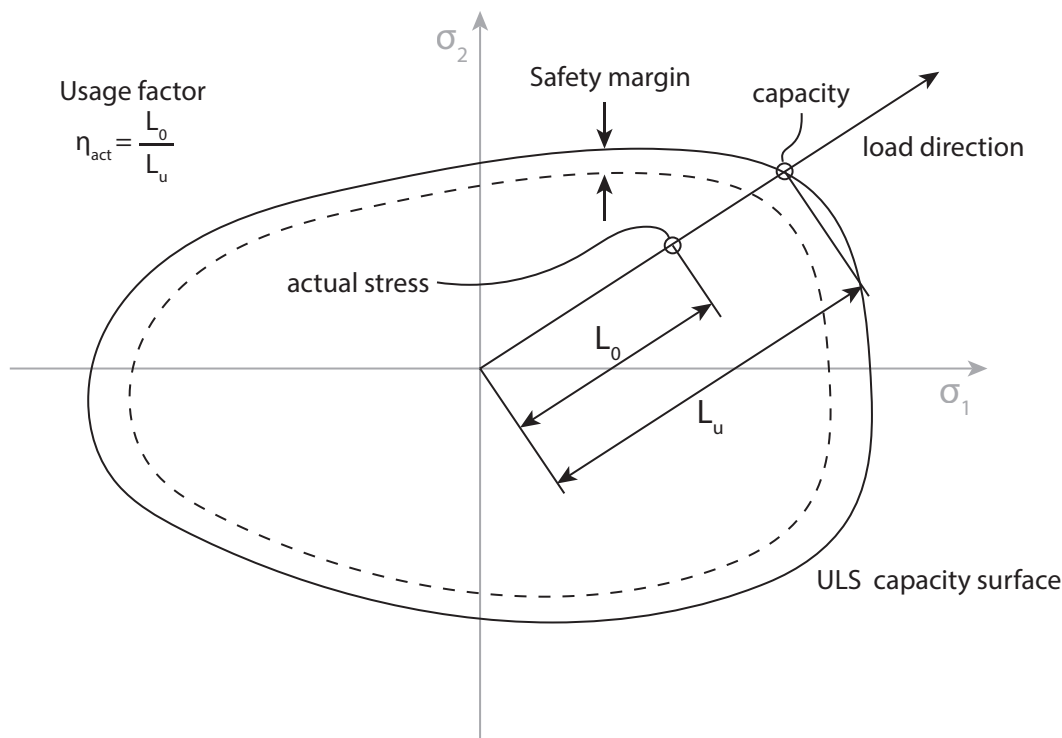


Figure 11: Ultimate capacity characteristics

The proportional load paths form straight lines in load space and the utilization is determined by the distance to the ultimate capacity surface. This gives a measure of how close to

the ultimate capacity or to potential safety limits the structure operates. Safety criteria are written as $\eta \leq \eta_{all}$ where the allowable usage η_{all} includes all relevant safety factors.

In this thesis the majority of the analyses are conducted using displacement control rather than load control. The edge-shortenings are applied in the same manner as explained above, by assuming a proportional biaxial strain history.

3.2 Nonlinear Finite Element Methods

Non-linear analyses may be necessary when documenting new designs and solutions that are not treated or adequately described in established rules. Considering elastic buckling, Non-linear Finite Element codes are convenient tools to map phenomena such as mode snapping and stress redistribution. Hereunder follows a brief review of important aspects when approaching such problems. The procedures are retrieved from the DNV GL Classification Guide for buckling (DNVGL (2015)) and the ABAQUS User Manual (Systèmes (2014)).

Standard non-linear FE-tools address four main types of non-linearities:

- Non-linear geometrical behaviour
- Non-linear material behaviour
- Non-linear contact effects
- Fracture

The two latter effects are generally not relevant in the elastic buckling problem, while the non-linear material behaviour dictates the onset of material yield. The main concern in this thesis is sensitivity to and application of geometrical non-linearity, hereunder initial imperfections.

3.2.1 Non-linear geometrical behaviour

Non-linear geometrical effects progress due to large deflections caused by external loads. For structures consistent of slender plates, large deflections may develop long before the onset of material non-linearity. In these cases the geometrical non-linear behaviour may be prominent even for minor out-of-plane distortions and initial imperfections. For the elastic plate buckling problem, these effects are dealt with by thin shell elements. The non-linear

behaviour is described by the large deflection plate theories due to von Kármán (Kármán (1910)) and Marguerre (Marguerre (1983)).

3.2.2 Nonlinear material behaviour

For metallic materials, the material non-linearity is defined by:

- a stress-strain curve
- a yield criteria (von Mises)
- a hardening rule (isotropic or kinematic)
- a flow rule

In this thesis, focus is on elastic buckling. Plasticity will not be further discussed. The assumed yield strength is merely used to define relative stresses and strains and analysis stopping criteria.

3.2.3 Geometrical imperfections

The initially imperfect plate needs to be considered in some way when assessed in an FE-code. The most common approach is to introduce the minimum eigenmode as the imperfect geometry, alternatively a combination of higher-degree buckling modes. However, the nature of initial out-of-flatness depends on numerous factors and alternative approaches may be considered for different cases. A more thorough discussion of the evaluation and application of initial imperfections relevant for stiffened plate panels is given in Chapter 2.2.

3.2.4 Element meshing

The mesh must be sufficiently refined for the various buckling modes to develop in a realistic manner. Accumulation of stresses and material yielding must be captured in local "hard-corners". DNV GL provides some specific advise on the meshing procedure for stiffened panels:

- Considering the local stiffness and buckling strength of individual plates, 6 elements across plates between stiffeners are required.
- Min. 3 elements across the stiffener web height and one element across the stiffener flange (two if T-bar)

- Elements should be close to quadratic and element aspect ratios above 3 should be avoided.

3.2.5 Load history

When the load history for a structural problem is unknown one may conveniently assume a proportional load-path. By introducing a reference load σ_0 the problem reduces to one variable; the load proportionality factor (LPF) λ . The load at any stage in the response history is found by multiplying the reference load with the corresponding LPF. The same goes for prescribed displacements.

3.2.6 Boundary conditions and extent of model

Boundary conditions must be defined in such a manner that all relevant deflection patterns may develop without any unphysical edge-effects. The latter are often visual in the ABAQUS deflection plots and may thereby be spotted and eliminated. The extent of the model should be adequate to allow for both local and global buckling modes and a realistic interference between these. For stiffened panels this implies minimum three frame spacings and six stiffener spacings.

4 Macro Material Modelling

The material law for an homogeneous isotropic material (Hooke's law) is defined by Young's Modulus E and the Poisson ratio ν . The two material parameters are constant and merely reflect the behaviour for minor deflections on a structural element of restricted size. For highly non-linear problems one will be far beyond the frame of reference where Hooke's law is valid. When approaching such problems, a modified macro material model may mimic relevant non-linearities in a quite sophisticated manner. In short, macro material modelling implies predicting the overall structural behaviour by coupling the material model to non-linear local effects. In this chapter a review of macro material concepts and the derivation of a closed-form solution for initial stiffness of imperfect plates will be presented. The theory and approach are directly retrieved from the article *Elastic Postbuckling Stiffness of Biaxially Compressed Rectangular plates*(Steen et al. (2008)).

4.1 Macro material concepts

An integrated plate in a ship hull must be able to cope with in-plane biaxial and shear loads. The relation between acting membrane stresses and in-plane edge-shortenings is written as:

$$\sigma_\alpha = \sigma_\alpha(\epsilon_1, \epsilon_2, \epsilon_3) \quad (7)$$

where σ_α represents σ_1 , σ_2 or σ_3 . 1, 2 and 3 denotes the principal directions in physical space; the in-plane longitudinal, in-plane transverse and in-plane shear direction respectively. The corresponding load-shortening relations may be written in a very compact manner by introducing the macro material characteristics matrix:

$$\begin{bmatrix} \Delta\sigma_1 \\ \Delta\sigma_2 \\ \Delta\sigma_3 \end{bmatrix} = \begin{bmatrix} C_{11} & C_{12} & C_{13} \\ C_{21} & C_{22} & C_{23} \\ C_{31} & C_{32} & C_{33} \end{bmatrix} \begin{bmatrix} \Delta\epsilon_1 \\ \Delta\epsilon_2 \\ \Delta\epsilon_3 \end{bmatrix} \quad (8)$$

The incremental form is required since the stiffness properties are state/load-dependent. This implies that the stiffness is reflected at a given stress- or strain-level, rather than at a material point. The macro material coefficients are defined as the derivative of each stress

component with respect to relevant strains, written as:

$$\begin{aligned} C_{\alpha\beta} &= \frac{\partial^2 \sigma_\alpha}{\partial \epsilon_\beta \partial \epsilon_\delta} \\ C_{\alpha\beta\delta} &= \frac{1}{2!} \frac{\partial \sigma_\alpha}{\partial \epsilon_\beta} \quad \alpha, \beta, \delta = 1, 2. \end{aligned} \quad (9)$$

The macro material model may, embedded in FE-tools, be utilized in modern design codes as a convenient alternative to non-linear procedures. By "lumping" the effects of relevant non-linearities together in the macro material coefficients, a linear analysis may realistically imitate the actual non-linear response, more precisely by modifying the macro material input.

The concept of gathering non-linearities in the material properties is not a new approach, and numerous methods may be found in literature (Paik and Thayamballi (2003)). However, the procedure has yet to prove the ability to describe all effects relevant for strength assessments and design of marine structures. It is desired to develop an improved and more rigorous concept, which may be part of the design procedures in the years to come. In the remainder of this chapter an abbreviated derivation of the analytical formulation for initial stiffness due to the presence of initial imperfections is derived.

4.2 Closed-form stiffness solution

Large in-plane loads is a highly relevant load-condition for integrated plates in stiffened panels in marine structures. In the case of pure biaxial loading the macro-material model reduces to the following:

$$\begin{bmatrix} \Delta\sigma_1 \\ \Delta\sigma_2 \end{bmatrix} = \begin{bmatrix} C_{11} & C_{12} \\ C_{21} & C_{22} \end{bmatrix} \begin{bmatrix} \Delta\epsilon_1 \\ \Delta\epsilon_2 \end{bmatrix} \quad (10)$$

For moderate stresses (or prescribed displacements) and small imperfection levels the stiffness matrix will be symmetrical. Considering a plate with a given geometry and imperfection level, the membrane strains and stresses are determined by Marguerre's compatibility equation (Marguerre (1983)) based on the kinematic relations due to the same person. The latter are given in Equation 11, from which the compatibility equation, Equation 12, is derived.

$$\begin{aligned}
 \epsilon_1 &= u_{1,1} + \frac{1}{2} w_{,1}^2 + w_{0,1} w_{,1} \\
 \epsilon_2 &= u_{2,2} + \frac{1}{2} w_{,2}^2 + w_{0,2} w_{,2} \\
 \epsilon_{12} &= u_{1,2} + u_{2,1} + w_{,1} w_{,2} + w_{0,1} w_{,2} + w_{,1} w_{0,2}
 \end{aligned} \tag{11}$$

$$\nabla^4 F = E[w_{,12}^2 - w_{,11} w_{,22} + 2w_{0,12} w_{,12} - w_{0,11} w_{,22} - w_{0,22} w_{,11}] \tag{12}$$

F is recognized as Airy's stress function while w and w_0 are the out-of-plane load-dependent deflection and the initial stress-free deflection respectively. The notation ",₁" denotes partial derivation with respect to x_1 . The compatibility equation implies straight in-plane plate edges.

The deflection mode is assumed to take on the same shape as the initial imperfection. The lateral deflection of a plate with length a and width b may be described mathematically by a Fourier series, here adopting one single Fourier term:

$$w = q_1 t \sin\left(\frac{m\pi}{a} x_1\right) \sin\left(\frac{n\pi}{b} x_2\right) \tag{13}$$

$$w_0 = q_{10} t \sin\left(\frac{m\pi}{a} x_1\right) \sin\left(\frac{n\pi}{b} x_2\right) \tag{14}$$

m and n denotes the number of half-waves across the plate length and width respectively (which corresponds to direction 1 and 2 with the adopted subscript convention). The values to adopt for a given case depends on the plate aspect ratio and the load condition. The deflection pattern may also be varied to study different structural effects. The unit-less coefficients q_1 and q_{10} denote the amplitudes of the deflection and the initial imperfection respectively, relative to the plate thickness:

$$q_1 = \frac{A_{mn}}{t} \tag{15}$$

$$q_{10} = \frac{A_{mn}^0}{t} \tag{16}$$

where A_{mn} and A_{mn}^0 are the relevant Fourier amplitudes. Now that the initial and load-dependent deflection patterns are determined, the compatibility equation(12) provides the

solution for the resulting internal membrane stresses:

$$\begin{aligned}\sigma_{11} &= -\sigma_1 - \frac{\pi^2 E}{8} (2q_{10}q_1 + q_1^2) \left[\left(\frac{tm}{a} \right)^2 \cos\left(\frac{2n\pi}{b}x_2\right) \right] \\ \sigma_{22} &= -\sigma_2 - \frac{\pi^2 E}{8} (2q_{10}q_1 + q_1^2) \left[\left(\frac{tn}{b} \right)^2 \cos\left(\frac{2m\pi}{a}x_1\right) \right] \\ \sigma_{12} &= 0\end{aligned}\quad (17)$$

Assuming a thin plate, plane stress theory is adopted. The membrane stresses are transformed to membrane strains by Hooke's Law:

$$\begin{aligned}\epsilon_{11} &= -\frac{1}{E}(\sigma_1 - \nu\sigma_2) - \frac{\pi^2 E}{8} (2q_{10}q_1 + q_1^2) \times \left[\left(\frac{tm}{a} \right)^2 \cos\left(\frac{2n\pi}{b}x_2\right) - \nu \left(\frac{tn}{b} \right)^2 \cos\left(\frac{2m\pi}{a}x_1\right) \right] \\ \epsilon_{22} &= -\frac{1}{E}(\sigma_2 - \nu\sigma_1) - \frac{\pi^2 E}{8} (2q_{10}q_1 + q_1^2) \times \left[\left(\frac{tn}{b} \right)^2 \cos\left(\frac{2m\pi}{a}x_1\right) - \nu \left(\frac{tm}{a} \right)^2 \cos\left(\frac{2n\pi}{b}x_2\right) \right]\end{aligned}\quad (18)$$

The relative plate shortenings are conventionally defined as:

$$\begin{aligned}\epsilon_1 &= \frac{1}{ab} \int u_{1,1} dA \\ \epsilon_2 &= \frac{1}{ab} \int u_{2,2} dA\end{aligned}\quad (19)$$

By using the kinematic relations and the derived expressions for the membrane strains (Eq. 18), $u_{1,1}$ and $u_{2,2}$ may be determined. Implemented in 19 we end up with the macro material model on total form:

$$\begin{aligned}\epsilon_1 &= \frac{1}{E}(\sigma_1 - \nu\sigma_2) + \frac{\pi^2}{8} (2q_{10}q_1 + q_1^2) \left(\frac{tm}{a} \right)^2 \\ \epsilon_2 &= \frac{1}{E}(\sigma_2 - \nu\sigma_1) + \frac{\pi^2}{8} (2q_{10}q_1 + q_1^2) \left(\frac{tn}{b} \right)^2\end{aligned}\quad (20)$$

Inverted, and assuming a deflection pattern equal to $m = n = 1$, these equations give the sought load-shortening relations:

$$\begin{aligned}\sigma_1 &= \frac{E}{1-\nu^2}(\epsilon_1 + \nu\epsilon_2) - \frac{\pi^2}{8} \frac{E}{1-\nu^2} \times (q_1^2 + 2q_{10}q_1)(k_1 + \nu k_2) \\ \sigma_2 &= \frac{E}{1-\nu^2}(\epsilon_2 + \nu\epsilon_1) - \frac{\pi^2}{8} \frac{E}{1-\nu^2} \times (q_1^2 + 2q_{10}q_1)(k_2 + \nu k_1)\end{aligned}\quad (21)$$

where k_1 and k_2 are constants defined by

$$k_1 = \frac{t^2}{a} \quad k_2 = \frac{t^2}{b}\quad (22)$$

From Eq. 21 and the stiffness relation defined in Eq. 9 the solution for the closed-form stiffness coefficients emerge:

$$C_{11} = \frac{E}{1-\nu^2} \left[1 - \frac{\pi^2}{4} (k_1 + \nu k_2) (q_1 + q_{10}) \frac{\delta q_1}{\partial \epsilon_1} \right] \quad (23)$$

$$C_{12} = \frac{E\nu}{1-\nu^2} \left[1 - \frac{\pi^2}{4} (k_1 + \nu k_2) (q_1 + q_{10}) \frac{\delta q_1}{\partial \epsilon_2} \right] = C_{21} \quad (24)$$

$$C_{22} = \frac{E}{1-\nu^2} \left[1 - \frac{\pi^2}{4} (k_2 + \nu k_1) (q_1 + q_{10}) \frac{\delta q_1}{\partial \epsilon_2} \right] \quad (25)$$

These coefficients may, for a plate with given dimensions and an initial load-independent imperfection defined by q_{10} , be derived for any equilibrium state given by a deflection coefficient q_1 and a load condition disclosed by either applied stresses (σ_1, σ_2) or edge-shortenings (ϵ_1, ϵ_2). The derivatives of the deflection parameter are found using the equilibrium equation for plate-shortening control, given by:

$$\Lambda_\epsilon = \frac{q_1}{q_1 + q_{10}} (1 + b_2(q_1^2 + 3q_1 q_{10} + 2q_{10}^2)) \quad (26)$$

The primary desire in this thesis is to utilize the macro material coefficients to mimic the initial load-independent stiffness. In order to filter out the effect of initial imperfections, the above is simplified to the case of zero external load. It may be proved that the stiffness coefficients, now denoted initial stiffness, may be written as:

$$\begin{aligned} C_{11} &= \frac{E}{1-\nu^2} \left[1 - 6 \frac{(k_1 + \nu k_2)^2}{A} \right] \\ C_{12} &= \frac{E\nu}{1-\nu^2} \left[1 - \frac{6}{\nu} \frac{(k_1 + \nu k_2)(k_2 + \nu k_1)}{A} \right] = C_{21} \\ C_{22} &= \frac{E}{1-\nu^2} \left[1 - 6 \frac{(k_2 + \nu k_1)^2}{A} \right] \end{aligned} \quad (27)$$

The load-independent stiffness coefficients are functions of the plate aspect ratio, the plate slenderness and the imperfection level. It is observed that the first part of the equations equals the linear elastic values, while the latter corresponds to the knock-down factor. The closed-form solution for initial stiffness is in the subsequent chapters recognized by a number of different names. Of these, the analytical solution/formulation/coefficients is most frequently used, in addition to the anisotropic method/coefficients when embedded in ABAQUS.

4.3 Macro material model embedded in FE-software

Considering the load-shortening relation of a compressed plate, the early response history may be linearized and conveniently mimicked by an anisotropic/orthotropic linear model. The analytical formulation for initial stiffness dictates the knockdown of the anisotropic coefficients for a given imperfection level. The general definition of such a material in FE-software is written as:

$$\begin{bmatrix} \epsilon_1 \\ \epsilon_2 \\ \gamma_{12} \end{bmatrix} = \begin{bmatrix} \frac{1}{E_1} & \frac{\nu_{12}}{E_1} & 0 \\ \frac{\nu_{12}}{E_1} & \frac{1}{E_2} & 0 \\ 0 & 0 & \frac{\nu_{12}}{G_{12}} \end{bmatrix} \begin{bmatrix} \sigma_{11} \\ \sigma_{22} \\ \tau_{12} \end{bmatrix} \quad (28)$$

The relation between the macro material model and the above stiffness definitions are given by (DNVGL (2015)):

$$E_1 = \frac{C_{11}C_{22} - C_{12}^2}{C_{22}} \quad (29)$$

$$E_2 = \frac{C_{11}C_{22} - C_{12}^2}{C_{11}} \quad (30)$$

$$\nu_{12} = \frac{C_{12}}{C_{22}} \quad \nu_{21} = \frac{C_{12}}{C_{11}} \quad (31)$$

$$G_{12} = \frac{1}{C_{33}} \quad (32)$$

These coefficients form the macro material input in the linear anisotropic material model of a single plate or the integrated plating of a larger configuration. It is important to note that the closed-form solution assumes a simply supported plate and a constant deflection pattern equal to half a sine-wave over both length and breadth. In comparison with non-linear analyses, the linear anisotropic model will fail to mimic the initial response if the actual boundary conditions or deflection pattern differ from the above.

5 Compressive Strength of Unstiffened Plates

As an introductory to the process of stress redistribution and the buckling phenomenon the compressive strength and stiffness of one specific rectangular plate is examined for five different proportional strain paths. The article *Elastic Postbuckling Stiffness of Biaxially Compressed Rectangular plates* (Steen et al. (2008)) is used as support and for comparison. A subsequent study of four plates with varying lengths under uni-axial and biaxial compression documents the correlation between aspect ratio and the buckling nature. The analyses are performed in Abaqus with displacement control. All plate models are considered as nearly perfect with a minor initial imperfection to set off the desired buckling mode. The results are presented as load-shortening curves and as load-paths mapped into the biaxial load-space.

5.1 Model description

The plate model has length $l = 3000mm$, width $b = 1000mm$ and thickness $t = 17mm$, and is depicted with the adopted coordinate system in Figure 12. An isotropic linear elastic material model is used, with material parameters defined as $E = 206000MPa$ and $\nu = 0.3$. Although not included in the material model, a yield strength of $315MPa$ is assumed, merely to use as reference in the presentation of the results.

5.1.1 Boundary conditions

The model is assumed to be integrated in a larger stiffened panel typical for a ship hull or deck structure. The presence of neighbouring plating is assumed to restrain the plate edges to remain straight. Due to the rotational stiffness imposed by adjacent stiffeners, the boundary conditions for the plate will be somewhere in between simply supported and clamped. For most panels constituting ship hulls the condition will be closer to that of simply supported due to the restricted rotational stiffness provided by stiffeners (Byklum (2002)). Local plate buckling implies no lateral distortions of the plate edges. The resulting constraints are given in Table 1, complemented by Figure 12. U denotes translation and the subscript notations 1, 2 and 3 correspond to the principal directions in xyz-space.





Boundary	Suppressed DOF's	Constraint	Colour code
Aft	U_3	Constrained to remain straight	
Fore	U_1, U_3	-	
Right	U_3	Constrained to remain straight	
Left	U_2, U_3	-	

Table 1: Boundary conditions, unstiffened plate

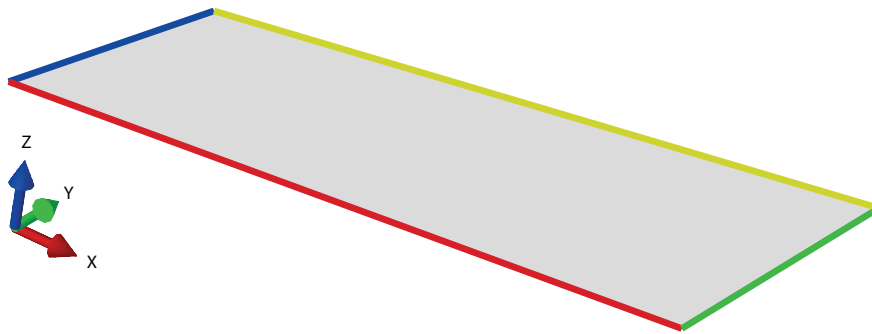


Figure 12: Plate model

Displacements are applied along the aft and right edge. An additional constraint against in-plane translation is applied to the right and aft edge for pure longitudinal and pure transverse compression respectively.

5.1.2 Mesh

The Abaqus model is meshed with square 4-node elements with reduced integration (S4R). 15 elements are used over the plate width. In terms of computational efficiency, the elements should be close to quadratic, which is achieved by requiring that the number of elements in the longitudinal direction is approximately $\frac{l}{b} \times 15$. No convergence study is conducted as 15 elements over the plate width is considered on the safe side with respect to computational accuracy (ref. Chapter 3.2).

5.1.3 Initial imperfections

For each displacement history the buckling mode corresponding to the minimum eigenmode is applied as initial imperfection. The relevant eigenmodes for the given geometry and load-conditions are depicted in Figure 13 to 15. The mode corresponding to each respective

displacement history is dictated by Figure 16. The models are to mimic perfect plates, hence a minor imperfection level corresponding to 1% of the thickness ($w_0 = \frac{t}{100} = 0.17mm$) is adopted, merely to trigger the preferred deflection mode.

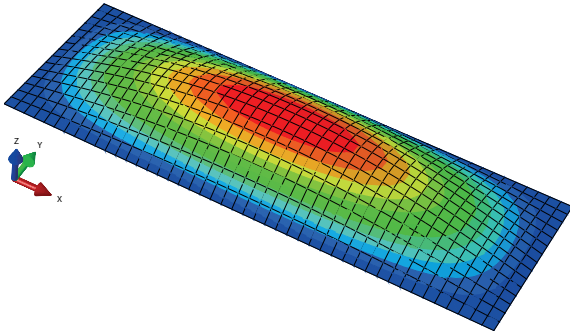


Figure 13: Eigenmode $m = 1$

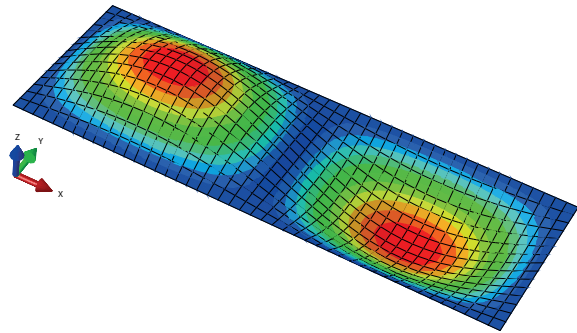


Figure 14: Eigenmode $m = 2$

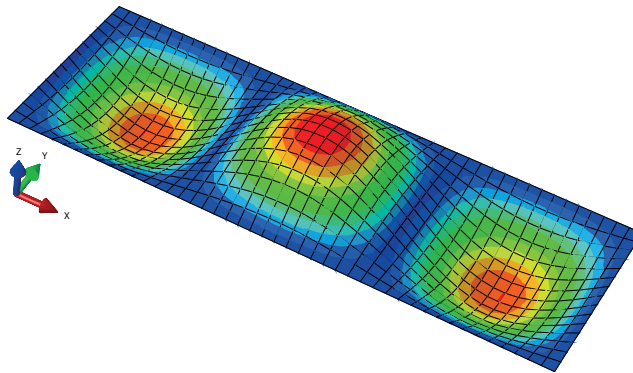


Figure 15: Eigenmode $m = 3$

The eigenmodes will hereafter be referred to as $m = 1$, $m = 2$ and $m = 3$, dictated by the number of half sine-waves across the plate length.

5.2 Analysis methodology

Analyses are carried out using displacement (or edge-shortening) control. The displacement histories are defined by the angle d between the ϵ_1 -axis and the relevant strain path in the biaxial strain-space, as displayed by the black lines in Figure 16. 1 and 2 denotes the x- and y-direction respectively. The straight coloured lines illustrate the elastic buckling limits corresponding to the relevant eigenmodes, and are calculated by equations derived in Steen et al. (2008). The strain paths' intersections with the eigenvalue boundaries dictate the stress levels at which the respective eigenmodes emerge. It is clear that the $m = 1$ mode is dominant in the majority of the biaxial strain-space.

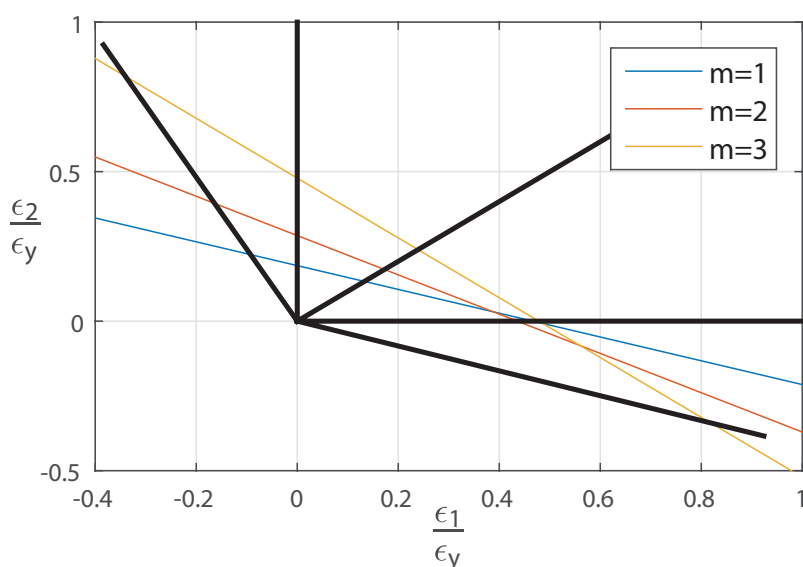


Figure 16: Proportional prescribed strain paths,
 $\odot: d = -22.5^\circ, 0^\circ, 45^\circ, 90^\circ, 112.5^\circ$

The minimum eigenmode for each strain history is used as imperfection geometry in the subsequent non-linear analyses. In the case of pure longitudinal edge-shortening ($d = 0^\circ$) the eigenvalues are clustered together. This indicates that the plate is highly prone to mode-snapping and sensitive to the initial imperfection mode. Three separate analyses are conducted adopting the three eigenmodes as imperfection geometry to capture all response events for this load case. Buckling analyses are carried out using the Static-Riks procedure. This is an arc-length based solution method which describes limit points and mode snapping effects without any problem. The yield strain ($\epsilon_y = \frac{\sigma_y}{E}$) is defined as analysis stopping criteria.

5.3 Results

Stresses in x- and y-direction, σ_1 and σ_2 respectively, are taken as the averaged membrane stresses along the plate edges, displayed in Figure 17. The stresses are retrieved from the middle integration point over the element thickness. Strains are given as overall nominal strain; $\epsilon_1 = \frac{\delta u_1}{l}$ and $\epsilon_2 = \frac{\delta u_2}{b}$. The results are made dimensionless by the yield strain and yield stress in the subsequent presentation of stress-paths and load-shortening curves.

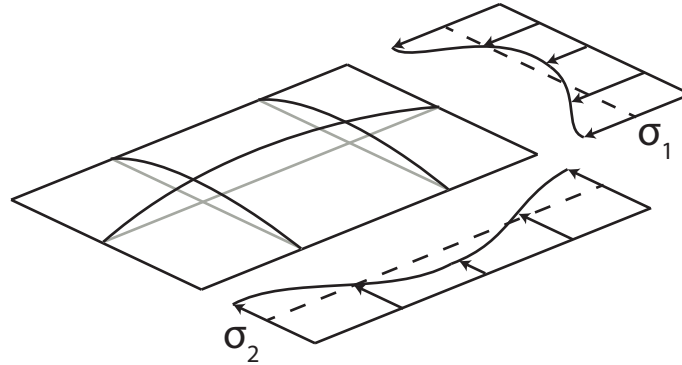


Figure 17: Biaxial membrane stresses

5.3.1 Biaxial Stress-paths

The stress paths in the biaxial stress space resulting from the five prescribed strain histories are given in Figure 18, accompanied by the minimum elastic eigenvalue boundaries mapped onto stress-space in Figure 19.

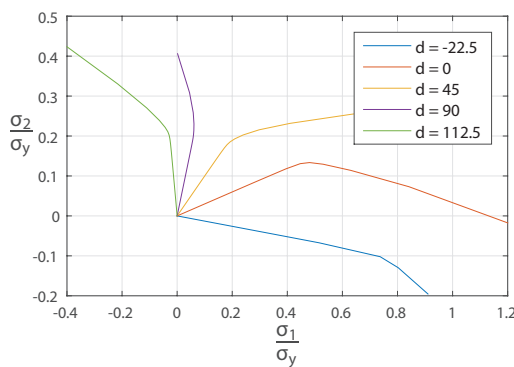


Figure 18: Biaxial stress-paths

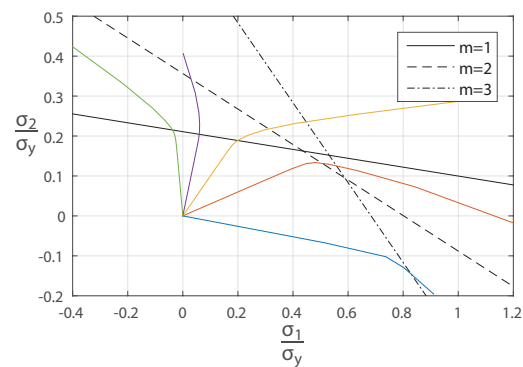


Figure 19: Stress-paths w. eigenvalue limits

All curves exhibit a clear bend as they pass the eigenvalue limit, demonstrating the stress redistribution that takes place when the plate buckles. The stress-paths will be used as support in the subsequent discussion of each shortening condition. In the remainder of this section, load-shortening curves are given for each strain history, presenting both of the orthogonal

stress resultants, σ_1 and σ_2 , as functions of either ϵ_1 or ϵ_2 . The variation of stresses in the shortening direction dictate the membrane stiffness of the system, while the stresses in the orthogonal to the shortening represent the coupled stiffness. The upper curve will always correspond to the transverse or longitudinal stiffness, while the lower curve dictate the coupled effect. The dashed lines correspond to the linear elastic stiffness. The load-dependent stiffness reduction and post-buckling stiffness for each displacement history are explicitly dictated by the figures given in Appendix A. All stiffness reductions given by percentage in subsequent discussions are retrieved from these.

5.3.2 $d = -22.5^\circ$

The strain path defined by $d = -22.5^\circ$ is characterized by a dominant longitudinal compression and tension in the transverse direction. The resulting stress path in Figure 18 illustrates that stress redistribution is initiated in the vicinity of the elastic buckling limit for mode $m = 3$. When the path crosses the boundary it experiences a sharp bend down, indicating a progressive growth of transverse tension.

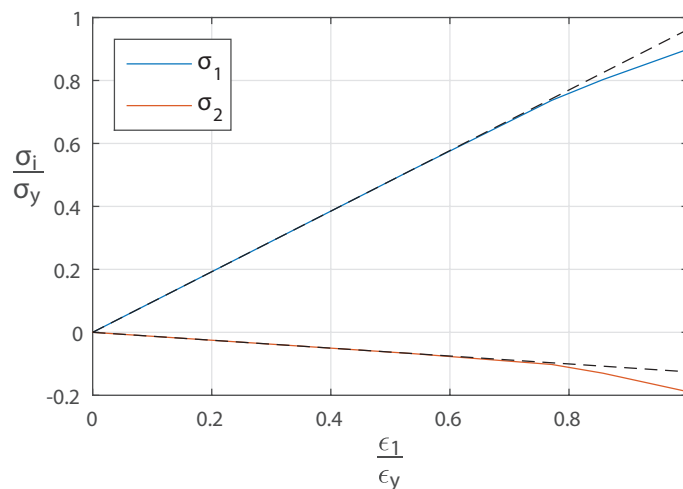


Figure 20: Load-shortening relation $d = -22.5^\circ$

The load-shortening relation in Figure 20 indicates that the transverse tension provide stiffening effects, resulting in a rather high elastic buckling strength. The stiffness for longitudinal compression experiences a knock-down in the order of 30%. The coupled stiffness is negative from the onset of compression due to initial tension in the transverse direction.

5.3.3 $d = 0^\circ$

For pure longitudinal shortening ($\epsilon_2 = 0$) the plate is seen to be highly prone to mode snapping, hence three analyses are conducted, adopting each of the three minimum eigenmodes as imperfection shape. The resulting load-shortening curves are given in Figure 21.

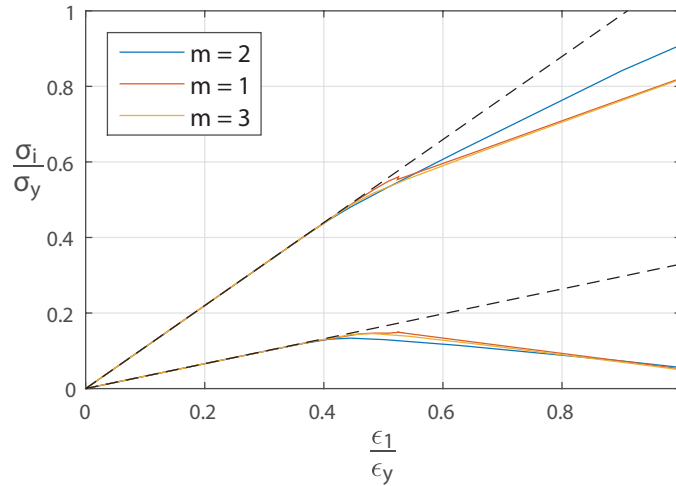


Figure 21: Load-shortening relation $d = 0^\circ$

It is observed that there is no difference in the initial stiffness of the three cases. The minimum eigenmode ($m = 2$) buckles slightly earlier than the two higher-degree imperfections at approximately 40% of the yield strain. The post-buckling stiffness reduction is in the order of 30%. Some contributions from the $m = 3$ mode emerge during deflection, although no snapping effects occur. The knock-down of longitudinal stiffness for the two higher-degree modes is seen to be larger than that of the minimum eigenmode. The second imperfection mode ($m = 1$) exhibit a sharp changeover into the $m = 3$ mode soon after the plate has buckled, recognized by the irregularity in the corresponding load-shortening curve. Since the $m = 3$ imperfection maintains its initiated deflection mode during buckling, the two higher-degree imperfection modes have equal post-buckling stiffness of about 50% of the linear value (interpreted by Figure 21).

As to the coupled stiffness, it is observed that the transverse stress starts off-loading as soon as the plates buckle and approaches negative stresses (tension) far into the post-buckling region. The reduction is in the order of 150%.

5.3.4 $d = 45^\circ$

The 45° condition corresponds to an equally weighed transverse and longitudinal strain history for which the minimum eigenmode equals the $m = 1$ mode. The load-shortening relations for longitudinal and transverse strains are equal, however plotted for longitudinal strains in Figure 22.

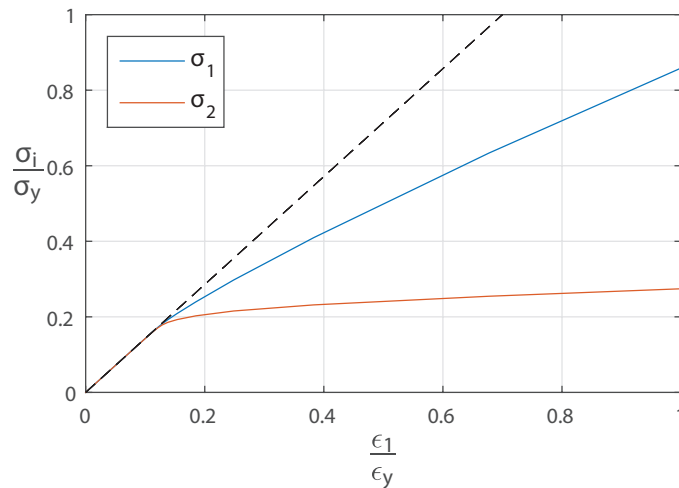


Figure 22: Load-shortening relation $d = 45^\circ$

The plate buckles at less than 20% of the yield strain. The stiffness against longitudinal shortening experiences a knock-down of almost 50%, while the coupled effect is barely present in the post-buckling range. Both curves form straight lines in the advanced strain range, which indicates that the $m = 1$ mode is maintained during deflection. Contributions from higher-degree modes are however seen in the deflection plot, recognized by a flattened buckle along the mid-plate followed by two initiated peaks towards the short-ends. The deflection mode is illustrated in Figure 36 in Chapter 6.

5.3.5 $d = 90^\circ$

For pure transverse edge-shortening ($\epsilon_1 = 0$) Figure 18 dictates that the higher-degree buckling modes are located at stress levels well above the eigenmode $m = 1$, hence the buckling response should be stable. The longitudinal stress starts off-loading as soon as the plate buckles, resulting in tension along the plate short-edges at higher strains.

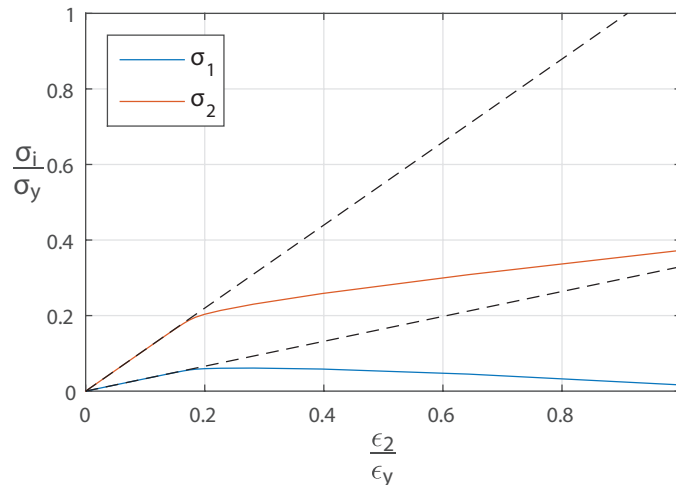


Figure 23: Load-shortening relation $d = 90^\circ$

The process of elastic buckling involves a drastic reduction of the transverse stiffness, in the order of 80%. The coupled stiffness approaches a negative level of -20% of the linear value. The deflection mode displays a flattened buckle along the mid-plate, depicted in Figure 35 in Chapter 6.

5.3.6 $d = 112^\circ$

The displacement history corresponding to 112° is characterized by compression in the transverse direction and longitudinal tensile stresses. Since transverse strain is dominating, this condition also displays the $m = 1$ as minimum eigenmode. The corresponding biaxial stress-path (Figure 18) illustrates a continuous increase of transverse compression accompanied by a minor increase of longitudinal tension in pace with increased strains. A clear bend is seen as the curve passes the elastic buckling limit, whereupon longitudinal tension starts building up more rapidly while the slope of transverse stresses is reduced. As the stress-path bends off to form an almost parallel slope with the $m = 2$ mode, the risk of mode-snapping at larger strains is minor.

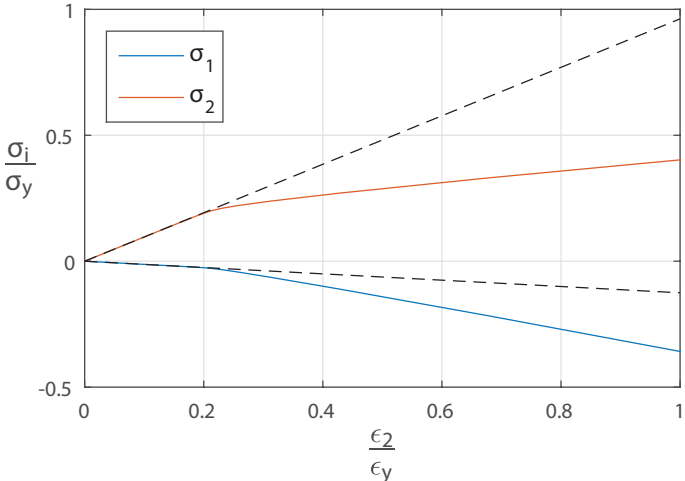


Figure 24: Load-shortening relation $d = 112.5^\circ$

A reduction in the order of 75% is seen for the stiffness against transverse shortening. It is observed that the longitudinal tension does not contribute noteworthy to the buckling strength nor the post-buckling stiffness, compared to the 90° condition. This is in contrast to the $d = -22.5^\circ$ condition where the transverse tension was seen to significantly strengthen the plate. The failure mode reveals the same flattened deflection pattern as seen for the previous strain history.

5.4 Effect of plate aspect ratio

Four plates with aspect ratios in the range $\alpha = 1, 2, 3, 4$, corresponding to models A1, A2, A3 and A4 are studied, each with plate width $b = 1000\text{mm}$ and thickness $t = 17\text{mm}$. Boundary conditions, material properties and the meshing approach are equally defined as in preceding analyses. The imperfection level is minor ($w_0 = 0.17\text{mm}$) and the minimum eigenmode is used as imperfection shape. Each model is studied under pure longitudinal ($d = 0^\circ$) and transverse ($d = 90^\circ$) displacement in addition to an equally weighed biaxial shortening condition ($d = 45^\circ$).

Stress-paths for all displacement histories are given for each model in Figure 25 to 28, supplemented by the eigenvalue boundaries corresponding to the minimum eigenmodes (black lines). The blue, yellow, and red curve corresponds to $d = 0^\circ, 45^\circ$ and 90° respectively. The eigenvalue boundaries effectively show how stress redistribution is initiated when the elastic buckling limit is reached.

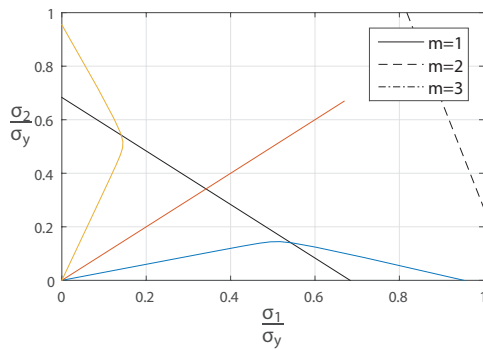


Figure 25: Biaxial stress-path, model A1

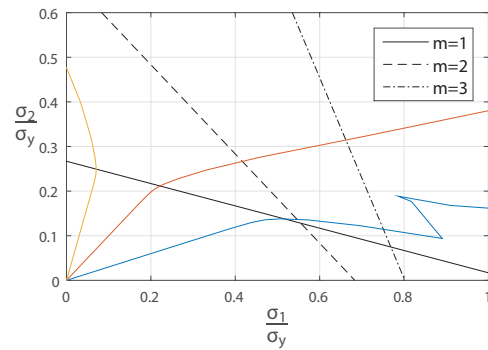


Figure 26: Biaxial stress-path, model A2

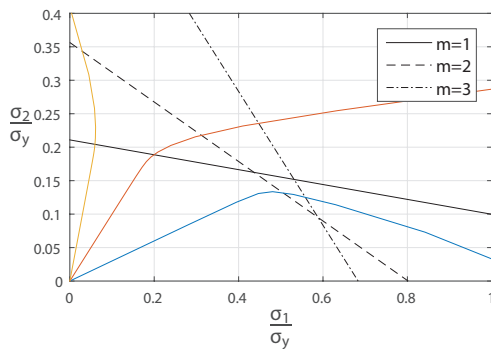


Figure 27: Biaxial stress-path, model A3

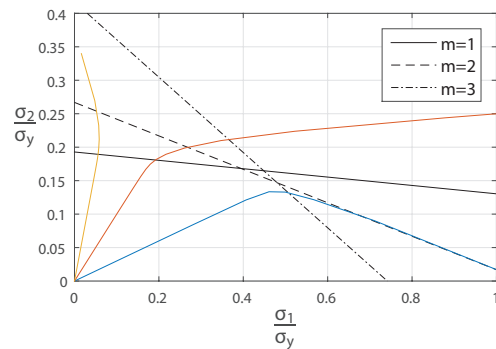


Figure 28: Biaxial stress-path, model A4

It is clear that the dominance of the $m = 1$ eigenmode is more pronounced for plates with aspect ratios below 2. For the square plate (Figure 25) the higher-degree eigenmodes are located far into the post-buckling region and are barely visual in the current plot. For this geometry the 45° strain history does not involve any stress redistribution, quite naturally since the load and deflection pattern are symmetric. Model A2 clearly exhibits mode-snapping effects for pure longitudinal shortening due to the cluster of eigenvalues near the buckling limit. The plate snaps directly from the $m = 1$ mode into the $m = 3$ mode for then to take on a mirrored $m = 1$ mode, a so-called snap-through effect.

At pure longitudinal edge-shortening the process of stress redistribution is observed to be almost identical for all models if disregarding the snapping effects in A2. When the plate buckles the transverse stress (σ_2) is relieved while the longitudinal stress (σ_1) increases at approximately the same rate as before buckling. Far into the post-buckling region the curves cross the x-axis, which indicates tensile stresses along the plate long-edges. For the biaxial load-case the higher aspect ratios are seen to involve a higher degree of load-shedding towards the plate short-edges than the shorter plates, accompanied by a more sudden relief of transverse stresses. For pure transverse shortening the stress redistribution and the transverse stress level at which the longitudinal stress is completely relieved is seen to be highly affected by the plate aspect ratio.

Considering the condition of pure transverse compression, Figure 29 and 30 depicts the load-dependent reduction of the stiffness coefficients C_{22} and C_{12} . The coefficients are made dimensionless by the linear elastic values.

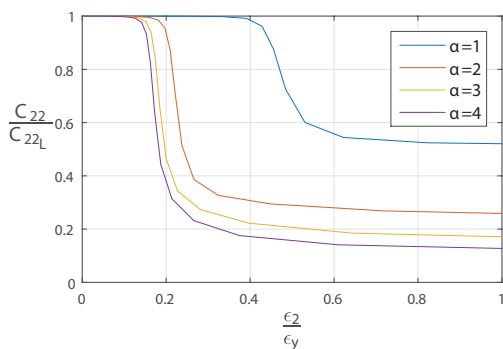


Figure 29: Reduction of coefficient C_{22}

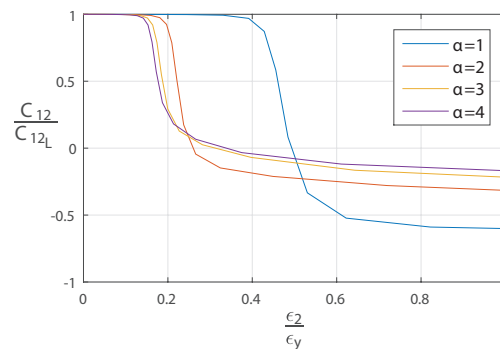


Figure 30: Reduction of coefficient C_{12}

Figure 29 efficiently shows the lower buckling strength against transverse compression displayed by longer plates. A more dramatic load-dependent loss of stiffness is also seen for higher aspect ratios, which approaches less than 20% of the linear elastic value in the ad-

vanced post-buckling range. All coefficients are positive for higher strains, indicating a positive post-buckling stiffness.

The variation of the coupled coefficient C_{12} in Figure 30 demonstrates a more dramatic reduction for the square plate than the longer plates. This indicates a more sudden relief of longitudinal stresses, also dictated by the corresponding stress-path in Figure 25. In the post-buckling range all plates display a negative coupled stiffness, and more so for the square plate.

Discussion Considering typical configurations of stiffened panels in marine structures, individual plates are often relatively long. The loss of stiffness has been observed to reach the order of 80% of the linear value for high aspect ratios. Thus, conventional linear design procedures predict membrane stresses way in excess of the actual level if the elastic buckling limit is exceeded. The buckling behaviour is recognized by a considerable load-shedding which undoubtedly must be accounted for if allowed in design.

The coupled effect between longitudinal and transverse displacement is of special interest as it even changes sign during the response history. The physical meaning of a negative coupled stiffness is more thoroughly discussed in Chapter 6.3.

6 Unstiffened Rectangular Plates with Initial Imperfections

Up until now a minor imperfection level of 1% of the plate thickness have been adopted. In reality, initial imperfections may reach amplitudes even in excess of the plate thickness and significantly alter the initial stiffness of the structure. In this chapter a study of the effect of imperfection amplitude is conducted, with the eventual aim to validate the closed-form solution for initial stiffness derived in Chapter 4.2. Since the latter is derived based on an assumed imperfection mode equal to the $m = n = 1$ eigenmode, only this shape is adopted as imperfection geometry. The effects of various imperfection modes are studied for the multi-bayed model introduced in Chapter 7.

6.1 Model description

Model A3 from the previous study is examined, only the thickness is reduced to $t = 12.5\text{mm}$ in order to accentuate the non-linear response. The material model and boundary conditions are defined as in preceding analyses. The imperfection level is varied from slight to severe by adopting Faulkner's imperfection model, introducing the imperfection scale factor $x = [0.025, 0.05, 0.1, 0.3]$. For the given geometry this corresponds to imperfection amplitudes of approximately $w_0 = 3\text{mm}, 6\text{mm}, 12\text{mm}$ and 37mm respectively.

6.2 Results

Due to the applied imperfection mode the plates are highly prone to mode-snapping under longitudinal compression. The corresponding load-shortening curves are thereby highly irregular and do not provide any useful information other than the initial stiffness. The below considerations of the edge-shortening relation only include transverse edge-shortening to demonstrate the initial knock-down, while the longitudinal coefficient is included in Figure 33. The load-shortening curve in Figure 31 dictate the load-dependent stiffness reduction for each imperfection level while Figure 32 represent the coupled stiffness. The initial stiffness is seen to be highly affected by the imperfection amplitude, while the post-buckling stiffness is equal for all models. It is observed that the greatest imperfection amplitude ($x = 0.3$) results in an initial stiffness equal to that of the buckled plates. This condition applies more to

a damaged condition than a typical fabrication level imperfection.

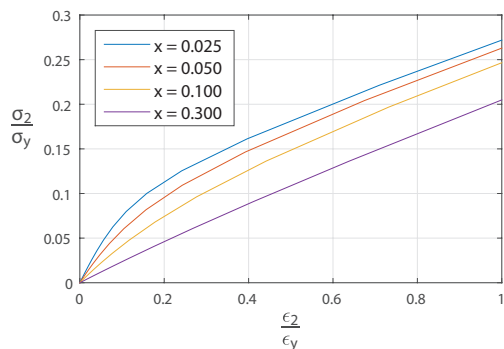


Figure 31: Transverse load-shortening relation, model A3

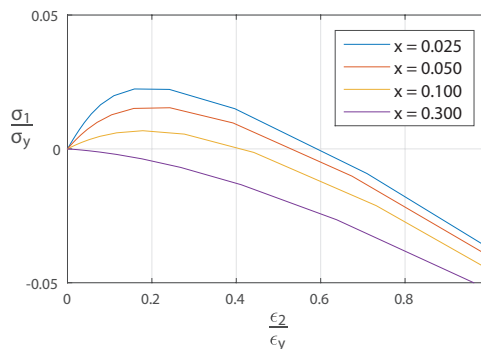


Figure 32: Coupled stiffness model A3

The knock-down of initial stiffness is also dictated by Figure 33, here as function of the Faulkner imperfection scale factor x . The coefficients are made dimensionless by the linear elastic values. It is clear that the longitudinal stiffness is hardly effected by the imperfection amplitude compared to the other two coefficients. Even for the damaged condition the longitudinal coefficient holds about 90% of the linear elastic value. This amplitude is seen to entail a negative coupled stiffness from the very onset of compression due to the large out-of-plane distortion.

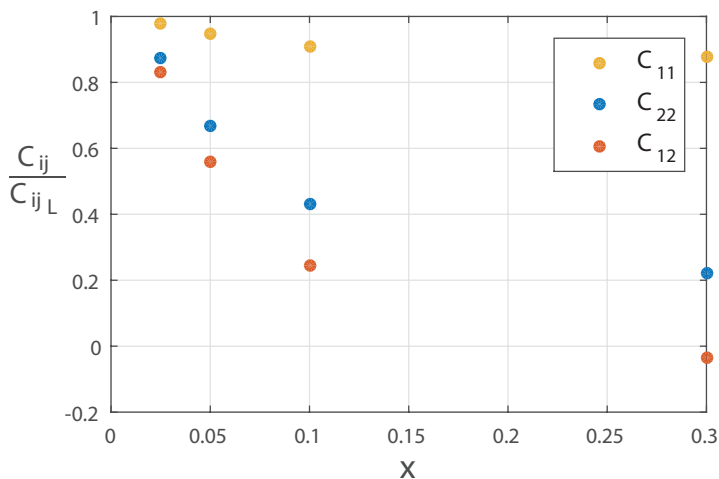


Figure 33: Knock-down of initial stiffness

The contours corresponding to out-of-plane distortion is given for the first analysis increment at transverse compression for each imperfection amplitude in Figure 34 to 36. For the minor imperfections the initial deflection is seen to take on the same shape as the initiated imperfection mode. The average imperfection ($x = 0.1$) is altered at the onset of compression

in terms of a flattened buckle in the mid-region. The highest amplitude immediately forces the plate into an advanced mode in the form of two initiated peaks towards the short-ends. These altered deflection modes are, in addition to the initial membrane stretching, the reason for the large loss of initial stiffness and are highly relevant in context of the subsequent validation of the closed-form solution.

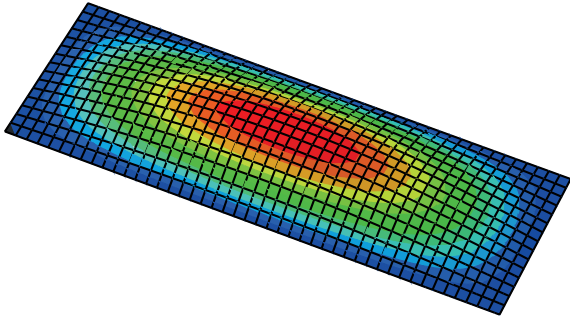


Figure 34: Deflection mode $x = 0.025/0.5$

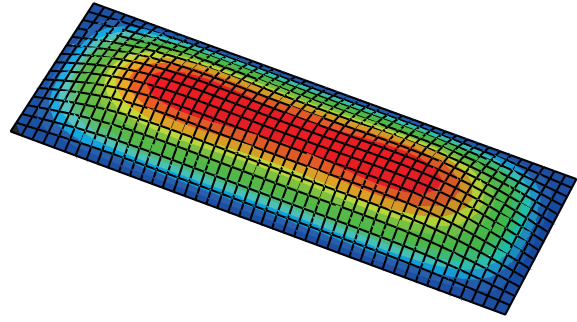


Figure 35: Deflection mode $x = 0.1$

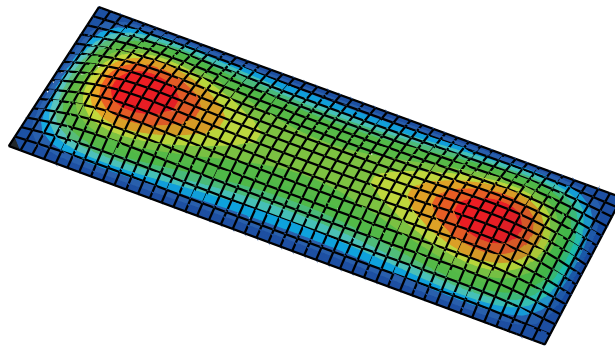


Figure 36: Deflection mode $x = 0.3$

6.3 Discussion of negative Poisson effect

The Poisson ratio for an isotropic, homogeneous material is defined as $-\frac{\epsilon_2}{\epsilon_1}$, normally taken as 0.3 for steel. This means that for a plate that is not restrained from in-plane translation, a shortening in the longitudinal direction will result in a lengthening (or negative strains) in the transverse direction, corresponding to a factor of 0.3. Similarly, if the unloaded edge is restrained from in-plane translation, a shortening in the orthogonal direction will result in compression along the unloaded edges. The coupled stiffness coefficient $C_{12}(=C_{21})$ may be regarded as an analogy to the Poisson effect as it relates transverse edge-shortening to axial stresses (and the other way around for C_{21}).

The physical understanding of a negative Poisson effect would suggest that a uni-axial

shortening results in a shortening in the orthogonal direction as well, or tension along the unloaded constrained edges. Such materials do exist in their initial form but for steel this phenomenon occurs due to membrane stretching at large out-of-plane distortions. When the deflection becomes large enough, the constrained edge wants to pull in to the centre of the plate which results in an unloading along the boundary, as depicted in Figure 37.

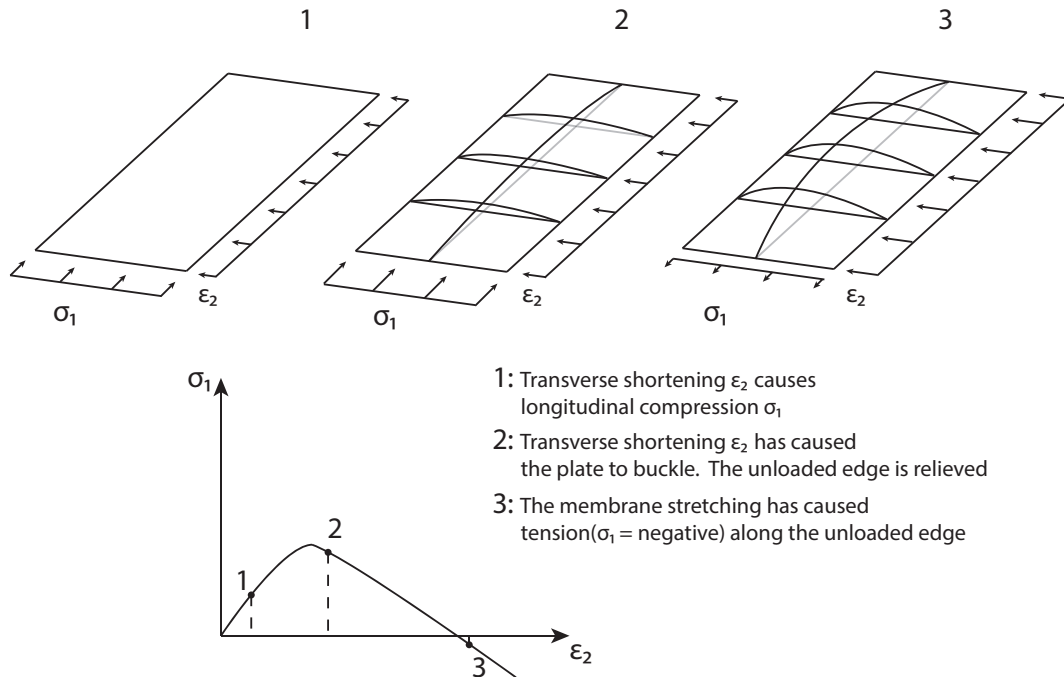


Figure 37: Poisson effect caused by membrane stretching

In the case of large initial imperfections and especially for lower aspect ratios the coupled stiffness may be found to be negative from the very onset of loads. This follows from the membrane stretching that has already taken place prior to loading. Assuming that the deflection pattern is constant and equal to the initial imperfection, one may look at it as though the initial imperfection has shifted the initial state from zero load to a point later in the displacement history, corresponding to stage 3 in Figure 37.

6.4 Validation of closed-form solution

The analytical solution for initial stiffness derived in Chapter 4.2 is a function of the plate aspect ratio, the plate slenderness and the imperfection level. To obtain a sound basis of comparison with numerical results, four models with aspect ratio $\alpha = 1, 2, 3, 4$, corresponding to model A1, A2, A3 and A4 are studied, each with plate thickness $t = 12.5mm$ and width $b = 1000mm$. Boundary conditions and material properties are defined as in preceding analyses. The $m = 1$ mode is applied as imperfection geometry, ranging from the minor to the major Faulkner imperfection amplitude. Thickness iterations are performed with model A4.

6.4.1 Extraction of initial stiffness coefficients

Prior to comparison of numerical and analytical results a study on how to most accurately retrieve the initial stiffness from the Abaqus analyses had to be carried out. Two almost identical analyses was performed for each imperfection level, the only difference being that one had linear geometry and the other had non-linear geometry. The initial stiffness was found by linear regression of the first increments of the non-linear analysis. Ideally, the initial stiffness in a non-linear analysis should coincide with the stiffness in an identical system with linear geometry, assuming the same imperfection level is applied. However, due to the highly non-linear nature of the response, considerable stiffness reduction occurred during the very first analysis increments. Good correlation between the linear and non-linear model was found for an initial increment size of 0.001, which corresponded to one thousandth of the yield strain, given the prescribed displacement. The initial coefficients using linear and non-linear geometry are compared in Table 2 to Table 5.

Scale factor x	0.025	0.05	0.1	0.3
Linear geometry	2.2183	2.1453	2.0607	1.9874
Non-linear geometry	2.2179	2.1449	2.0605	1.9872

Table 2: Comparison of C_{11} [$\times 10^5 MPa$]

Scale factor x	0.025	0.05	0.1	0.3
Linear geometry	0.5646	0.3808	0.1674	-0.2286
Non-linear geometry	0.5637	0.3798	0.1668	-0.0231

Table 3: Comparison of C_{21} [$\times 10^5 MPa$]

Scale factor x	0.025	0.05	0.1	0.3
Linear geometry	0.5646	0.3809	0.1674	-0.2256
Non-linear geometry	0.5579	0.3732	0.1640	-0.0234

Table 4: Comparison of C_{12} [$\times 10^5 MPa$]

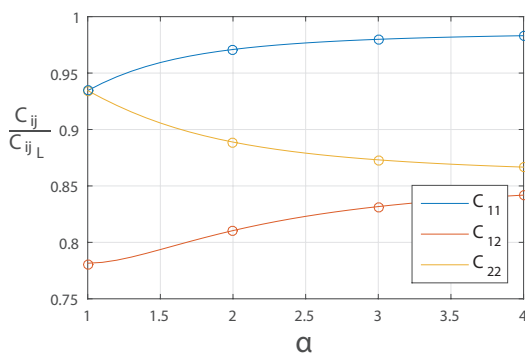
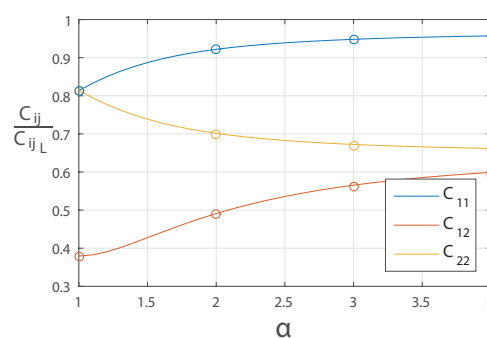
Scale factor x	0.025	0.05	0.1	0.3
Linear geometry	1.9754	1.5129	0.9758	0.4994
Non-linear geometry	1.9585	1.4938	0.9679	0.4985

Table 5: Comparison of C_{22} [$\times 10^5 MPa$]

The deviations between the two models are minor. Slightly higher values are provided using linear geometry. When only interested in the exact values for the initial stiffness coefficients, the linear analysis is considered more accurate.

6.4.2 Initial stiffness vs. plate aspect ratio

In Figure 38 to Figure 41 the initial stiffness coefficients obtained in Abaqus are compared with the closed-form solution(CF) as function of the plate aspect ratio for each imperfection level. The plate thickness is constant equal to $t = 12.5mm$. The continuous lines correspond to the analytical formulas, while the scatter applies to the Abaqus measurements. High agreement is seen for small imperfection levels (Figure 38 and 39) while the numerical results for C_{22} and C_{12} are on the lower side for the more prominent imperfection amplitudes (Figure 40 and 41). The deviations are greater for large aspect ratios.

Figure 38: CF vs. Abaqus, $w_0 = 3mm$, $t = 12.5mm$ Figure 39: CF vs. Abaqus, $w_0 = 6mm$, $t = 12.5mm$

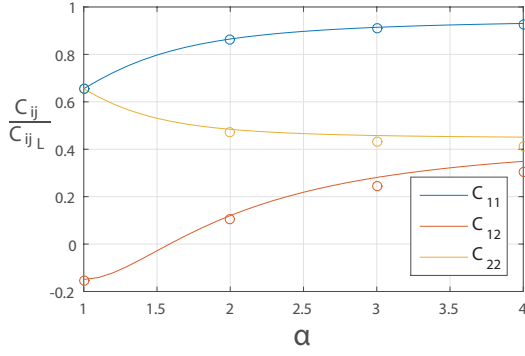


Figure 40: CF vs. Abaqus, $w_0 = 12\text{mm}$, $t = 12.5\text{mm}$

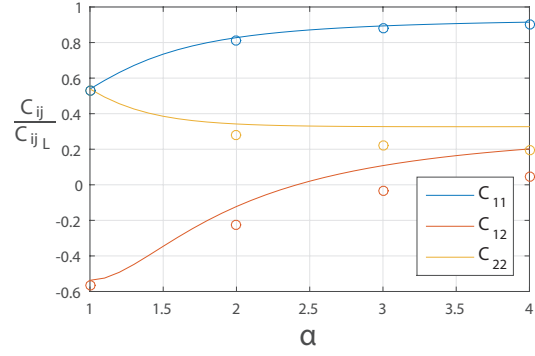


Figure 41: CF vs. Abaqus, $w_0 = 37\text{mm}$, $t = 12.5\text{mm}$

The deviations for large imperfections and longer plates may be explained by the immediate deflection modes for the various imperfection amplitudes given by Figure 34 to 36. The greater initial amplitudes alter the initial deflection mode in terms of a flattened buckle, followed by two initiated peaks towards the plate short-ends. This behaviour entails a stiffness reduction that is not reflected by the analytical solution, which presumes a constant deflection in the $m = 1$ mode. Hence, the analytical formulation fails to reproduce the actual initial stiffness for plates with high aspect ratios and considerable imperfection levels ($w_0 > t_{plate}$). The longitudinal stiffness is observed to be almost unaffected by the altered deflection mode as the numerical results coincide with the analytical prediction of C_{11} for all imperfection amplitudes and aspect ratios.

6.4.3 Initial stiffness vs. plate slenderness

In Figure 42 to Figure 45 the initial stiffness coefficients obtained in Abaqus are compared with the closed-form solution as function of the plate slenderness ($\frac{s}{t}$) for each imperfection level. The numerical results are retrieved from model A4, hence the aspect ratio is constant equal to $\alpha = 4$. The continuous lines correspond to the analytical formulas, while the scatter applies to the Abaqus measurements.

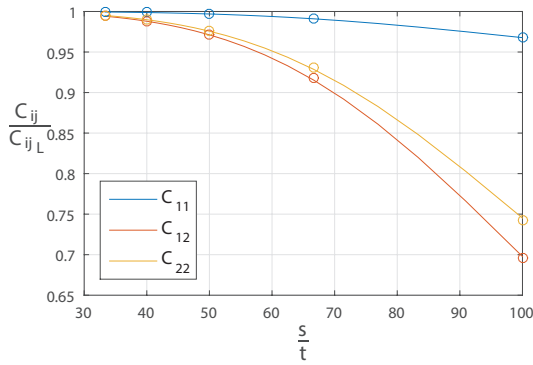


Figure 42: CF vs. Abaqus, $w_0 = 3\text{mm}$, $\alpha = 4$

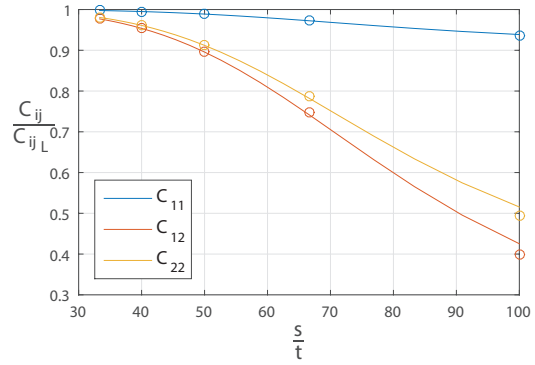


Figure 43: CF vs. Abaqus, $w_0 = 6\text{mm}$, $\alpha = 4$

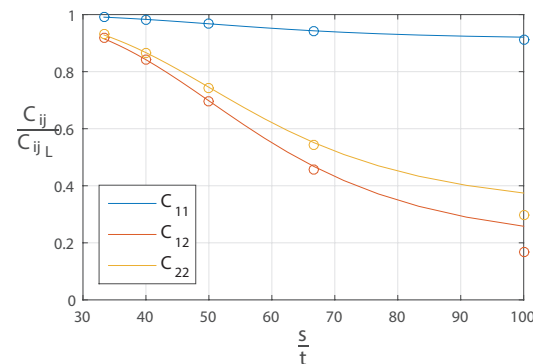


Figure 44: CF vs. Abaqus, $w_0 = 12\text{mm}$, $\alpha = 4$

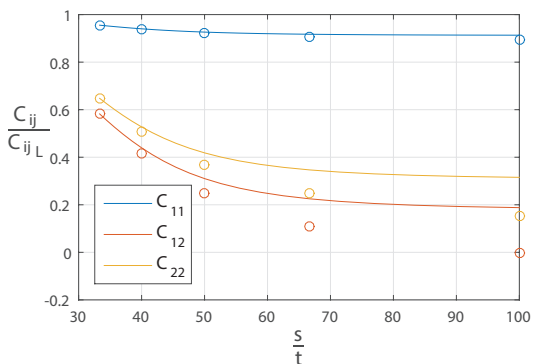


Figure 45: CF vs. Abaqus, $w_0 = 37\text{mm}$, $\alpha = 4$

Also here the analytical and numerical solution coincide well for small imperfections levels, while deviations grow larger at more prominent amplitudes. The differences are greater for the slender plate models. As understood from the previous comparison this is due to the immediate deviation from the applied imperfection mode. The stockier plates possess adequate stiffness to withhold the pure $m = n = 1$ mode at the onset of edge-shortening, while the slender plates immediately take on an altered deflection.

Discussion Based on the above considerations the closed-form formulations for initial stiffness of imperfect plates are considered verified for small to moderate imperfections levels ($w_0 < t_{plate}$). In the case of larger imperfections ($w_0 > t_{plate}$), the solution is more accurate for plates with low aspect ratios ($\alpha < 3$) and moderate slenderness ($\frac{s}{t} < 60$) due to adequate strength to maintain the initial imperfection mode at the onset of compression.

From a design perspective, one would rather overestimate the membrane stresses in the plating than the redistribution to supporting structure. The analytical predictions being

higher (stiffer) than the numerical results is thus on the "safe side" with respect to a potential practical application.

7 Multi-bayed Panel with Initial Imperfections

Adopting the eigenmode (hereafter also referred to as EM) as imperfection geometry in a buckling problem is considered a conservative approach as it generally reduces the stiffness and ultimate strength of the system. However, this method fails to capture some of the effects introduced by more realistic imperfection geometries. The purpose of the present study is to examine the effect of the imperfect geometry on the initial plate membrane stiffness and the emergence of resulting deflection modes. A number of studies within this field have already been conducted by DNV GL (Slettum (2014a), Slettum (2014b)), however here with focus on the ultimate capacity. The analyses performed in the present chapter are perfectly linear elastic but the mentioned reports are used as support.

7.1 Model description

A multi-bayed model similar to the typical configuration of stiffened panels in marine structures is introduced. The panel is assumed to be located between two heavier longitudinal girders or stringers. It spans over three transverse frames and five longitudinal stiffeners with half a stiffener length in the fore and aft end. The stiffener spacing is 850mm , the frame spacing 3000mm and the plate thickness 12mm . The main dimensions are visualized in Figure 46. The stiffeners are not physically modelled, hence the stiffener dimensions are not given (see Boundary Conditions). The material model is isotropic linear elastic with Young's modulus $E = 206000\text{MPa}$ and Poisson ratio $\nu = 0.3$.

7.1.1 Boundary conditions

Since focus is on local elastic buckling and initial stiffness, stiffeners and frames are modelled as constraints against vertical translation rather than physically present. This implies that the rotational stiffness imposed by stiffeners and potential interaction effects with global buckling modes are not considered. The former is addressed in Chapter 9 while the latter is generally prevented by applying adequately heavy stiffeners. Since global deflection is neglected, the extent of the model does not need to envelope more than one frame-span. However, for a better visual comparison with the later stiffened panel, all three spans are included.

Due to the assumed presence of heavier longitudinal girders along the right and left

boundary, these edges are clamped and restrained from vertical translation. The aft and fore boundary are located midway between two transverse frames, hence symmetry conditions are applied. The loaded edges (aft and right boundary) are constrained to remain straight during deflection. All boundary conditions are given in Table 6, supplemented by Figure 46. The notations 1, 2 and 3 correspond to the principal directions in xyz-space. U denotes translation, while UR denotes rotation.






Boundary	Suppressed DOF's	Constraint	Colour Code
Aft	UR_2, UR_3	Constrained to remain straight	
Fore	U_1, UR_2, UR_3	-	
Right	U_3, UR_1, UR_2, UR_3	Constrained to remain straight	
Left	$U_2, U_3, UR_1, UR_2, UR_3$	-	
Stiffeners and frames	U_3	-	

Table 6: Boundary conditions, multi-bayed model

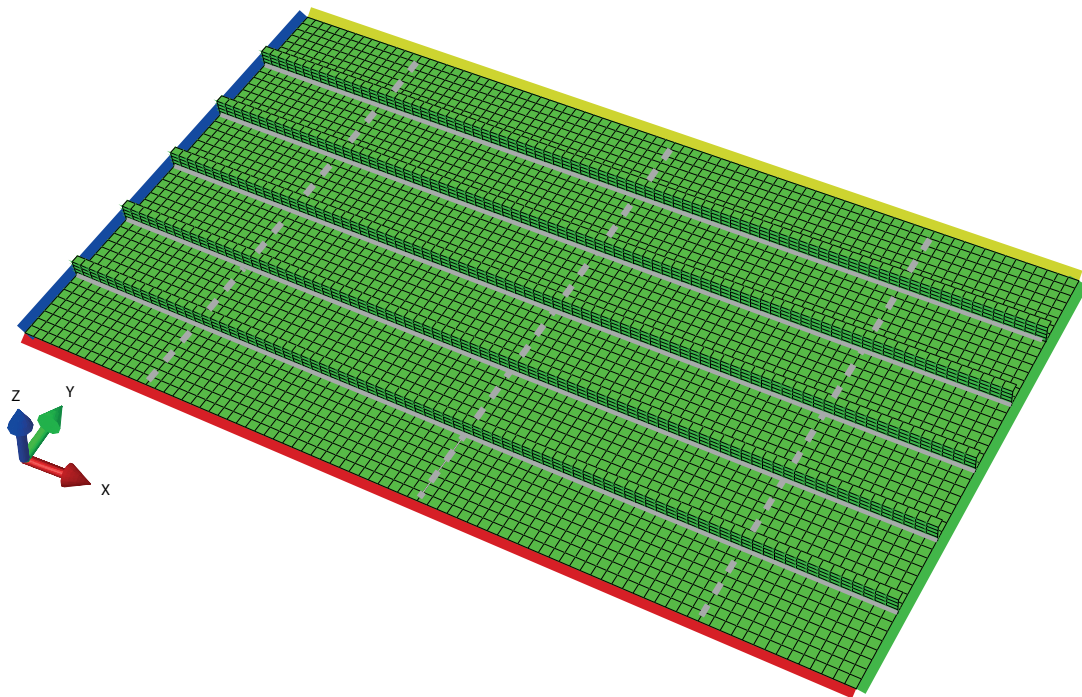


Figure 46: Multi-bayed model

Displacements are applied along the aft and right boundary. The above boundary conditions apply to both longitudinal and transverse compression. An additional constraint against in-plane translation is applied to the right and aft edge for the pure longitudinal and pure transverse condition, respectively. This is in order to get a measure of the uniaxial stiffness without contributions from the coupled effects.

7.1.2 Mesh

In previous analyses, 15 elements have been used across the plate width. Since these models are very simple, the refinement of the mesh does not noticeably influence the computational efficiency. When introducing larger models this becomes more of a concern. Even though the multi-bayed model is not very complex, a brief study is performed adopting 15 and 8 elements across the plate width.

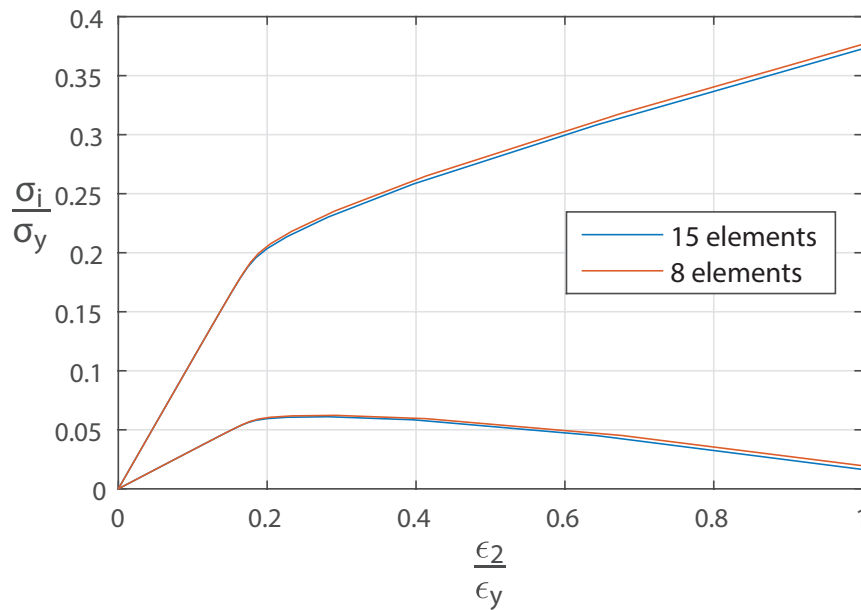


Figure 47: Load-shortening relation, 15 elem. vs. 8 elem.

As depicted in the load-shortening curve for transverse (upper) and longitudinal (lower) stresses in Figure 47 there is no deviation in initial stiffness while the post-buckling curves barely are distinguishable. Hence, 8 elements between longitudinal stiffeners is used in subsequent analyses. The element type is the square four-node element with reduced integration (S4R).

7.2 Initial imperfections

The imperfection pattern is varied from a complete eigenmode to a pure "Hungry-Horse"-shape by the relative weight fractions 0.01/0.99, 0.2/0.8 and 0.4/0.6. The geometries are applied using a script provided by DNV GL (Appendix B) which requires a contribution from both the eigenmode and the "Hungry-Horse" in each imperfection geometry. Hence, the modes corresponding to a pure eigenmode or HH-geometry have a 1% contribution from

the other mode. Initial imperfections are only applied to the plating. The imperfection amplitude is scaled according to Faulkner's imperfection model, corresponding to initial amplitudes of $w_0 = 2mm, 5mm, 9mm$ and $28mm$ approximately. Table 7 and 8 show the resulting imperfection modes corresponding to pure longitudinal and pure transverse displacement respectively. The out-of-plane geometry is amplified by a factor of 100.

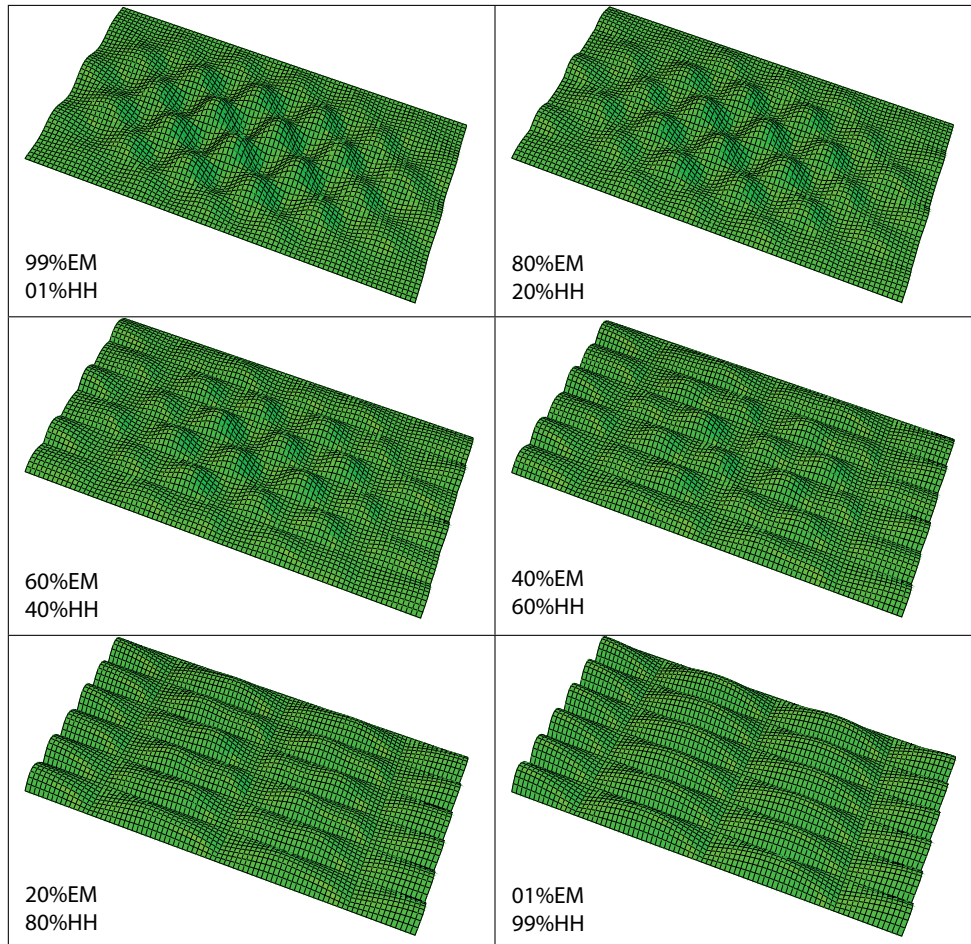


Table 7: Weighed imperfection modes, longitudinal shortening, scale = 100

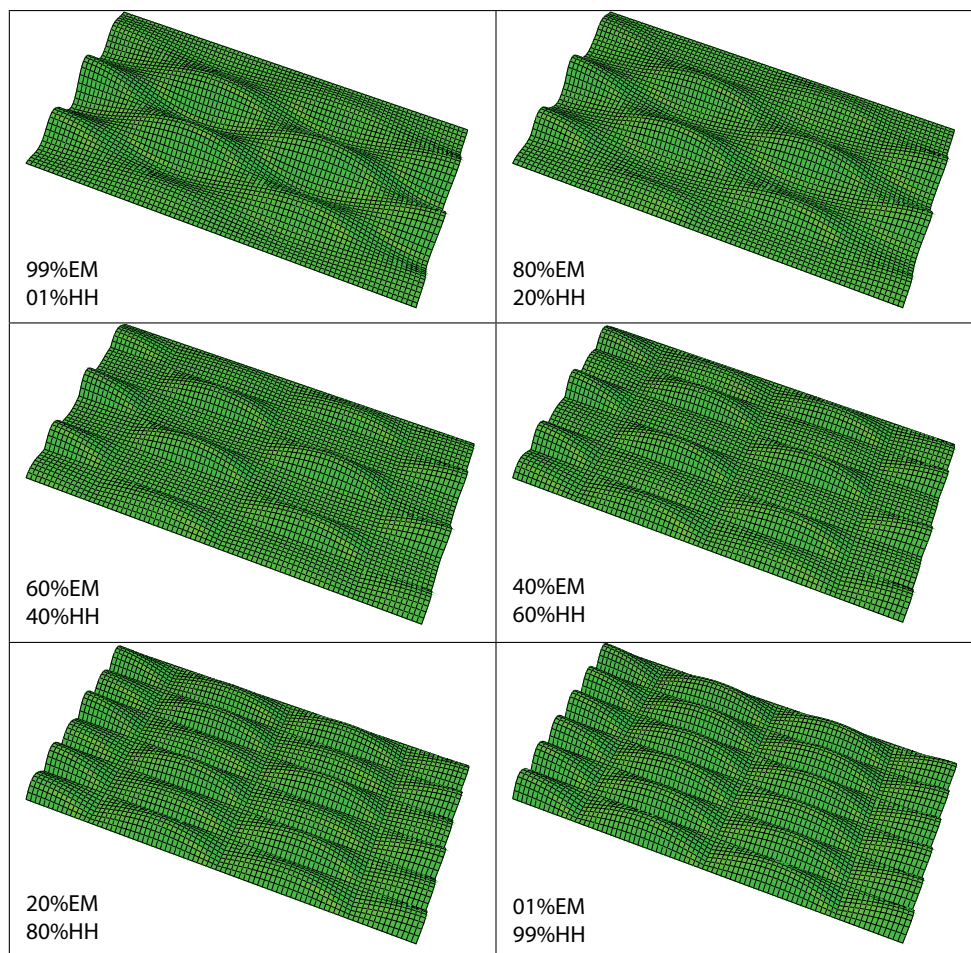


Table 8: Weighed imperfection modes, transverse shortening, scale = 100

7.3 Results

Transverse and longitudinal stresses are taken as the averaged membrane stresses along the left and fore boundary respectively. Strains are taken as overall engineering strain $\epsilon_1 = \frac{\delta u_1}{l}$ and $\epsilon_2 = \frac{\delta u_2}{b}$. The load-shortening relation could also be presented for a single frame-span rather than for the whole model. It was however easier to retrieve the results in the given manner and the stiffness properties would be equal due to the vertical constraints along stiffeners and frames. The results are normalized with respect to an assumed yield strength of $\sigma_y = 315$ and the yield strain $\epsilon_y = \frac{\sigma_y}{E}$. As focus is on initial stiffness and emergence of elastic buckling modes exclusively, no consideration is given to ultimate capacity and local accumulation of stresses. The results are presented up until the yield strain (or below for a better appearance), although this includes states in excess of the ultimate capacity.

7.3.1 Longitudinal compression

Figure 48 to 51 display the load-shortening relation for all imperfection shapes and amplitudes under longitudinal edge-shortening. The dashed line corresponds to the linear elastic stiffness.

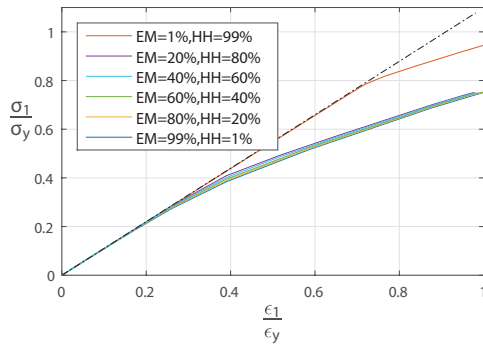


Figure 48: Longitudinal load-shortening relation, $w_0 = 2\text{ mm}$

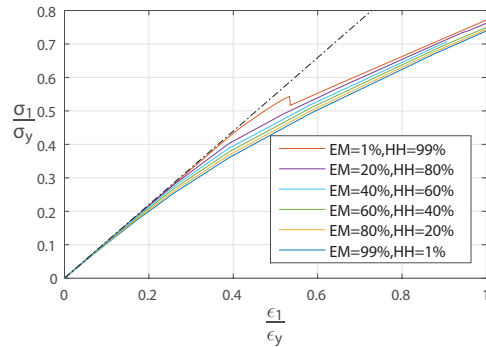


Figure 49: Longitudinal load-shortening relation, $w_0 = 5\text{ mm}$

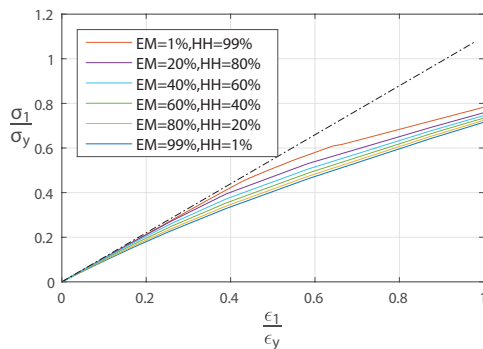


Figure 50: Longitudinal load-shortening relation, $w_0 = 9\text{ mm}$

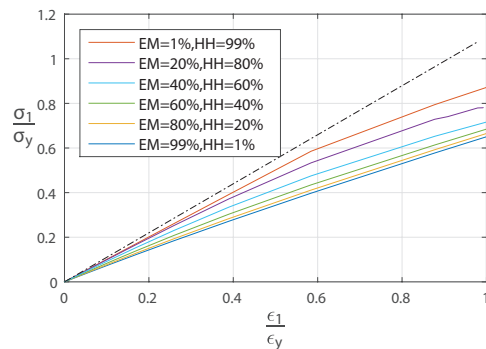


Figure 51: Longitudinal load-shortening relation, $w_0 = 28\text{ mm}$

The "Hungry-Horse" exhibits a greater initial stiffness than the modes with eigenmode contributions, and more so the larger the initial amplitude. For the minor imperfection level, $w = 2\text{ mm}$ displayed in Figure 48, the variations between the imperfection modes are considered negligible. However, the HH-curve is seen to cling to the linear elastic value up to a strain level far in excess of what is seen for the other imperfections. The corresponding deflection mode in Figure 52 relates that the panel has taken on an advanced buckling mode with five half-waves across each plate length due to the high stresses. For this particular case Abaqus had troubles finding a converging solution, hence a number of iterations had to be performed to obtain the load-shortening relation for the whole strain range. Other compositions of increment size, applied shortening and analysis solution method gave a much

earlier deviation from the linear stiffness and a deflection mode similar to the eigenmode. Nonetheless, the presented plot effectively displays the reluctance of letting the eigenmode emerge, which is also observed by the snapping effect in the adjacent figure, Figure 49.

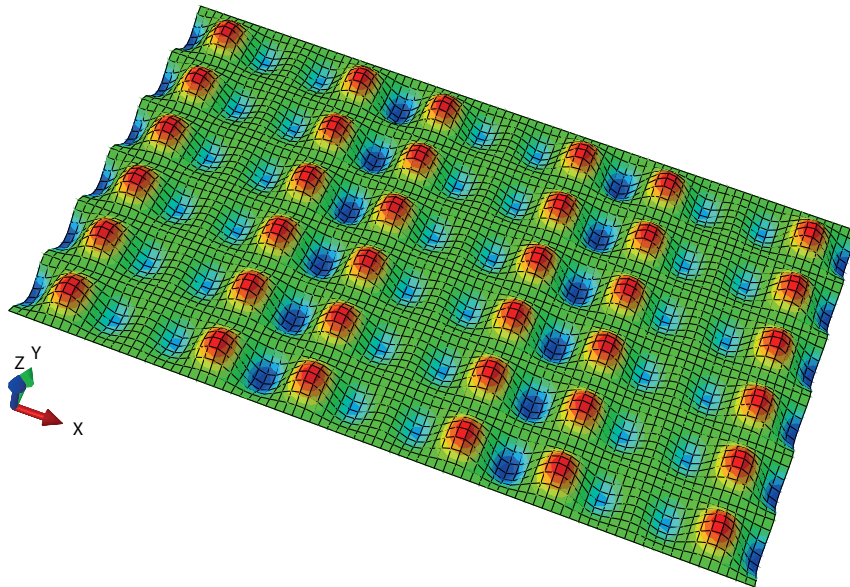


Figure 52: Longitudinal deflection mode, $w_0 = 2\text{mm HH}$, scale=30

The greater imperfection amplitudes exhibit a smooth transition into the longitudinal eigenmode for all initial geometries. The eigenmode imperfection is clearly more affected by the initial amplitude than the "Hungry-Horse". The latter lies fairly close to the linear elastic stiffness even for the major imperfection, or rather damaged condition.

7.3.2 Transverse compression

Figure 53 to 56 display the load-shortening relation for each imperfection mode and amplitude under transverse compression.

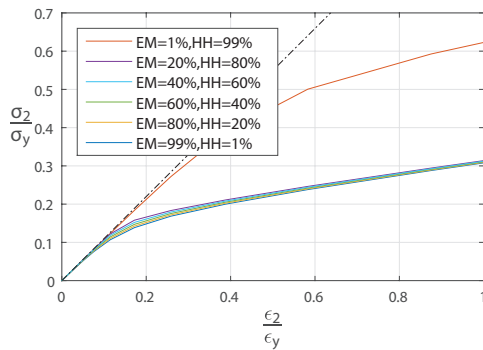


Figure 53: Transverse load-shortening relation, $w_0 = 2\text{ mm}$

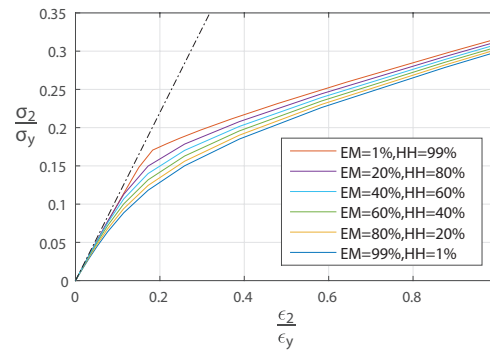


Figure 54: Transverse load-shortening relation, $w_0 = 5\text{ mm}$

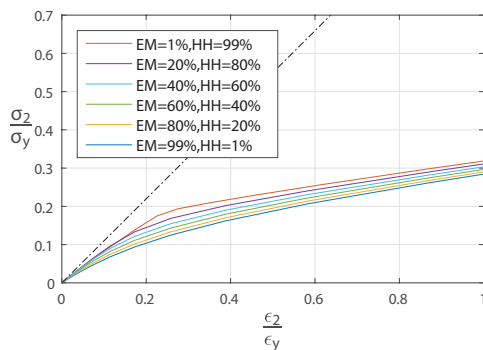


Figure 55: Transverse load-shortening relation, $w_0 = 9\text{ mm}$

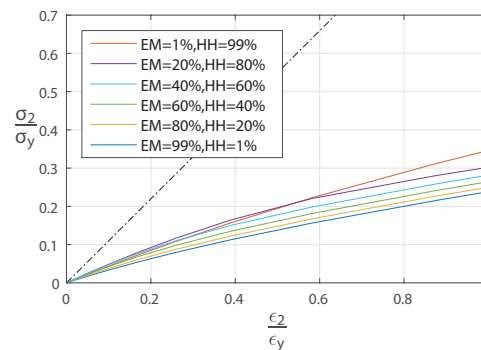


Figure 56: Transverse load-shortening relation, $w_0 = 28\text{ mm}$

The transverse stiffness is seen to be more affected by the amplitude of the initial imperfection than for longitudinal compression. For the minor imperfection level the initial stiffness of the "Hungry-Horse" coincides with the linear elastic value, while the greater amplitudes display a more prominent knock-down for all imperfection geometries. According to Figure 56, the major imperfection amplitude impose a lower initial stiffness for the "Hungry-Horse" geometry than the two closest imperfection modes. The post-buckling stiffness is equal for all imperfections, except for the "Hungry-Horse" for the two utmost imperfection levels. As for longitudinal compression the minor imperfection, $w_0 = 2\text{ mm}$ in Figure 53, displays a far greater elastic buckling strength than the other geometries. The corresponding deflection mode in Figure 57 indicates that the panel maintains the HH-mode during deflection. A

similar trend is seen for the major amplitude, dictated by Figure 56, for which the deflection mode is given in Figure 58.

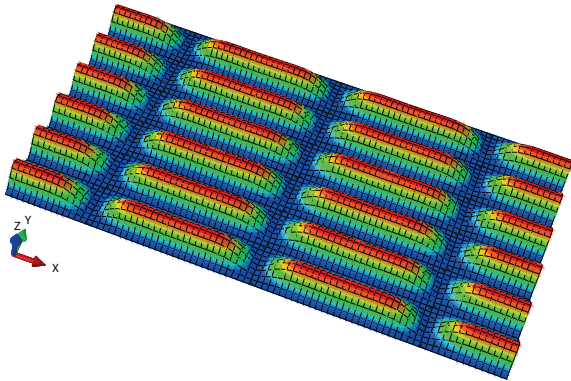


Figure 57: Transverse deflection mode, $w_0 = 2\text{mm HH}$, scale=30

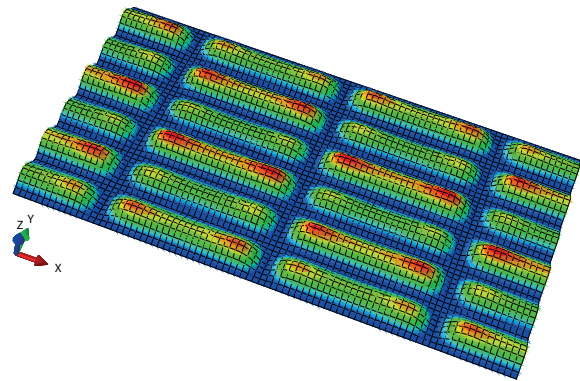


Figure 58: Transverse deflection mode, $w_0 = 28\text{mm HH}$, scale=30

Despite of the similar deflection mode, the minor imperfection exhibits a much greater initial stiffness and buckling resistance than the major imperfection amplitude, or damaged condition. The post-buckling stiffness of the former is more or less equal to the initial stiffness of the latter. Nonetheless, the "Hungry-Horse" buckling mode displays a greater post-buckling stiffness than the eigenmode deflection.

Discussion The overall sensitivity to the imperfection geometry regarding the emergence of deflection modes is considered to be relatively low. The eigenmode emerges without noteworthy counteracting effects for most imperfection geometries. Considering the relatively slender configuration of the plating ($\lambda = 1.46$ assuming $\sigma_y = 315\text{MPa}$), the elastic buckling strength is rather low and the response thereby governed by the minimum eigenmode. A more pronounced effect of the various imperfections on the resulting deflection pattern might be seen for stockier plates, although the initial amplitudes would be lower. The deviating results seen for the major amplitude is considered more relevant in the context of structural damage than from a design perspective. The minor "Hungry-Horse" imperfection displayed stiffness characteristics similar to a perfect plate for both longitudinal and transverse compression. In this case the modelling of the initial imperfection could have been omitted regarding an accurate prediction of the initial stiffness.

8 Multi-bayed Panel Subjected to Lateral Pressure

Stiffened panels in marine structures may, in addition to in-plane loads, be subjected to lateral pressure. Some examples are the external bottom and lower sides of the hull, the double bottom plating and deck panels. One way of coping with the effects of lateral pressure is to treat the load as an additional contribution to the initial imperfection. However, this does not necessary capture the actual distribution of membrane stresses, considering potential tensile stresses imposed by the lateral deflection. In the current chapter, a study on the effect of lateral pressure on the initial and load-dependent membrane stiffness and the emergence of buckling mode is performed. The pure "Hungry-Horse" mode and the eigenmode imperfection from previous analyses are evaluated. The imperfection level is average, corresponding to $w_0 = 9mm$. Stiffeners and frames are still modelled as constraints to capture the impact on the local buckling behaviour. Material properties and boundary conditions are defined as in previous analyses.

8.1 Analysis methodology

The pressure and the in-plane displacements are applied in separate analysis steps. First the lateral pressure is gradually stepped up to the desired level by using the General Static solution method, whereupon the pressure is propagated into the next step where the in-plane displacement is applied, also using General Static. The displacements are applied along the right and aft edge. Analyses are run for four lateral pressures at pure longitudinal and pure transverse compression. Under the action of lateral pressure solely, both the aft and right plate edge are free to move in the plane.

8.2 Results

As focus is on the simultaneous action of pressure and in-plane loads, membrane stresses are retrieved along the fore and left boundary from the second analysis step. Stresses and displacements caused during the action of lateral pressure only are withdrawn to be able to compare the actual in-plane stiffness during in-plane compression.

The applied pressures were first chosen considering a reasonable utilisation with respect to bending stresses and an assumed yield strength of $\sigma_y = 315MPa$. Minor effects were seen for these levels. A larger pressure taken as the maximum load provided by PULS for the given

panel, $P = 0.132\text{MPa}$, and yet another greater pressure were therefore also examined. The two latter loads are not relevant considering regular tolerance levels but are merely applied to capture effects that were not seen for the pressures first chosen. Focus is still on initial stiffness and elastic buckling, hence the proximity to ultimate capacity limits or local yielding are not considered.

8.2.1 Longitudinal compression

The pressure forces the initial longitudinal eigenmode imperfection into a shape resembling a compromise with the "Hungry-Horse", as depicted in Figure 59. The HH-imperfection is affected in terms of an increased initial amplitude.

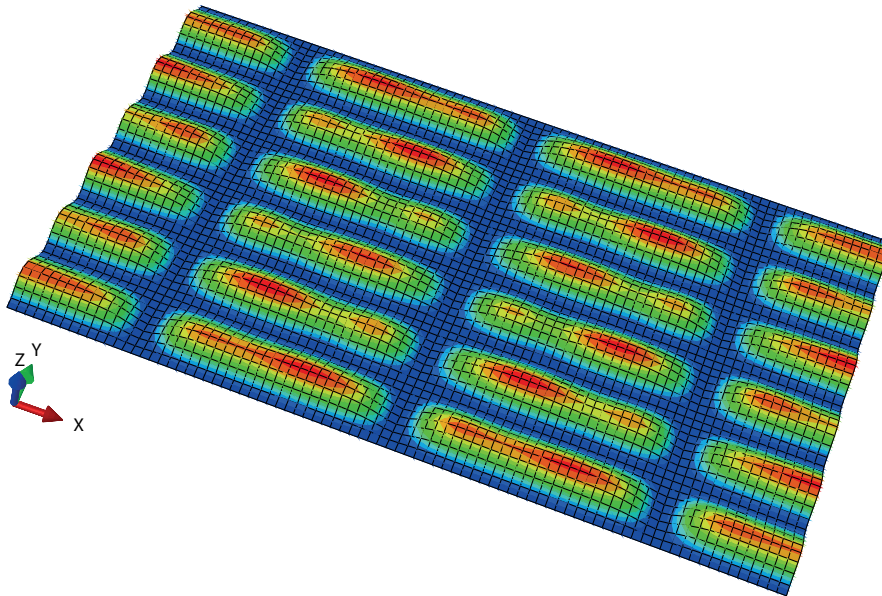


Figure 59: Deflection mode, $P = 0.2\text{MPa}$, $w_0 = 9\text{mm EM}$, scale=30

Despite the above, the eigenmode emerges without noteworthy resistance for all pressure levels, dictated by the load-shortening curves in Figure 60. The buckling behaviour is thereof nearly equal and the curves more or less coincide. The barely distinguishable dashed line corresponds to the pure longitudinal shortening condition considered earlier. The lateral pressure is seen to add on to the stiffness, although the deviations are negligible.

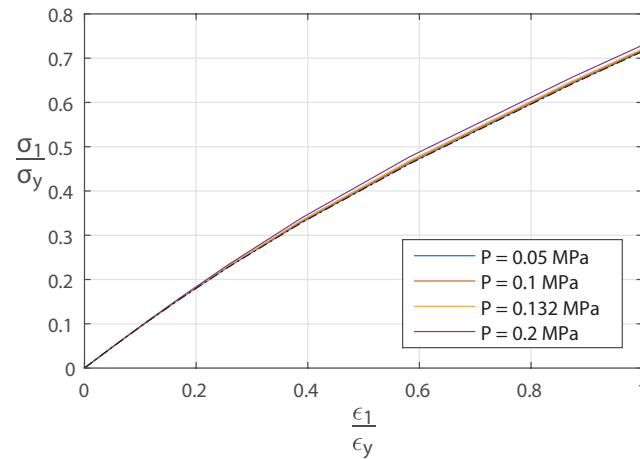


Figure 60: Longitudinal load-shortening relation, $w_0 = 9\text{ mm EM}$

More distinct deviations are observed for the "Hungry- Horse", for which the load-shortening relation is given in Figure 61. While the non-pressure condition has a slightly larger initial stiffness (dashed line), the pressure adds on to the load-dependent stiffness, resulting in a distinguishable increase of the elastic buckling limit. All conditions finally take on the longitudinal eigenmode, except the largest pressure condition, for which the response is close to linear for the whole response range. The corresponding deflection mode is given in Figure 62, which displays an overall HH-mode with some initiated contributions from the longitudinal eigenmode.

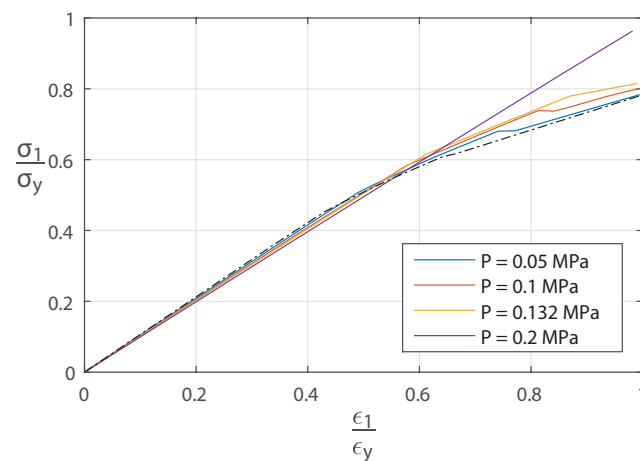


Figure 61: Longitudinal load-shortening relation, $w_0 = 9\text{ mm HH}$

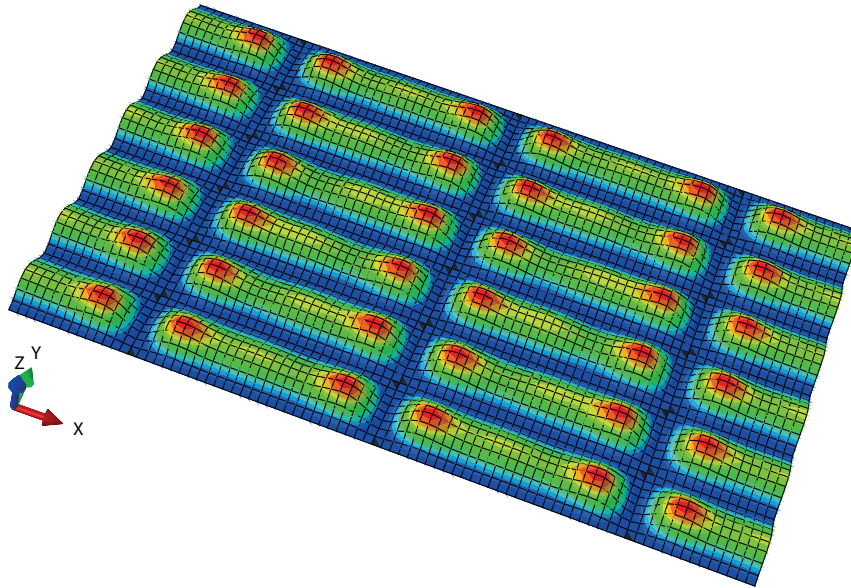


Figure 62: Longitudinal deflection mode, $P = 0.2\text{MPa}$, $w_0 = 9\text{mm HH}$, scale=30

8.2.2 Transverse compression

The lateral pressures forces the sinusoidal eigenmode imperfection into a shape resembling the "Hungry-Horse", shown for $P = 0.2\text{MPa}$ in Figure 63.

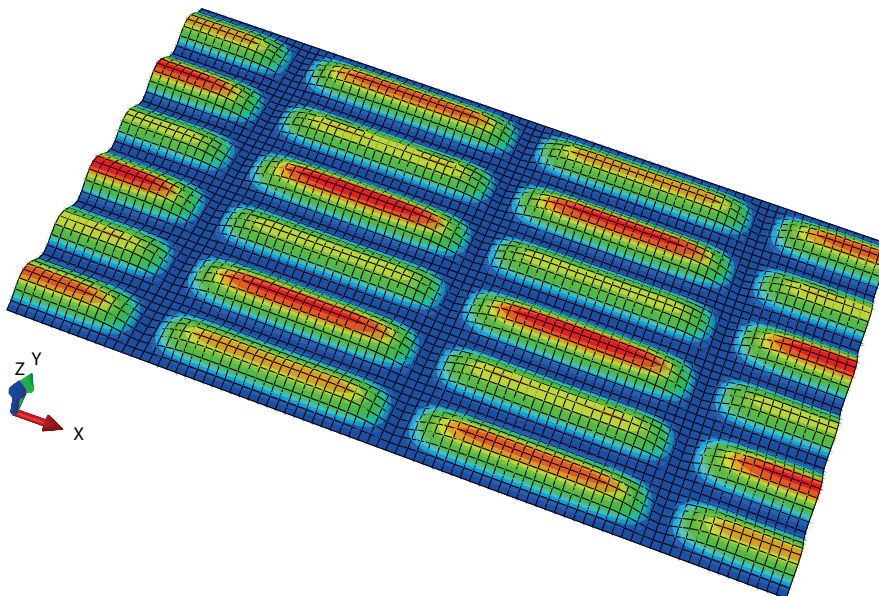


Figure 63: Deflection mode, $P = 0.2\text{MPa}$, $w_0 = 9\text{mm EM}$, scale=30

As for longitudinal shortening, the eigenmode emerges regardless of the altered imperfection mode. It is clear that only small contributions from the eigenmode geometry is needed to set off the deflection. The buckling behaviour, dictated by Figure 64, disclose that the lateral pressure has little effect on the in-plane stiffness. A slight increase is seen for increasing

pressures but the deviations are minor. The non-pressure condition is not distinguishable in the current plot but coincides with the lowest pressure level.

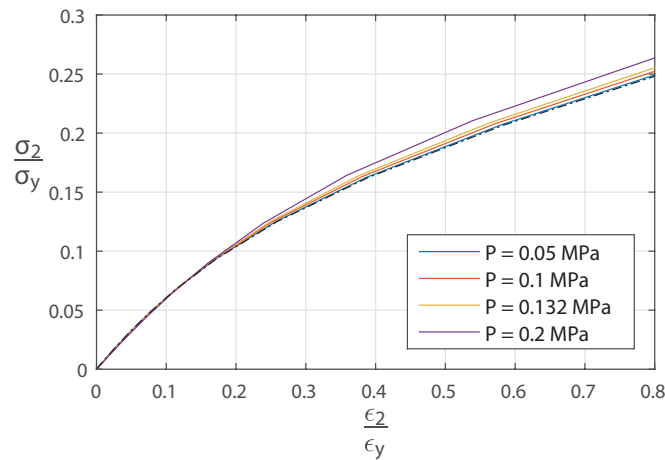


Figure 64: Transverse load-shortening relation, $w_0 = 9\text{ mm EM}$

For the "Hungry-Horse" a distinct effect of the applied pressure is observed even for the lower pressure levels in terms of a reduced initial stiffness and an increased buckling strength. The in-plane stiffness, dictated by Figure 65, displays a much higher load-dependent stiffness for the greatest pressure condition. The corresponding deflection mode in Figure 66 shows that the HH-mode is more or less maintained during deflection. However, the curve exhibits a bend in the advanced strain range, which indicates that the panel is about to give in to the eigenmode. This is also reflected by the deflection mode, where every other plate has a lower amplitude.

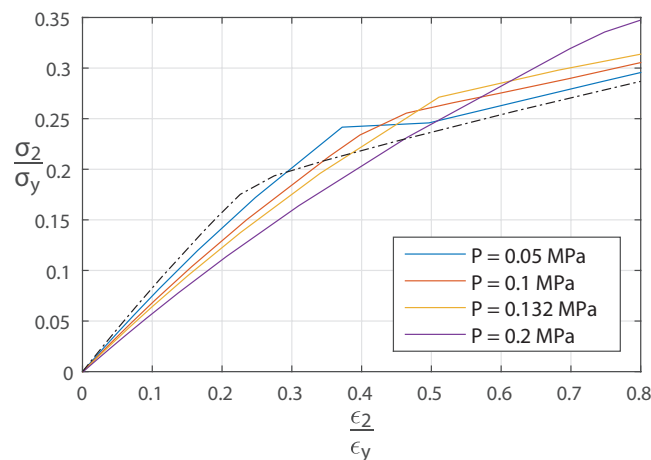


Figure 65: Transverse load-shortening relation, $w_0 = 9\text{ mm HH}$

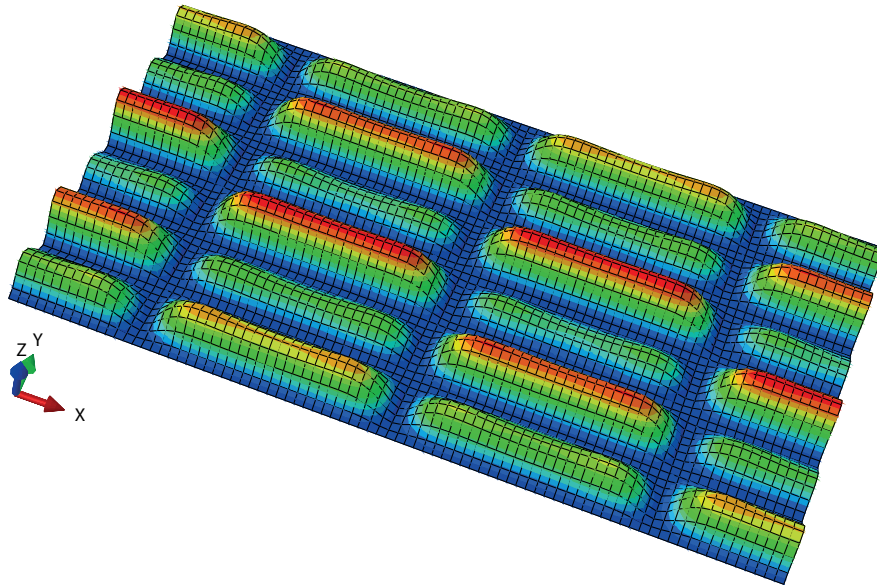


Figure 66: Transverse deflection mode, $P = 0.2\text{MPa}$, $w_0 = 9\text{mm HH}$, scale=30

Discussion The sensitivity to lateral pressure for panels with eigenmode imperfections are considered negligible with respect to the in-plane stiffness. Some effects were seen for the "Hungry-Horse" imperfection for both longitudinal and transverse compression in the form of a reduced initial stiffness and an increased elastic buckling limit. This having in mind that the two larger pressures were far in excess of relevant load-levels. The general observation was that the deflection is governed by the in-plane loads, not the pressure effects.

9 Stiffened Multi-bayed Panel

The ULS design principles accept local plate buckling, provided that the longitudinal stiffeners exhibit adequate strength to prevent global buckling. In modelling, this may only be checked by including the stiffener geometry. Interaction effects between local and global buckling modes may be identified and the rotational stiffness imposed by stiffeners may alter the emergence of local buckling modes, compared to the previous constrained model.

9.1 Model description

Longitudinal angle stiffeners, with dimensions 200/6 + 90/11 [mm], are added to the multi-bayed panel, as depicted in Figure 67. The stiffener geometry is chosen quite randomly, the only requirement being to possess enough stiffness to prevent global buckling. Transverse frames are modelled as vertical constraints as before and the previous constraints along the plate/stiffener junctions are removed. To prevent stiffener tripping the nodes in the junctions between frames and stiffeners are constrained to follow the displacement in the y-direction. Besides the above, the boundary conditions are defined as for the previous model. All boundary conditions are given in Table 9 and depicted in Figure 67.






Boundary	Suppressed DOF's	Constraint	Colour Code
Aft	UR_2, UR_3	Constrained to remain straight	
Fore	U_1, UR_2, UR_3	-	
Right	U_3, UR_1, UR_2, UR_3	Constrained to remain straight	
Left	$U_2, U_3, UR_1, UR_2, UR_3$	-	
Frames	U_3	-	

Table 9: Boundary conditions, stiffened multi-bayed model

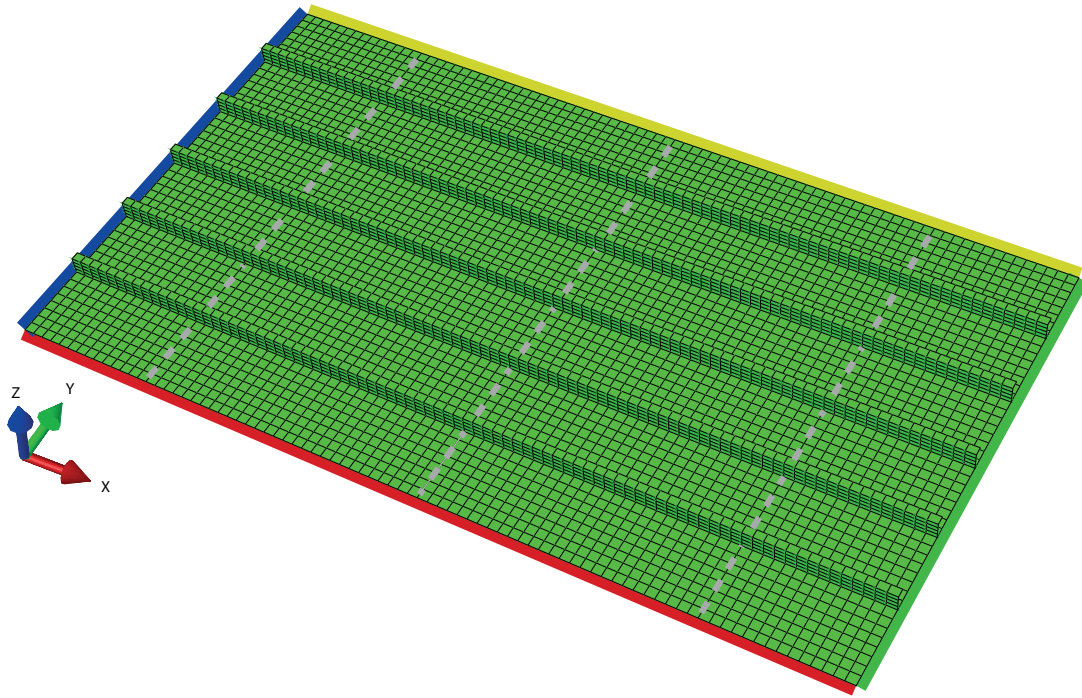


Figure 67: Stiffened multi-bayed model

The aft and right boundary are restrained from in-plane translation for transverse and longitudinal compression respectively. The panel studied in the two previous chapters will hereafter be referred to as the constrained panel.

9.2 Results

For the stresses to be comparable with the constrained panel, membrane stresses are retrieved along the fore and left edge in the plating only. Strains are overall engineering strain. A check was performed on the membrane stiffness of a single frame-span, which was found to coincide with the behaviour of the global panel for the considered strain range.

9.2.1 Longitudinal compression

The load-shortening curves for longitudinal edge-shortening are given for the average imperfection level in Figure 68 and 69. The effect of the rotational stiffness imposed by stiffeners is seen to have minor impact on the behaviour. For the "Hungry-Horse" imperfection the stiffened model has a slightly higher post-buckling stiffness than the constrained model. The deviations are however negligible.

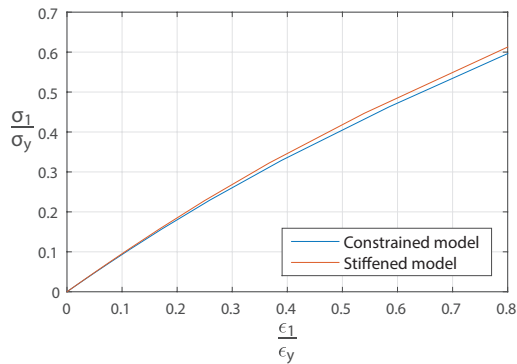


Figure 68: Longitudinal load-shortening relation, $w_0 = 9\text{mm EM}$

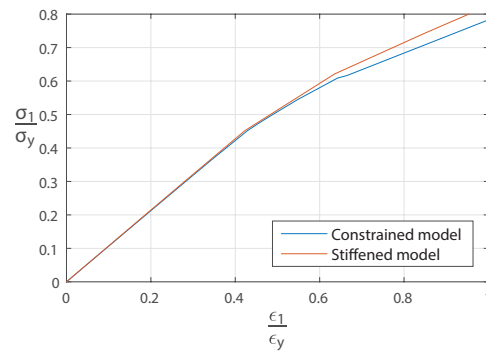


Figure 69: Longitudinal load-shortening relation, $w_0 = 9\text{mm HH}$

The load-shortening curve for the minor imperfection level is given in Figure 70. In Chapter 7 the HH-imperfection was found to possess a much higher post-buckling stiffness than the other constrained panels due to the emergence of an advanced buckling mode. Abaqus was unable to find a converging solution for the stiffened panel, but a reasonable assumption is that the panel in reality takes on a deflection mode closer to that of the eigenmode rather than the much stiffer geometry seen before.

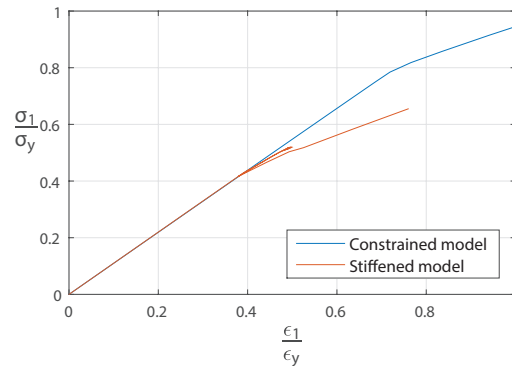


Figure 70: Longitudinal load-shortening relation, $w_0 = 2\text{mm HH}$

9.2.2 Transverse compression

The stiffener contribution in the transverse direction is minor, as expected. The slight deviations in the transverse load-shortening curves, Figure 71 and 72, stem from the additional rotational stiffness in the plate/stiffener intersection lines.

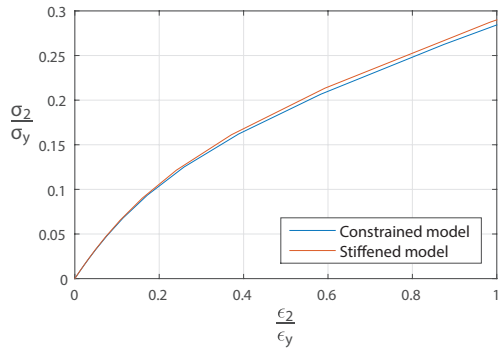


Figure 71: Transverse load-shortening relation, $w_0 = 9mm$ EM

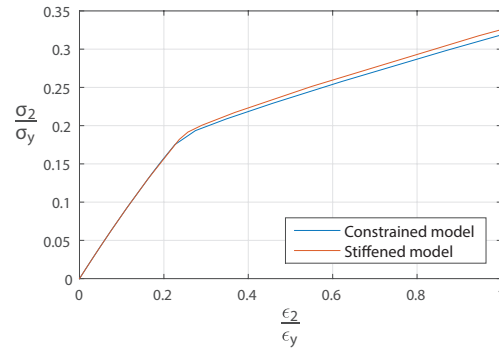


Figure 72: Transverse load-shortening relation, $w_0 = 9mm$ HH

In Chapter 7 the constrained panel with a minor "Hungry-Horse" imperfection was found to exhibit a much greater stiffness than the eigenmode contributions due to the maintenance of the HH-mode during deflection. The stiffened panel is however seen to take on the eigenmode, displaying a more realistic post-buckling stiffness in Figure 73.

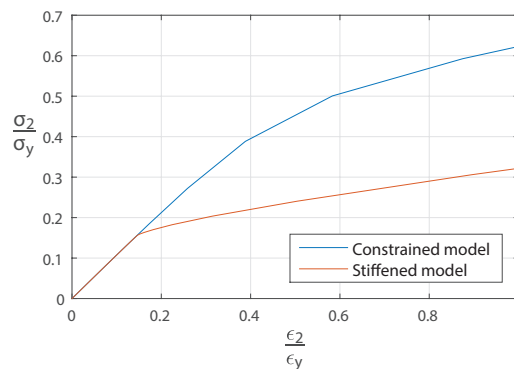


Figure 73: Transverse load-shortening relation, $w_0 = 2mm$ HH

Discussion The overall effects of the presence of longitudinal stiffeners are minor. The initial plate stiffness was unaffected, although some deviations in the post-buckling range were distinguishable for the "Hungry-Horse" imperfection. The presence of stiffeners did not seem to affect the emergence of the eigenmode at all, although no converging solution was found for the minor longitudinal eigenmode imperfection. It may be that the chosen stiffener dimensions were too small to impose adequate rotational stiffness to affect the growth of deflection modes. With more time, additional analyses with beefed-up stiffeners could have been performed. This was not prioritized considering the present scope.

A study on the effect of lateral pressure was also performed on the stiffened panel. No distinct deviations were seen between the stiffened and constrained model, other than that

the stiffeners naturally experienced some additional deflection subjected to lateral pressure only. This had however little impact on the in-plane stiffness and the induced stresses were way beyond yield in the stiffener flanges. This indicates that the applied loads were not very realistic for the considered configuration. The results are included in Appendix C but not further discussed.

10 Car-deck

In Chapter 6.4 the closed-form formulations for the initial macro material coefficients are tested and validated. In the current chapter, the practical use of the macro material model is addressed. The feature of serving as input in a linear model is tested for a larger configuration, representing a car-deck. A linear and coarsely meshed model with embedded anisotropic coefficients is compared with a "real" non-linear model with refined mesh. The results are supplemented with curves from a model representing the standard linear isotropic (Rule) procedure. The agreement between the linear results for initial stiffness and the actual behaviour is evaluated. As a continuance of the above, the macro material input is tuned to mimic the load-dependent behaviour of the non-linear panel.

10.1 Model description

A larger model of a car-deck configuration provided by DNV GL (Lars Brubak) is introduced. In the longitudinal direction two pillar lengths are modelled with half a pillar length in the aft and fore end. The two pillars are located on the center-line girder, as depicted in Appendix D. This encloses 6 transverse frame lengths in total. As the deck is symmetric about the center-line, only half of the full-breadth model is included. This encloses 19 longitudinal L-beam stiffeners in addition to 3 channel profiles. Two heavier girders support the deck in the center-line, whereof one is included in the half-breadth model. The overall configuration is given in Figure 74, while the scantlings are provided in Appendix D.

The aft and fore boundary are located midway between two transverse frames, hence symmetry conditions are applied. The two loaded edges (aft and left boundary) are restrained to remain straight due to the presence of adjacent plating and intersection with the ship side. The left boundary is clamped considering the connection to vertical transverse girders along the ship sides, while symmetry conditions are applied to the right edge. The two pillars are restrained from vertical translation. All boundary conditions are given in Table 10, complemented by Figure 74. The subscripts 1, 2, and 3 correspond to direction x , z , and y respectively, given the axis system defined in Figure 74.





Boundary	Suppressed DOF's	Constraint	Colour Code
Aft	UR_2, UR_3	Constrained to remain straight	
Fore	U_1, UR_2, UR_3	-	
Right	U_3, UR_1, UR_2	-	
Left	U_2, UR_1, UR_2, UR_3	Constrained to remain straight	
Pillars	U_2	-	-

Table 10: Boundary conditions, Car-deck model

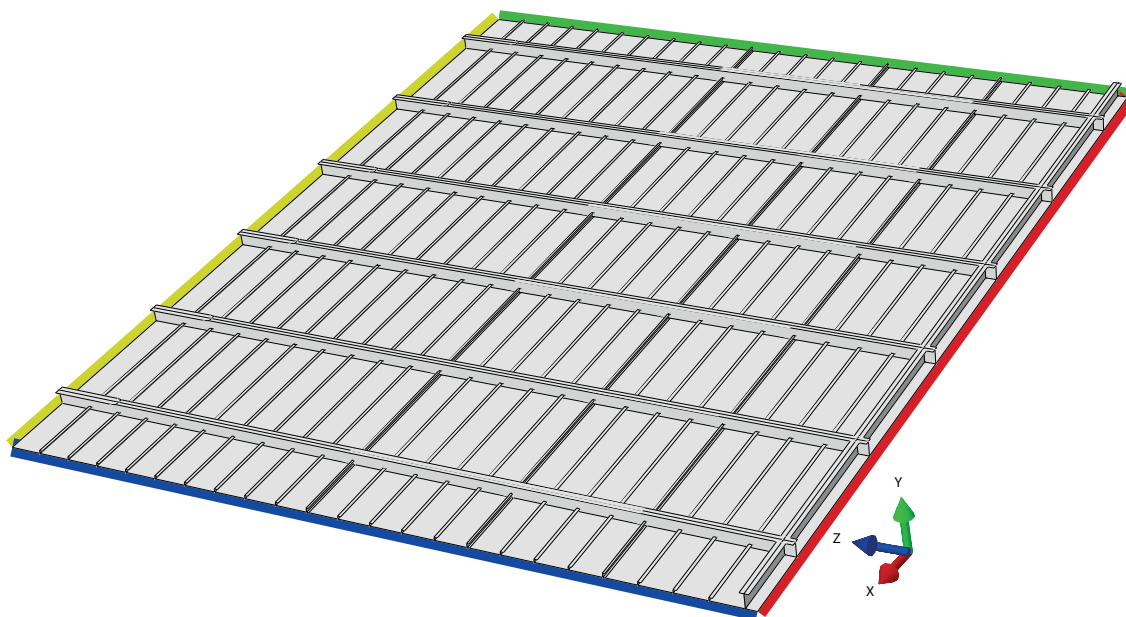


Figure 74: Car-deck model

Prescribed displacements are applied along the aft and left boundary. The above boundary conditions apply to both longitudinal and transverse compression. In addition, the aft and left boundary are restrained from in-plane translation for transverse and longitudinal compression, respectively.

10.1.1 Non-linear isotropic model

The isotropic material is defined as linear elastic with Young's Modulus $E = 206000MPa$ and $\nu = 0.3$. The model is meshed adopting the same approach as in previous analyses, using 8 elements across the plate width. The element size is equal for the supporting structure. Although no plasticity is included in the analyses, the actual yield strength of $235MPa$ is used as reference in the presentation of results.

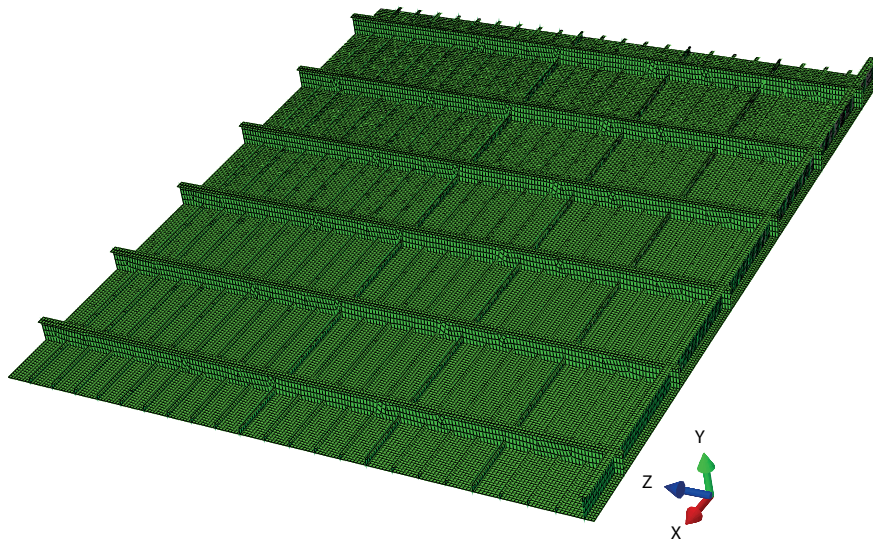


Figure 75: Non-linear isotropic model, fine mesh

10.1.2 Initial imperfection

An imperfection pattern similar that of the transverse eigenmode is assigned to the whole deck, i.e a pure sinusoidal deflection with one half-wave across both the plate length and width, Figure 76. The imperfect geometry is applied by the same imperfection script as used for the multi-bayed panel (Appendix B), only slightly modified to fit the car-deck geometry. The imperfection amplitudes are assigned according to Faulkner's imperfection model, corresponding to $w_0 = 3mm, 5mm, 11mm$ and $32mm$ approximately. (Analyses were primarily performed adopting the "Hungry-Horse" imperfection, which came out as too stiff compared to the anisotropic model. This is because the HH-imperfection results in a constraint closer to that of clamped along the plate edges. This is not captured by the anisotropic model as it is derived assuming simply supported plates.)

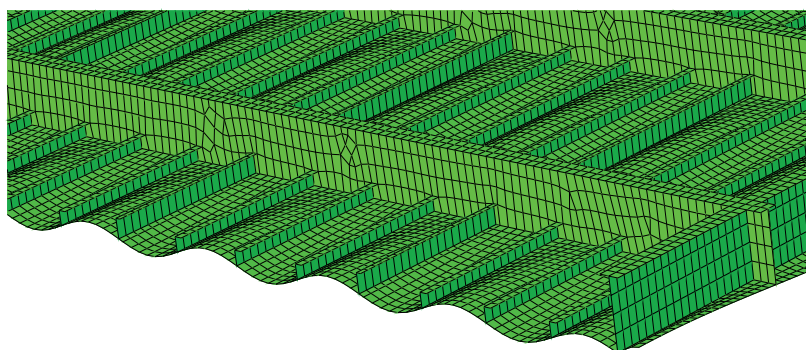


Figure 76: Initial imperfection

10.1.3 Linear anisotropic model

A lamina material model is chosen to represent the anisotropic material properties of the plating. The material input consists of the four parameters E_1 , E_2 , ν_{12} and G_{12} (G_{13} and G_{23} are kept constant equal to 1). G_{12} is not affected by the initial imperfection, hence the modification of stiffness is defined by the three former coefficients. The exact values are defined by the closed-form formulation for initial stiffness at each imperfection level (ref. Chapter 4) and conveniently calculated by the excel sheet given in Appendix E. One element across plates between longitudinal stiffeners is adopted. The supporting structure is more refined, as it represents the actual isotropic linear elastic material.

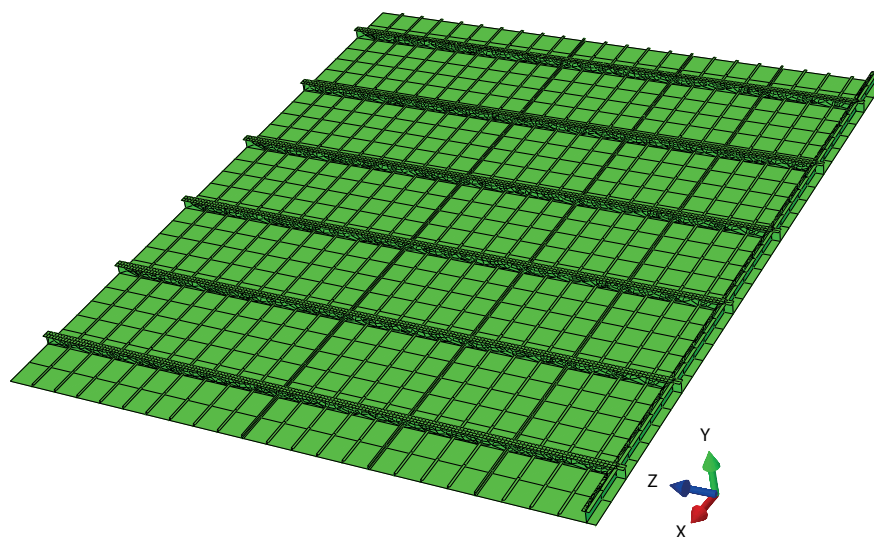


Figure 77: Linear anisotropic model, coarse mesh

10.1.4 Linear isotropic (Rule) model

In addition to the above a coarsely meshed linear isotropic model is introduced to represent the standard isotropic Rule model. The rule model is identical to the linear anisotropic model in configuration and meshing, however fully linear isotropic. Hence, no imperfections or non-linear effects are included.

10.2 Study of initial stiffness

Analyses are run for pure longitudinal and pure transverse compression. The stiffness reduction in the non-linear panel is found to be equal for all integrated plates, thus the local stiffness is expressed by the load-shortening relation of a randomly chosen plate. Membrane stresses and strains from all three models are retrieved from a plate located in the middle frame-span. The exact location is given in Appendix D, denoted "regular plate". Despite of the definition of coordinate system and corresponding subscripts, the transverse stress is hereafter denoted σ_2 . Thus, direction 2 corresponds to the z-direction in Figure 74. This is merely to obtain consistency in the presentation of results throughout the thesis.

Figure 78 to 81 display the load-shortening curves for longitudinal compression with the whole range of imperfection amplitudes. The dashed line corresponds to the Rule model. The non-linear panel behaves close to linearly for all imperfections, resulting in a nearly constant longitudinal stiffness. In accordance with previous analyses on the compressive strength of unstiffened plates, the initial longitudinal stiffness lies in the vicinity of the elastic value for the given imperfection geometry. The anisotropic models are seen to coincide with the non-linear curves before the latter slightly bends off. The curves are stopped at different shortenings due to numerical difficulties at larger strains.

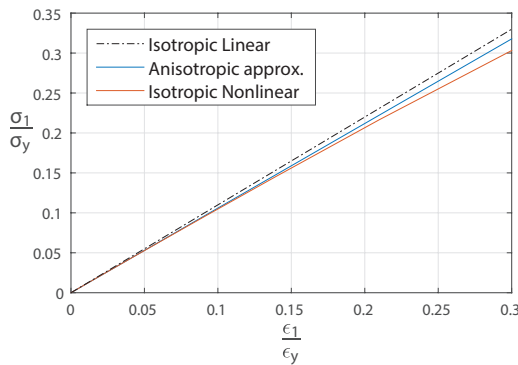


Figure 78: Longitudinal load-shortening relation, $w_0 = 3\text{mm}$

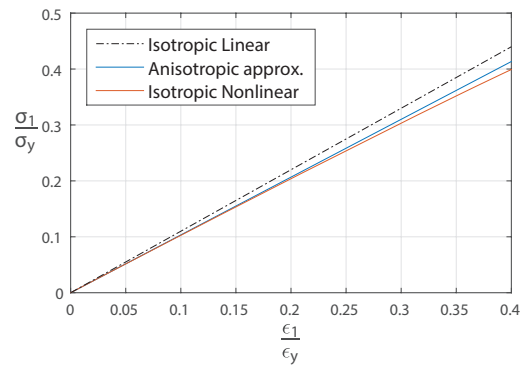


Figure 79: Longitudinal load-shortening relation, $w_0 = 5\text{mm}$

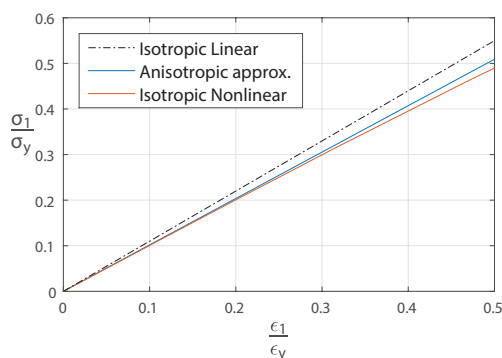


Figure 80: Longitudinal load-shortening relation, $w_0 = 11\text{ mm}$

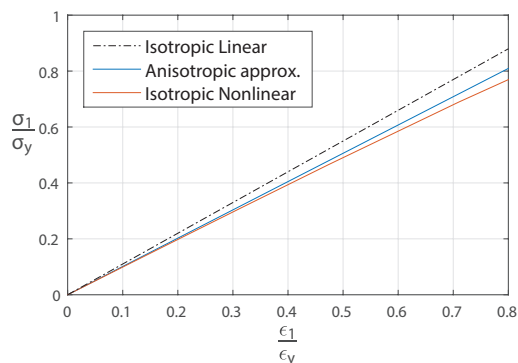


Figure 81: Longitudinal load-shortening relation, $w_0 = 32\text{ mm}$

A more distinct non-linear behaviour is seen for transverse edge-shortening. For the two lower imperfection amplitudes the anisotropic model is seen to coincide well with the initial stiffness of the non-linear model, Figure 82 and 83. Considering the greater imperfections, Figure 84 and 85, the stiffness predicted by the anisotropic model is in excess of the non-linear curve, however much closer to "reality" than the Rule model. This is due to the deflection behaviour seen for individual plates with a large aspect ratio and great imperfections, ref. Chapter 6.4. Instead of the pure half-wave deflection mode, the large out-of-plane distortion imposes an altered mode in the form of a flattened buckle and two initiated peaks.

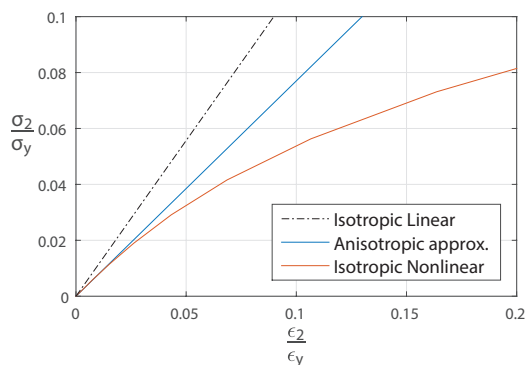


Figure 82: Transverse load-shortening relation, $w_0 = 3\text{ mm}$

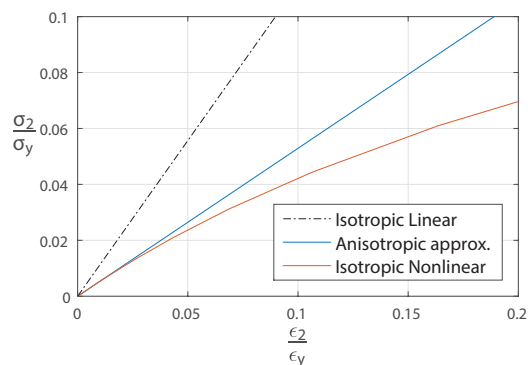


Figure 83: Transverse load-shortening relation, $w_0 = 5\text{ mm}$

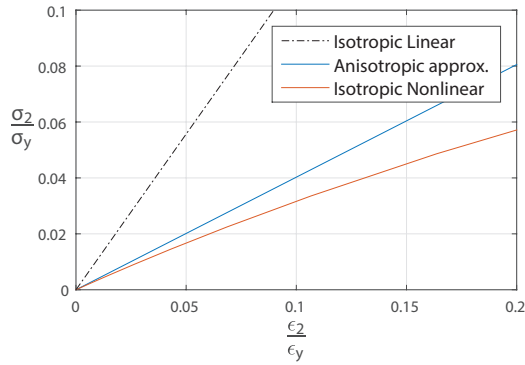


Figure 84: Transverse load-shortening relation, $w_0 = 11\text{ mm}$

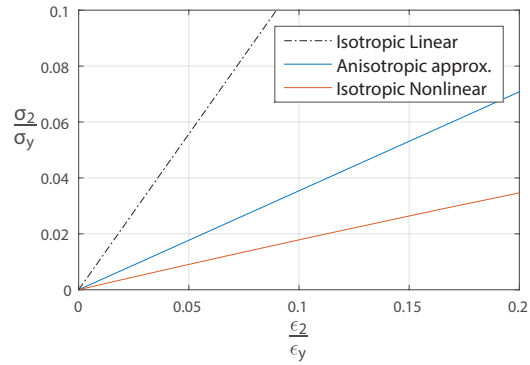


Figure 85: Transverse load-shortening relation, $w_0 = 32\text{ mm}$

The panels are loaded far beyond the elastic buckling limit. Due to the highly non-linear response at transverse compression, the linearisation of the initial response is only valid for a small range of strains. If the anisotropic model were to be used in design, only the area in the vicinity of the elastic buckling limit would be relevant. To get a measure of the stress redistribution to transverse frames the panels are run with load-control, allowing for some non-linearities to develop in the plating. The resulting axial stresses in the middle transverse frame are displayed for each imperfection level in Figure 86 to 89. The axial stresses are denoted σ_1 due to the local definition of stresses in the Abaqus model, which corresponds to the transverse direction.

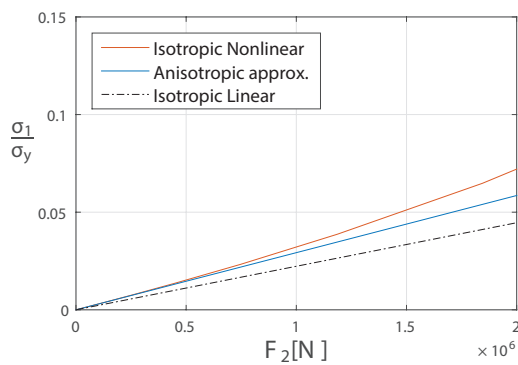


Figure 86: Axial stresses in middle frame, $w_0 = 3\text{ mm}$

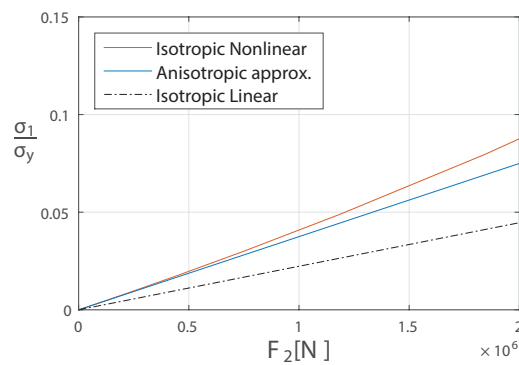


Figure 87: Axial stresses in middle frame, $w_0 = 5\text{ mm}$

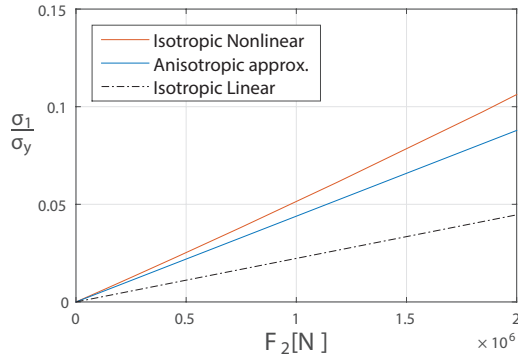


Figure 88: Axial stresses in middle frame, $w_0 = 11\text{mm}$

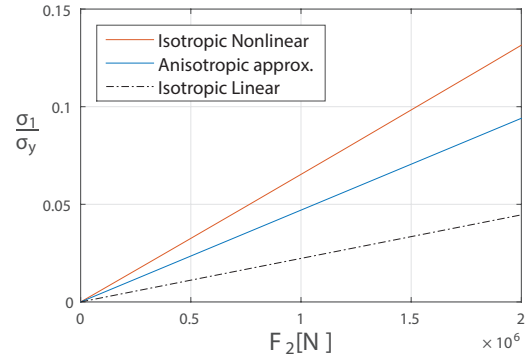


Figure 89: Axial stresses in middle frame, $w_0 = 32\text{mm}$

Figure 86 and 87 illustrate that the early stress redistribution to transverse frames is successfully mimicked by the anisotropic approximation. For the larger amplitudes, Figure 88 and 89, the anisotropic plates have been proved to stiff, resulting in less stresses taken by supporting frames. The Rule models naturally display lower stresses as no redistribution is accounted for in the material model. The global load-shortening relation (overall shortening vs. membrane stresses in frames and plating) for the two minor imperfection levels are given in Figure 90 and 91. The anisotropic model coincides with the initial non-linear behaviour.

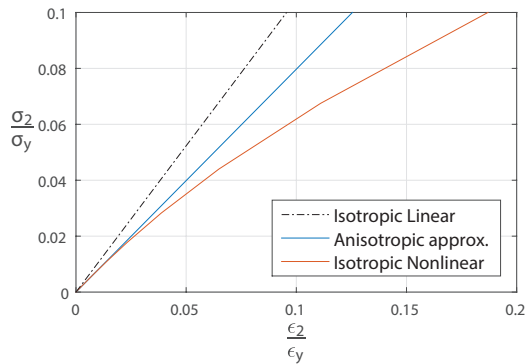


Figure 90: Global transverse stiffness, $w_0 = 3\text{mm}$

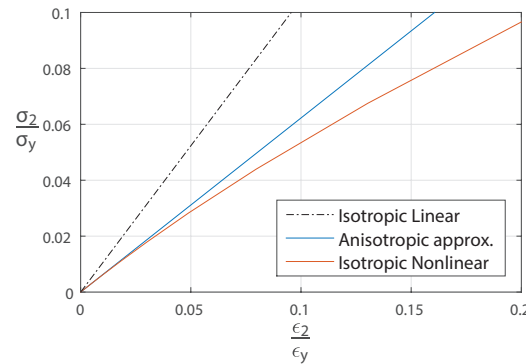


Figure 91: Global transverse stiffness, $w_0 = 5\text{mm}$

Discussion The macro material approach has been proved to successfully mimic the initial behaviour of a larger configuration consisting of imperfect plates. The anisotropic model gives lower stresses in the panel plating compared to the standard linear procedure, and thus a more realistic measure of stresses in the supporting structure. As for the validation of the closed-form solution for initial stiffness, the larger imperfection amplitudes gave higher estimates of the initial stiffness using the macro material approach than the non-linear system.

From a design perspective, this is on the "safe side" with respect to the prediction of plate membrane stresses. One would rather overestimate the stress levels in the plating (and thus underestimate the load-shedding), than overestimating the stresses in the supporting structure.

The macro material approach may give room for reduction of the plate thickness due to the lower utilization of plating. This again relies on the relative utilization of adjacent structural elements and other relevant load-conditions. This issue is further treated in Section 10.4.

It should be noted that even though the anisotropic model is seen to imitate the non-linear behaviour in a satisfying manner, the actual proximity to reality will heavily depend on the chosen imperfection geometry and size. In the present study, the same imperfection mode and amplitude are applied to all integrated plates. In reality, the probability of this occurring is minor, as discussed in Chapter 2.2. Studies should be performed adopting a more randomly distributed imperfection pattern to identify potential corrections of the estimated anisotropic stiffness.

10.2.1 Applicability of macro material model under lateral pressure

A most relevant load-condition for a car-deck structure is lateral pressure. In Chapter 8 a number of studies on a multi-bayed panel documented a relatively low sensitivity to relevant pressure levels in terms of in-plane stiffness. The car-deck model is however of a much greater extent, thus the global effects of lateral loads may be more prominent. The aim of the current study is to determine whether the pressure condition alters the accuracy of the anisotropic approximation of membrane stiffness, potentially how much the material coefficients must be knocked down to mimic the pressure effects. The models corresponding to the minor imperfection level from the preceding study are used. The deck-load is modelled as a uniform distributed pressure of $P = 0.002MPa$ and applied in a separate analysis step prior to onset of in-plane transverse compression.

The membrane carrying of the lateral pressure causes tension in the plates close to the center-line girder and the left boundary, while the plates positioned in the middle of the deck are in compression. This results in larger local deflections in the middle plating than for the outer plates, displayed by Figure 92.

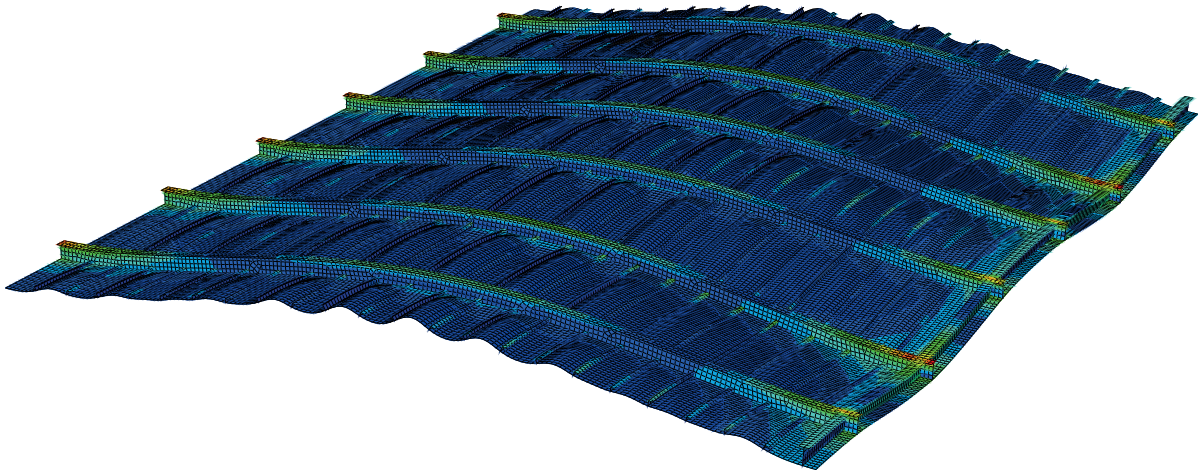


Figure 92: Deflection caused by lateral pressure, scale=50

The resulting membrane stiffness at the onset of transverse compression is dictated by Figure 93 where the blue line corresponds to the plate considered in previous analyses and the yellow applies to a plate in the middle frame-span in the middle of the deck, denoted "middle plate" in Appendix D. It is clear that the middle plate has suffered the most from the global bending, while the outer plate more or less coincides with the linear anisotropic solution. Some minor stiffening effects are seen for the latter case as a result of the initial tensile stresses. The resulting overall stiffness of the panel (stresses in plating and frames along left boundary vs. overall nominal strain), dictated by Figure 94, confirms that the loss of stiffness in the mid-panel area is larger than the stiffening effects along the edges. Hence, the anisotropic model predicts a much stiffer structure than the non-linear system.

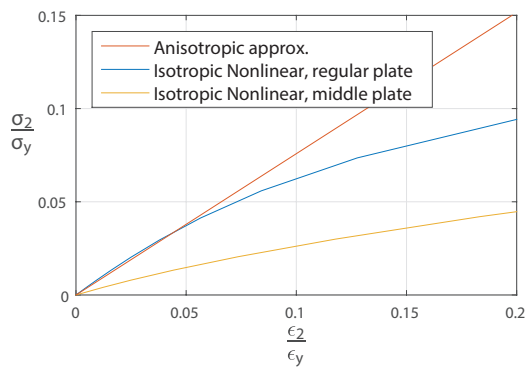


Figure 93: Local stiffness

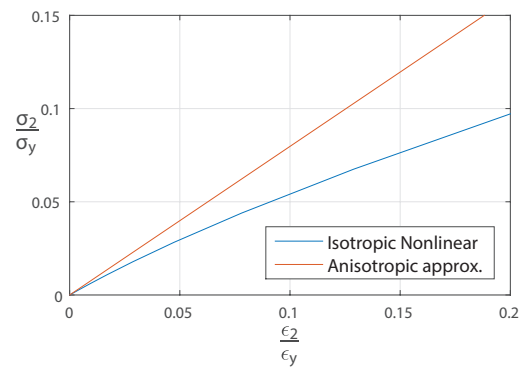


Figure 94: Global stiffness

Discussion Due to the global bending of the panel and the resulting variation of local out-of-plane distortions in the non-linear model, the overall in-plane stiffness of the anisotropic and non-linear model does not coincide after exposure of lateral pressure. On a local level

the agreement between the non-linear model and the anisotropic approximation depends on the location of the considered plate. Potentially, an averaged stiffness reduction caused by lateral pressure applied to the whole anisotropic plating would give a more correct overall stiffness at the onset of compression. Also, one could model part of the deck with the original anisotropic stiffness, while the middle-part, that is most affected by the pressure, could be assigned a knock-down corresponding to the pressure level. The stiffness reduction caused by lateral pressure would then be included in the linear procedure in the same manner as initial imperfections and the membrane stiffness at the onset of compression could perhaps be reproduced.

The effects of lateral pressure are clearly more prominent for the larger car-deck panel than for the multi-bayed model in Chapter 8. The macro material model may be more applicable for models with a lesser extent and a higher degree of constraint against vertical translation in the event of lateral loads.

10.3 Load-dependent stiffness correction

Up until now the macro material model has been used to mimic the initial stiffness reduction due to imperfections. A further aim is to reproduce the load-dependent non-linear response by modifying the anisotropic coefficients. The objective for such a procedure is to be able to predict local and global stress levels at prescribed load-states. This may especially come in hand considering a possible acceptance of local elastic plate buckling in design procedures. Since lateral pressure gave a poor compliance with the non-linear behaviour, this load-condition is excluded in the current study. Longitudinal edge-shortening does not involve an appreciable loss of stiffness for the adopted imperfection geometry, hence only transverse compression is applied. Although the relevance of this load-condition alone is rather restricted for the current panel, this study is merely performed to study the applicability of a load-dependent linear material model in the prediction of stiffness reduction and stress redistribution. The displacements that are studied are in excess of the elastic buckling limit for individual plates. This was done on purpose to obtain a pronounced effect of the tuning of the material input. A potential application in design would imply displacements in the vicinity of elastic buckling and thus much smaller margins regarding the tuning of the macro-material coefficients.

10.3.1 Anisotropic approximation of single plate model

To first get some feeling with embedding load-dependent coefficients in the macro material model, the problem is reduced to a single plate between longitudinal stiffeners and transverse frames. The dimensions are defined as $l = 3600\text{mm}$, $b = 750\text{mm}$ and $t = 6\text{mm}$. The plate is clamped across both short-ends to mimic the constraints imposed by heavier transverse frames. The longitudinal stiffeners are rather small, hence free rotation about the stiffener axis is applied along the plate long-edges. A minor imperfection level is chosen, corresponding to $w_0 = 3\text{mm}$. A non-linear analysis is conducted to obtain the load-dependent stiffness at given edge-shortenings. It is important to note that the load-dependent stiffness in this context is understood as the secant stiffness corresponding to a chosen load-state, not the incremental stiffness. Three states in the response history are chosen, for which the secant coefficients C_{22} and C_{12} are calculated. The macro material input in the form of the transverse coefficient E_2 and the Poisson ratio ν_{12} are determined by the equations given in Chapter 4.3. The exact values for the load-dependent coefficients are found in Appendix F.

The longitudinal coefficient E_1 is taken as the value given by the closed-form solution for initial stiffness, as it has been proved to be nearly constant during deflection. The coefficients corresponding to each target shortening are embedded in the anisotropic material model of three identical plates. The resulting load-shortening curves and coupled stiffness relations are given in Figure 95 and 96 respectively, complimented by the non-linear load-shortening relation.

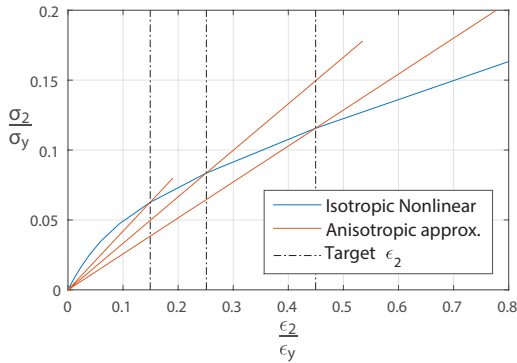


Figure 95: Anisotropic prediction of transverse stresses

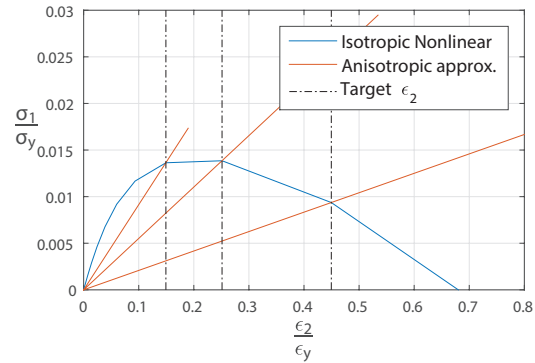


Figure 96: Anisotropic prediction of longitudinal stresses

Transverse and longitudinal stresses are seen to be successfully reproduced by the anisotropic models at the target shortenings.

10.3.2 Anisotropic approximation of car-deck using integrated plate

The desire is to utilize the single non-linear plate model to mimic the stiffness reduction of an integrated plate in the global car-deck model, and so the redistribution of stresses to supporting frames. However, the approximated boundary conditions in the above model most likely differ from the actual constraints imposed by neighbouring stiffeners and frames. Thus, the actual stiffness will differ accordingly. An intermediate study is performed using the load-shortening relation for an integrated plate in the non-linear car-deck model to obtain the load-dependent stiffness coefficients. The imperfection level is minor as before. The plate located in the mid-span close to the center-line girders, denoted "regular plate" in Appendix D, is evaluated. The strain is taken as the overall nominal strain of the isolated plate. Again, three states in the response history are chosen, for which the stiffness properties are calculated and embedded in the plating of the corresponding linear anisotropic car-deck models. The exact load-dependent coefficients for the integrated plate are found in Appendix F. Stiffeners and frames are assigned a linear elastic isotropic material as before.

Figure 97 and 98 display the variation of transverse and longitudinal membrane stresses in the chosen integrated plate.

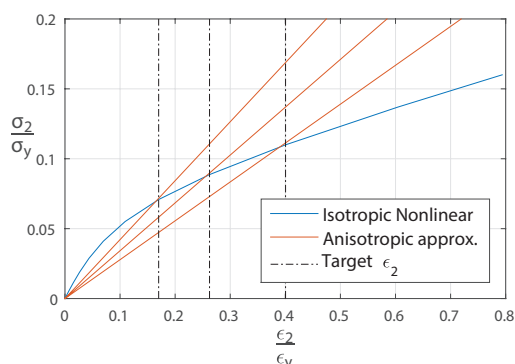


Figure 97: Anisotropic prediction of transverse stresses, integrated plate

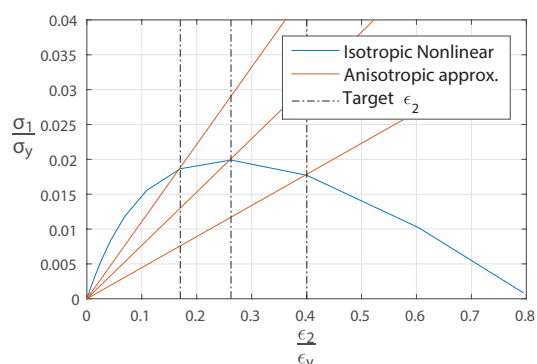


Figure 98: Anisotropic prediction of longitudinal stresses, integrated plate

The membrane stresses are successfully reproduced by the linear models at the target shortenings. For the largest strain, at approximately 40% of the yield strain, the anisotropic approximation is seen to be slightly stiffer than expected, however barely visual in the current plots. This suggests that the local behaviour of the macro material model and the non-linear model may differ for larger displacements. This is, however, far into the post-buckling region, thus neglected in the present study.

10.3.3 Anisotropic approximation of car-deck using single plate model

The stiffness coefficients obtained from the three states in the response history of the single plate model (Section 10.3.1) are embedded in the anisotropic material properties of the car-deck plating for comparison with the previous study. The final aim is to tune the coefficients to mimic the behaviour of the integrated plate. The resulting load-shortening relations are given in Figure 99 and 100, supplemented by the curve obtained from the non-linear single plate model and the curve corresponding to the integrated plate in the non-linear car-deck model.

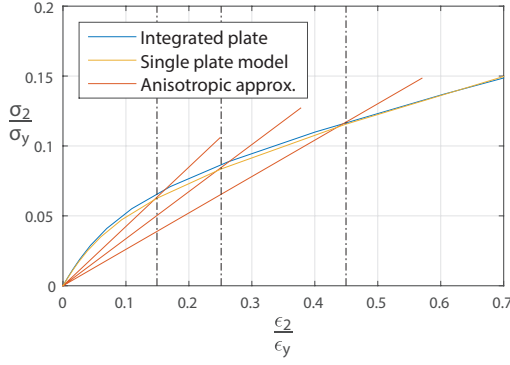


Figure 99: Anisotropic prediction of transverse stresses, single plate

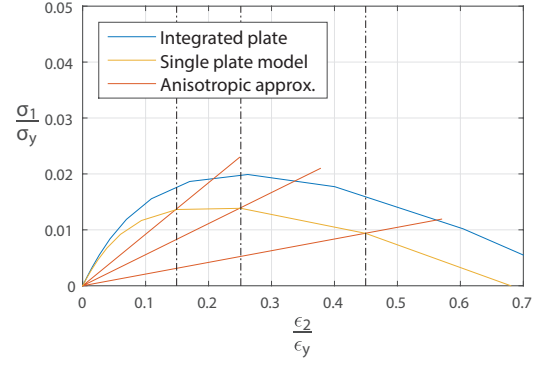


Figure 100: Anisotropic prediction of longitudinal stresses, single plate

The load-shortening relation for transverse stresses is seen to be almost identical for the single plate model and the integrated plate, implying that the approximated boundary conditions are realistic. Transverse stresses are thereby quite accurately reproduced by the anisotropic models, although slightly too low to completely coincide with the integrated plate at the target shortenings. Considering the coupled stiffness the anisotropic models are too flexible to reproduce the actual longitudinal stresses.

The anisotropic stiffness coefficients are tuned according to the actual stress levels (blue line) at the target shortenings in the above curves. The percentage increase of each coefficient are given in Table 11 and 12. Since the approximation was found to be slightly too stiff for the greatest shortening, no increase is performed for this case. The tabulated values are rounded for a better appearance, hence the calculated percentages do not completely coincide with the given coefficients.

$\frac{\epsilon_2}{\epsilon_y}$	E_2 [MPa] Single plate model	E_2 [MPa] Integrated plate	Relative increase
0.15	84779	86978	3%
0.25	67912	69728	3%
0.45	52889	53137	0%

Table 11: Tuning of E_2

$\frac{\epsilon_2}{\epsilon_y}$	ν_{12} Single plate model	ν_{12} Integrated plate	Relative increase
0.15	0.22	0.27	24%
0.25	0.17	0.23	37%
0.45	0.08	0.14	68%

Table 12: Tuning of ν_{12}

The resulting load-shortening curves after tuning of the material input are given in Figure

101 and 102, complemented by the non-linear curves corresponding to the single and integrated plate. The linear approximations are now seen to mimic the actual stress levels in the integrated plate at the target shortenings, however still slightly too stiff for the greatest displacement.

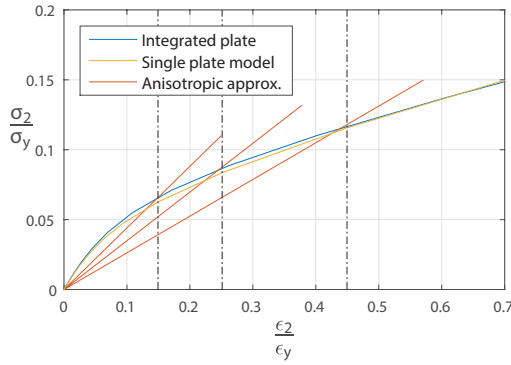


Figure 101: Anisotropic prediction of transverse stresses, tuned coefficients

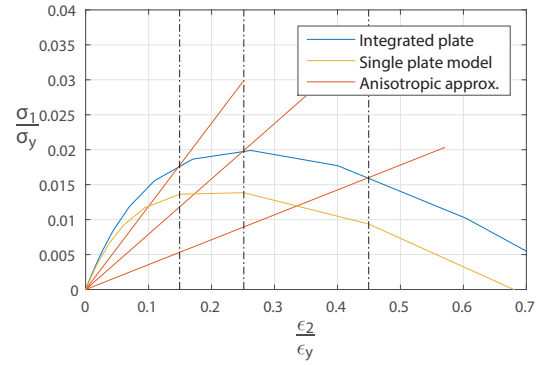


Figure 102: Anisotropic prediction of longitudinal stresses, tuned coefficients

To obtain the variation of membrane stresses in the frames, identical analyses are run, only with load-control. Since the stresses are plotted versus the applied force, no indication of the target state may be given, but the results seems reasonable. The anisotropic models predict increased stresses in the transverse frames for a progressively increasing force.

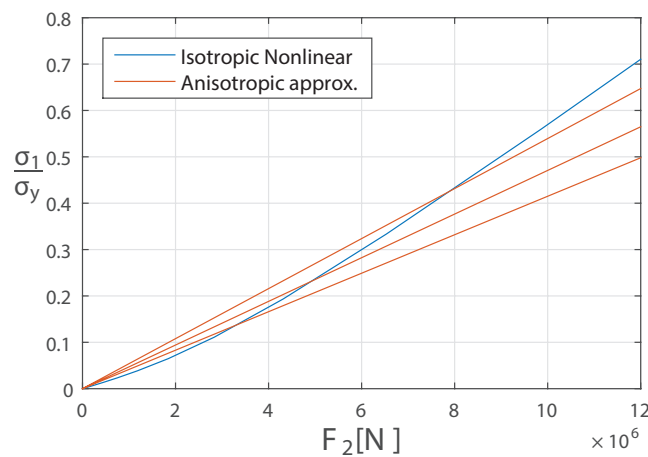


Figure 103: Membrane stresses in frame

The global transverse stiffness is found by averaging the stresses in both frames and plates across the left boundary, plotted versus the overall transverse shortening in Figure 104. The global transverse stresses are realistically reproduced by the anisotropic models, which indicates that the stresses in the frames are correct. For the largest strain the anisotropic approx-

imation is slightly too flexible. This is surprising since the anisotropic model was proved to be too stiff on a local level for the same displacement. No indication as to why this occurred was found, but again the strain level in question is far into the post-buckling region. The actual area of application involve strain levels in the vicinity of elastic buckling.

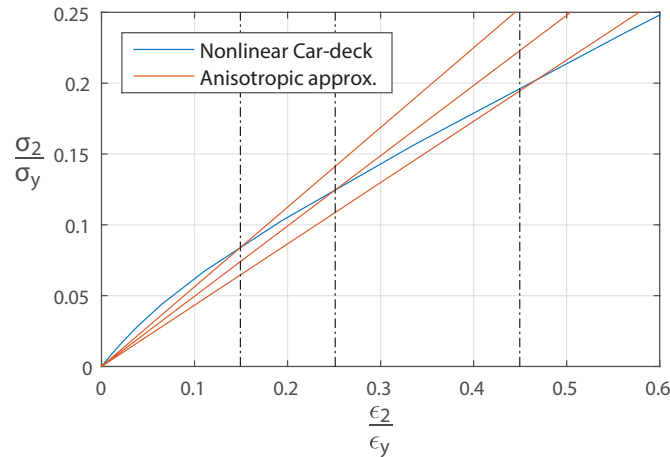


Figure 104: Global stiffness

Discussion A method for predicting the load-dependent stress redistribution of a specific configuration of a car-deck has been proposed. Load-dependent in this context applies to a given target shortening. Both longitudinal and transverse plate membrane stresses were successfully reproduced by tuning the anisotropic material input. Global stresses were also accurately predicted, indicating that the stress redistribution to transverse frames was correct. The required increase of the material coefficients depended on the compliance between the boundary conditions of the reference plate model and the actual boundary conditions imposed by stiffeners and frames.

The objective of introducing a load-dependent macro-material model in design is to be able to predict the stress redistribution at a prescribed load state in the vicinity of the elastic buckling limit. Thus, the procedure represents an alternative to non-linear procedures. A drawback with the approach presented herein is the dependence of a known prescribed displacement. A more general application would require a macro material input based on a target stress-level. Also, using a single plate as reference requires an equal load-dependent behaviour for all integrated plates in the panel. This was fulfilled for the evaluated load condition but may not be true for other loads (e.g. lateral pressure).

10.4 Optimization of deck structure

The macro-material modification of initial stiffness has been proved to give a lower utilization of the plating compared to standard linear isotropic procedures. This enables a potential for steel savings, provided that the supporting structure is not fully utilized.

The anisotropic car-deck model only copes with membrane stresses, hence thickness iterations may only be performed with respect to in-plane loads or displacements. Even though longitudinal shortening is more relevant for the current panel, this condition is characterized by a minor effect of the adopted initial imperfection and a more or less linear response for the relevant strain range (ref. Section 10.2). Longitudinal compression thereby gives little room for thickness iteration as the utilization in the anisotropic and isotropic Rule model is almost equal. Hence, the panel is optimized with respect to transverse compression with a later yield check under the simultaneous action of lateral pressure. This having in mind that in the case of lateral pressure the anisotropic approximation of initial stiffness is no longer fulfilled. The minor Faulkner imperfection, $w_0 = 3\text{ mm}$, is evaluated as it lies fairly close to the model imperfection commonly used by DNV GL ($w_0 = \frac{s}{200}$). Yield-checks are done manually, merely to get an idea of the proximity to potential collapse.

Iterations with the plate thickness are performed with the linear anisotropic model with the aim to mimic the plate membrane stresses in the standard linear isotropic model. The results are retrieved from the same plate as before, denoted "regular plate" in Appendix D. The variation of stresses in plates and frames are most conveniently displayed as function of the applied force, hence the analyses are run with load control. The panel is loaded slightly in excess of the apparent elastic buckling limit of individual plates.

In Figure 105 the transverse membrane stresses of the plating in the linear isotropic and anisotropic model are presented versus the applied transverse force. The curves are supplemented with the stresses corresponding to the non-linear isotropic model (dashed line). The thickness of the anisotropic plating is progressively reduced from 6mm to 3 mm. The resulting increase of stresses in transverse frames is given in Figure 106.

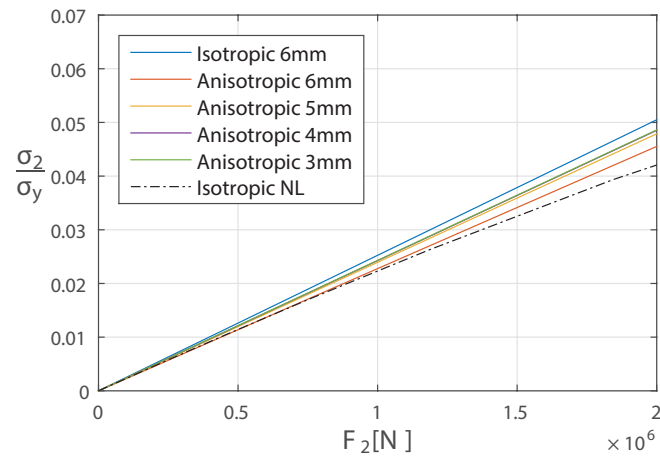


Figure 105: Transverse membrane stresses in plate

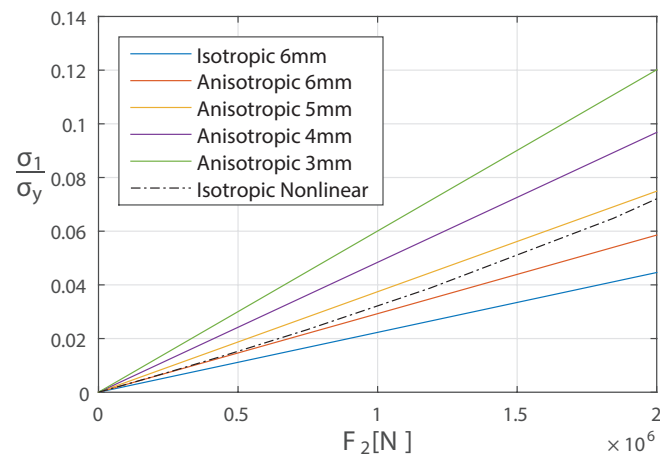


Figure 106: Transverse membrane stresses in frame

The relative increase of the plate membrane stresses is seen to cease for each iteration (3mm and 4mm completely coincide), while the corresponding increase of axial stresses in the frames grows more rapidly. Individual plates are observed to buckle at about half of the applied force. Adopting the onset of elastic buckling as limit criteria, the usage of frames is minor for all panels. Hence, with respect to the utilization of frames under transverse compression only, there exist some potential for reducing the plate thickness.

Under the simultaneous action of transverse compression and lateral pressure ($P = 0.002\text{MPa}$) the capacity in the non-linear model is found to be governed by yielding in the intersections between the center-line girders and the frame flanges. The vonMises stresses for the area in question are given for all panels in Figure 107. The utilization of the flange is seen to be considerable for lateral pressure only, in the order of 50% for the thicker panels, while the

3mm and 4mm panels move towards 60% utilization. Some reduction of the plate thickness is possible considering the utilization of the frame flange, again adopting elastic buckling as limit criteria. Reducing the plate thickness will of course entail a reduced buckling limit, hence the relevant range of the applied transverse force will in reality be smaller.

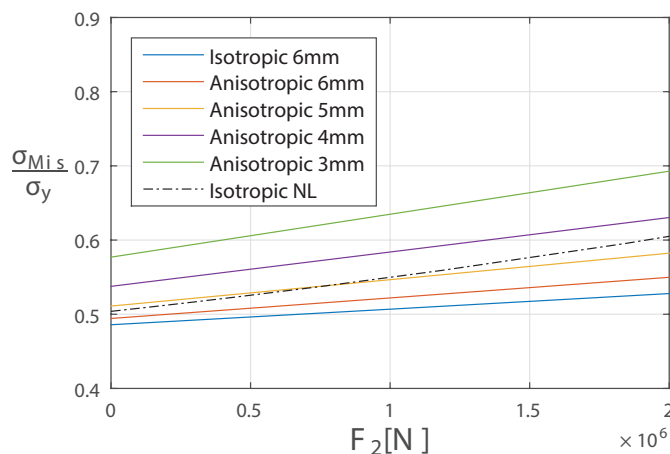


Figure 107: Stress accumulation in mid-frame flange

Discussion The above considerations forms an extremely superficial study, primarily performed to point at features of the macro material model that may enable steel savings under a very restricted load-condition. Due to the minor utilization of transverse frames when adopting elastic buckling of individual plates as limit criteria, the plate thickness may be reduced without consideration of axial stresses in the supporting structure. Having said so, the considered panel is obviously dimensioned with respect to other load-conditions than transverse compression. A potential reduction of plate thickness will fully rely on whether relevant loads and safety criteria allow for it.

Since the potential of thickness reduction was more relevant for transverse compression with the adopted imperfection geometry, the anisotropic approach might not be of much practical use for the given car-deck configuration. The present study has, however, identified a theoretical possibility of saving steel when replacing the standard isotropic procedure with the modified macro material approach. The possibility of actually doing so depends on the configuration and operation of the considered panel.

Cutting steel based on an assumed imperfection requires a confident assumption regarding the imperfection size and geometry, as this dictates the resulting utilization of the plating in the anisotropic model. The approach adopted in this thesis applies an equal initial dis-

tortion to all integrated plates, which compared to the more randomly nature of actual imperfection patterns probably gives a lower overall plate utilization than the actual condition. With this in mind, the room for steel savings may in fact be much smaller or even negligible considering the real stress levels in the plating.

11 Concluding Remarks

11.1 Conclusion

A linear Finite Element approach developed by DNV GL has been tested and evaluated from the perspective of being applicable in dimensioning of redundant plated structures. The presented procedure mimics the initial loss of stiffness imposed by imperfections by use of so-called macro material coefficients embedded in a linear anisotropic model. The coefficients are defined by a closed-form solution as function of the plate geometry and imperfection level. In the long run the aim is to be able to predict the load-dependent stress redistribution in the same manner, so as to cope with modern design criteria without the need for non-linear procedures. In the preceding studies and analyses in this thesis, both the imitation of initial and load-dependent behaviour are addressed.

The evaluation of the macro material procedure was based on a number of parametric studies on perfect and imperfect unstiffened plates and multi-bayed panels typical for redundant plated structures. The results showed a considerable loss of stiffness in the vicinity of the elastic buckling limit, followed by a nearly constant post-buckling stiffness. This implies an extensive load-shedding to supporting structural elements that is not captured by standard linear procedures.

A series of parametric studies with variations of the plate aspect ratio, plate slenderness and the imperfection level lead to the validation of the closed-form solution for initial stiffness. A high agreement between numerical and analytical results was seen for lower imperfection levels, $w_0 < t_{plate}$. Considerable deviations were observed for high aspect and slenderness ratios with large initial amplitudes, $w_0 > t_{plate}$, with the numerical results being on the lower side. This was found to be due to an immediate altered deflection mode imposed by the large initial out-of-plane distortions. This effect is not captured by the closed-form solution, which presumes a constant deflection mode equal to the initial imperfection.

The practical application of the macro material procedure was evaluated using a model of a specific car-deck configuration. A coarsely meshed anisotropic model with modified initial stiffness properties was compared to a fine-mesh non-linear isotropic model with initial geometrical imperfections. The models showed high agreement for the initial stiffness at typical fabrication level imperfections, while deviations were seen for larger initial amplitudes. For a strain range in the proximity of elastic buckling of individual plates the stresses

in supporting frames were accurately reproduced by the anisotropic approximation.

An attempt on imitating the load-dependent non-linear behaviour of the car-deck panel was performed using the characteristics of a single plate model. The non-linear behaviour of the plate dictated the tuning of the macro material input at certain target load-states. A transverse edge-shortening condition was examined, for which the anisotropic models successfully reproduced both transverse and longitudinal stresses in the plating at the target shortenings. The corresponding axial stresses in the transverse frames showed a realistic trend.

In conclusion, the macro material model serve two convenient applications in design. First, the anisotropic imitation of initial stiffness displays a lower utilization of the panel plating than standard linear procedures. Thus, it provides a potential for steel savings if the supporting structure is not fully utilized. Iterations were performed with respect to plate thickness to identify such a potential for the specific car-deck model. The study documented a theoretical possibility of cutting steel by replacing the standard linear approach with the anisotropic procedure. The final verification of this being a conservative approach will however fully rely on the configuration of the considered panel and whether all relevant load-conditions and safety criteria allow for it.

The second application of the macro material model is most relevant in the context of coping with modern design criteria. Allowing for elastic plate buckling implies a larger degree of non-linearity and thus more prominent shortcomings of established design procedures. The use of a modified linear procedure to predict the stress redistribution accompanying elastic buckling represents an alternative to more sophisticated methods. The load-dependent procedure suggested in this thesis was proved to quite accurately predict the stresses in plating and supporting structure at prescribed load-states. The method however only copes with in-plane loads, and would need a generalization with respect to relevant load-conditions to be truly applicable and conservative as a design procedure.

Even though the analyses performed in this thesis are very basic considering the various aspects of the design process, the tuning of the macro material input has been proved to successfully mimic the desired structural behaviour. A conservative implementation in design would require a larger basis of evaluated configurations and load conditions, in addition to more confident assumptions regarding modelling of initial imperfections. Nonetheless, the studies herein document a potential for predicting both initial and load-dependent non-

linear effects by essentially using a linear procedure.

11.2 Further work

The effect of lateral pressure on the in-plane stiffness of a stiffened panel was found to depend on the extent and constraints of the model. For the considered car-deck configuration, the exposure of lateral pressure altered the local plate membrane stiffness, resulting in a poor overall compliance between the linear anisotropic and the non-linear model. Further studies on the effects of other simultaneous acting loads than the in-plane displacement condition should be performed. A more general application of the macro material prediction of both initial and load-dependent stiffness should cope with all relevant load conditions regardless of the extent of the model.

Having good knowledge on the elastic buckling strength and loss of stiffness of supported plates, it might be possible to achieve more general and explicit formulations of the load-dependent behaviour of redundant plated panels. For in-plane loads solely and minor bending of bearing elements, the load-dependent macro-material input could be expressed as function of the individual plate geometry and imperfection level, similar to the closed-form solution for initial stiffness. The expressions would also be dependent on the constraints imposed by adjacent structure. For a more rigorous approach, the effects of other load-conditions and the potential bending of frames should be considered. The feature of reproducing load-dependent stresses by the behaviour of one single plate model requires an equal stiffness reduction for the whole plating. Potential deviations from this must be identified and accounted for in the model.

The desire of saving steel by introducing the macro material model in design requires better knowledge and confidence with respect to realistic modelling of imperfections. The utilization in the plating of the anisotropic model must be sure to mimic the actual stress levels within reasonable margins. Doing so, potential steel savings could be identified for redundant plated structures with similar configuration and operation.

Including initial imperfections in modelling and design will always be characterized by a certain degree of uncertainty. Simplifications are inevitable for an efficient application. However, with the procedures used today there is a considerable difference between imperfections used in design and real distortions. Studies should be performed on how to efficiently include more random deflection patterns in design. This includes getting more

knowledge and exact data on real fabrication level imperfections in order to more confidently predict the initial geometries and amplitudes.

References

- Amdahl, J. (2013). *TMR4205 Buckling and Ultimate Strength of Marine Structures*. NTNU.
- Brubak, L. and Helleland, J. (2007). Semi-analytical postbuckling and strength analysis of arbitrarily stiffened plates in local and global bending. *Thin-Walled Structures*, 45.
- Brush, D. and Almroth, B. (1975). *Buckling of Bars, Plates and Shells*. McGraw-Hill.
- Byklum, E. (2002). *Ultimate strength analysis of stiffened steel and aluminium panels using semi-analytical methods*. PhD thesis, Norwegian University of Science and Technology.
- Byklum, E. and Amdahl, J. (2002). Nonlinear buckling analysis and ultimate strength prediction of stiffened steel and aluminum panels. In *The Second International Conference on Advances in Structural Engineering and Mechanics*.
- Byklum, E., Steen, E., and Amdahl, J. (2004). A semi-analytical model for global buckling and postbuckling analysis of stiffened panels. *Thin-Walled Structures*, 42.
- Carlsen, C. and Czujko, J. (1978). The specification of tolerances for post-welding distortions of stiffened plates in compression. *The Structural Engineer*, 56A.
- DNVGL (2010a). *Offshore Standard DNV-OS-C401 - Fabrication and Testing of Offshore Structures*. DNV GL.
- DNVGL (2010b). *Recommended Practice DNV-RP-C201 - Buckling Strength of Plated Structures*. DNV GL.
- DNVGL (2015). *Class Guideline - DNVGL-CG-0128 - Buckling*. DNV GL.
- Faulkner, D. (1975). A review of effective plating for use in the analysis of stiffened plating in bending and compression. *Journal of Ship Research*, 19, No. 1, pp.1-17.
- IACS (2013). *No. 47 - Shipbuilding and Repair Quality Standard, Part A*. International Association of Classification Societies Ltd.
- Kármán, T. v. (1910). Festigkeitsprobleme im maschinenbau. *Encyklopädie der mathematischen Wissenschaften*, IV/4.

- Marguerre, K. (1983). Zur theorie der gekrümmten platte grosser formeänderung. *In: Proceedings of the 5th international congress for applied mechanics.*
- Paik, J., Kim, B., and Seo, J. (2008a). Methods for ultimate limit state assessment of ships and ship-shaped offshore structures: Part i - unstiffened panels. *Ocean Engineering*, 35.
- Paik, J., Kim, B., and Seo, J. (2008b). Methods for ultimate limit state assessment of ships and ship-shaped offshore structures: Part ii - stiffened panels. *Ocean Engineering*, 35.
- Paik, J. and Thayamballi, A. (2003). *Ultimate Limit State Design of Steel-plated Structures.* John Wiley and Sons Ltd.
- Palm, A. (2014). Buckling and load shedding in redundant plated ship structures.
- Singer, J., Arbocz, J., and Weller, T. (1998). *Buckling Experiments: Experimental Methods in Buckling of Thin-Walled Structures.* Wiley.
- Slettum, E. (2014a). Buckling study of integrated plating. Technical report, DNV GL.
- Slettum, E. (2014b). Buckling study of stiffened panels. Technical report, DNV GL.
- Steen, E., Byklum, E., and Helleland, J. (2008). Elastic postbuckling stiffness of biaxially compressed rectangular plates. *Engineering Structures*, 30.
- Steen, E., Byklum, E., and Vilming, K. (2004a). *PULS verification manual-PULS Version 2.0.* DNV Report No. 2003-0769, Rev.01.
- Steen, E. and Østvold, T. (2000). Basis for a new buckling model for strength assessment of stiffened panels. In *DNV Seminar: Buckling and Ultimate Strength of Ship Structures, Høvik.*
- Steen, E., Østvold, T., and Valsgård, S. (2001). A new design model for ultimate and buckling strength assessment of stiffened plates. *Practical Design of Ships and other Floating Structures.*
- Steen, E., Vilming, K., and Østvold, T. (2004b). Computerized buckling models for ultimate strength assessment of stiffened ship hull panels. *Practical Design of Ships and other Floating Structures*, 1.
- Systèmes, D. (2014). *Abaqus User Manual 6.14.*

Ventsel, E. and Krauthammer, T. (2001). *Thin Plates and Shells*. Marcel Dekker, Inc.

Appendices

A Load-dependent stiffness reduction

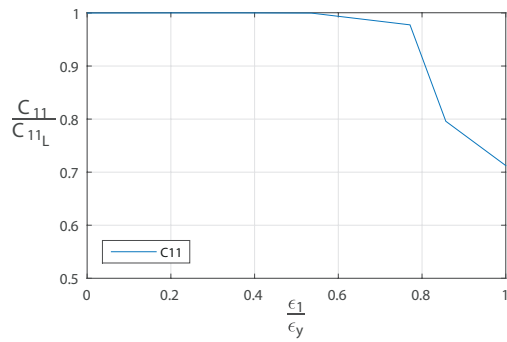


Figure 108: Variation of C_{11} , $d = -22.5^\circ$

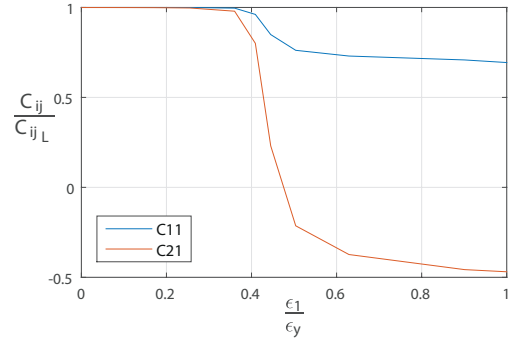


Figure 109: Variation of C_{11} and C_{21} , $d = 0^\circ$

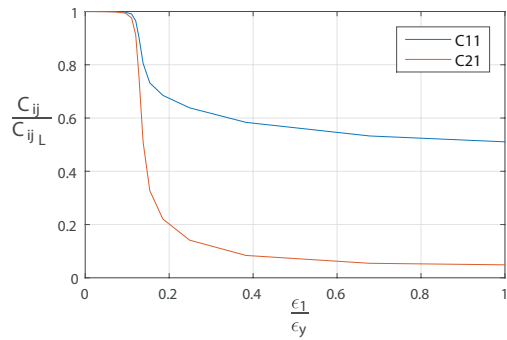


Figure 110: Variation of C_{11} and C_{21} , $d = 45^\circ$

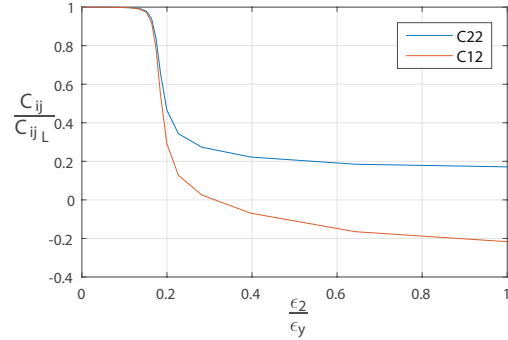


Figure 111: Variation of C_{22} and C_{12} , $d = 90^\circ$

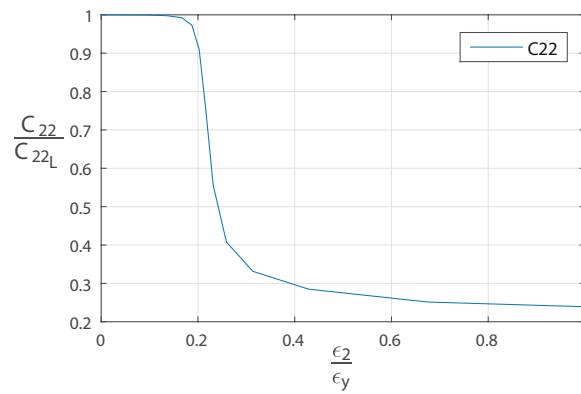


Figure 112: Variation of C_{22} , $d = 112.5^\circ$

Comment: The coupled stiffness for the first and last displacement history are not captured by the current plots as the tensile stresses gave an apparent negative coupled effect at the onset of loads.

B Python Imperfection Script


```
#####  
#                                                                                               #  
#           Weighed Eigenmode/Hungry-Horse imperfection                                       #  
#                               Author: DNV GL                                                 #  
#####  
  
import os, os.path, math, string, time  
from odbAccess import *  
from abaqus import *  
from visualization import *  
  
Analysisname='multibayed'  
  
#####  
#                                                                                               #  
#           Define fundamental parameters and constants                                       #  
#                                                                                               #  
#####  
  
pi = 3.1415926535897932384626433832795  
frame_space = 3000  
stiff_space = 850  
num_stiff = 5  
input_base_name = 'multibayed_n1'  
  
# Imperfection amplitude to be used as reference  
ref_ampl = 0.005*stiff_space  
  
# csi_coeff = (imperfection amplitude)/(reference amplitude)  
csi_vector = [0.5, 1.1, 2.2, 6.5]  
  
# comb_coefficients used for combining HH and EV imperfections  
comb_coefficients = [0.01, 0.99]  
  
#####  
  
# Scaled imperfection  
ImperfectionScaleFactor=1  
Imp_HH = ref_ampl*ImperfectionScaleFactor  
Imp_EV = ref_ampl*ImperfectionScaleFactor  
  
# Specify odb  
odbName=Analysisname+'.odb'  
odb=openOdb(odbName)  
  
if ImperfectionScaleFactor == 1:  
    FileName_HH='imperfection_HH.imp'  
    FileName_EV='imperfection_EV.imp'  
    FileName_total='imperfection_combined'  
else:  
    FileName_HH='imperfection_HH-scale'%s' % ImperfectionScaleFactor+'.imp'  
    FileName_EV='imperfection_EV-scale'%s' % ImperfectionScaleFactor+'.imp'  
    FileName_total='imperfection_combined-scale'%s' % ImperfectionScaleFactor  
  
# Open file for writing imperfection data  
ImperfectionFile_HH = open(FileName_HH, 'w+')  
ImperfectionFile_EV = open(FileName_EV, 'w+')  
  
# Define step name  
StepName='Step-1'
```

```

# Localize correct increment within the given step
FrameNo=1
Output1=odb.steps[StepName].frames[FrameNo].fieldOutputs['U']
OutputC=odb.steps[StepName].frames[FrameNo].fieldOutputs['COORD']

#####
#
#           Hungry horse imperfection
#
#####

for ValueC in OutputC.values:
    InstanceC=ValueC.instance.name
    NodeC=ValueC.nodeLabel

    # Initializing HH displacement
    Gdx = 0
    Gdy = 0
    Gdz = 0

    # Get coordinates
    x=ValueC.data[0]
    y=ValueC.data[1]
    z=ValueC.data[2]

    # HH_displacement (plate)
    Gdz = Imp_HH*abs(sin(pi*(x +
    (frame_space/2))/frame_space))*abs(sin(pi*y/stiff_space))

    if InstanceC:
        OutputString_HH=('%s' % NodeC)+(', ' '%s' % Gdx)+(', ' '%s' %
        Gdy)+(', ' '%s' % Gdz)+'\n'
        ImperfectionFile_HH.write(OutputString_HH)

# Close file after writing imperfection data
ImperfectionFile_HH.close()

#####
#
#           Eigenvalue imperfection
#
#####

# Max out_of_plane_disp and adjusting EV scale-factor
EV_max=0

for Value in Output1.values:
    Instance=Value.instance.name
    Node=Value.nodeLabel

    # Initializing EV displacement
    Ldx = 0
    Ldy = 0
    Ldz = 0

    Ldx=Value.data[0]
    Ldy=Value.data[1]
    Ldz=Value.data[2]
    Ldtot=(Ldx**2+Ldy**2+Ldz**2)**0.5
    if Ldtot > EV_max:
        EV_max = Ldtot

EV_max_outOfPlaneDisp = -1*EV_max
Scaling_EV = Imp_EV/EV_max_outOfPlaneDisp

```



```

for Value1 in Output1.values:

    Instance1=Value1.instance.name
    Node1=Value1.nodeLabel

    Ldx=Value1.data[0]*Scaling_EV
    Ldy=Value1.data[1]*Scaling_EV
    Ldz=Value1.data[2]*Scaling_EV

    if Instance1:
        OutputString_EV=(' %s' % Node1)+'(, ' %s' % Ldx)+'(, ' %s' % Ldy)+'(, ' %s' % Ldz)+'\n'
        ImperfectionFile_EV.write(OutputString_EV)

ImperfectionFile_EV.close()

#####
#
#           Combined imperfections
#
#####

# Create .bat file to run all analyses
bat_runme = "./" + "/non-linear_analyses_runme.bat"
bat_runme_w = open( bat_runme, 'w' )

for csi_coeff in csi_vector:

    # Create subfolder for the current csi_coeff
    subfolder_name = ("csi_""%05.3f" % (csi_coeff))
    if os.path.isdir( ( "./" + subfolder_name ) ) != 1:
        os.mkdir( ( "./" + subfolder_name ) )

    # Create .bat file to summarize analyses in subfolder
    bat_analyses_summary = "./" + subfolder_name +
    "/non-linear_analyses_csi_""%05.3f"% (csi_coeff) + ".bat"
    bat_analyses_summary_w = open( bat_analyses_summary, 'w' )

    #Combining HH and EV imperfections
    for index in range(0,len(comb_coefficients)):
        coeff_HH = comb_coefficients[index]
        coeff_EV = comb_coefficients[-1*index - 1]

        # Imperfections to be combined
        ImperfectionFile_HH = open(FileName_HH,'r')
        ImperfectionFile_EV = open(FileName_EV,'r')

        # Open file for writing imperfection data
        FileName_combined = FileName_total + '_HH_""%05.3f' % coeff_HH +
        '_EV_""%05.3f' % coeff_EV + '_csi_""%05.3f' % csi_coeff + '.imp'
        ImperfectionFile_combined = open("./" + subfolder_name + "/" +
        FileName_combined,'w+')

        # Writing input file
        input_base = input_base_name + '.inp'

        finp = open( (input_base ), 'r' )
        jobname = input_base_name + '_HH_""%05.3f' % coeff_HH + '_EV_""%05.3f' %
        coeff_EV
        fout = open( ( "./" + subfolder_name + "/" + jobname + '.inp' ), 'w' )
        bat_analyses_summary_w.write( 'call abaqus job=%s interactive \n' % jobname )
        bat_runme_w.write( 'cd %s \n' % subfolder_name )
        bat_runme_w.write( 'call abaqus job=%s interactive \n' % jobname )
        bat_runme_w.write( 'cd .. \n' )

```

```

for line in finp:
    if line.startswith('*IMPERFECTION'):
        fout.write(line.replace(line, (*IMPERFECTION, INPUT=' +
            FileName_combined + '\n')))
    else:
        fout.write(line)

fout.close()
finp.close()

# Reading and combining imperfection data
for line1, line2 in zip(ImperfectionFile_EV, ImperfectionFile_HH):

    nodeno_EV=line1.split(',')[0]
    x_EV = float(line1.split(',')[1])
    y_EV = float(line1.split(',')[2])
    z_EV = float(line1.split(',')[3])

    nodeno_HH=line2.split(',')[0]
    x_HH = float(line2.split(',')[1])
    y_HH = float(line2.split(',')[2])
    z_HH = float(line2.split(',')[3])

    if nodeno_EV==nodeno_HH:
        nodeno=nodeno_EV
        dx = csi_coeff * (coeff_EV*x_EV + coeff_HH*x_HH)
        dy = csi_coeff * (coeff_EV*y_EV + coeff_HH*y_HH)
        dz = csi_coeff * (coeff_EV*z_EV + coeff_HH*z_HH)
    else:
        print 'ERROR: The node numbers in EV and HH imperfection files does
            not correspond'

        break

    # Writing combined imperfection
    OutputString_combined=('%s' % nodeno)+(', ' '%s' % dx)+(', ' '%s' %
        dy)+(', ' '%s' % dz)+'\n'
    ImperfectionFile_combined.write(OutputString_combined)
    ImperfectionFile_combined.close()
    ImperfectionFile_HH.close()
    ImperfectionFile_EV.close()
    bat_analyses_summary_w.close()
bat_runme_w.close()

```

C Stiffened multi-bayed panel under lateral pressure

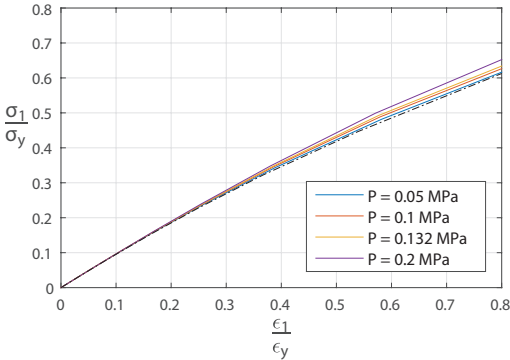


Figure 113: Longitudinal load-shortening relation, $w_0 = 9\text{mm EM}$

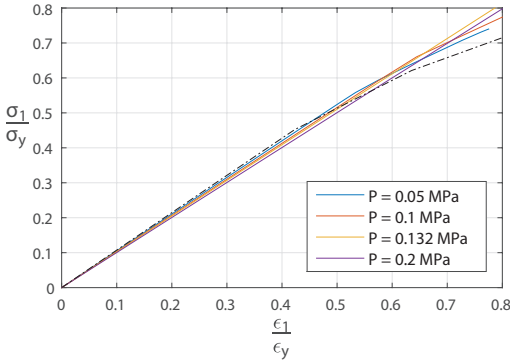


Figure 114: Longitudinal load-shortening relation, $w_0 = 9\text{mm HH}$

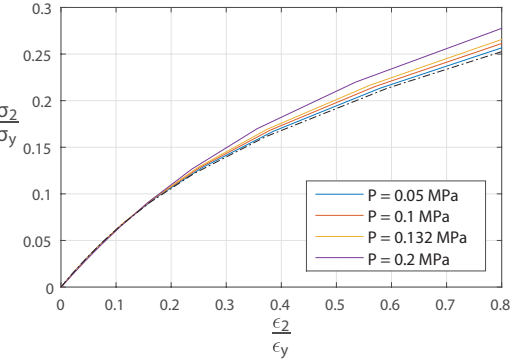


Figure 115: Transverse load-shortening relation, $w_0 = 9\text{mm EM}$

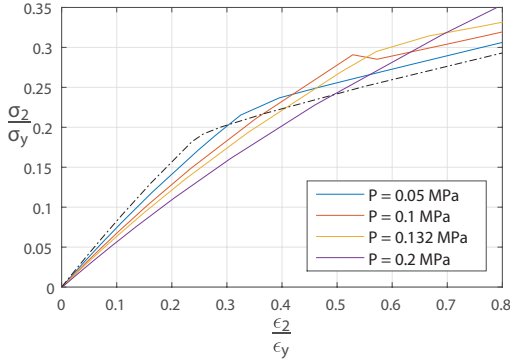
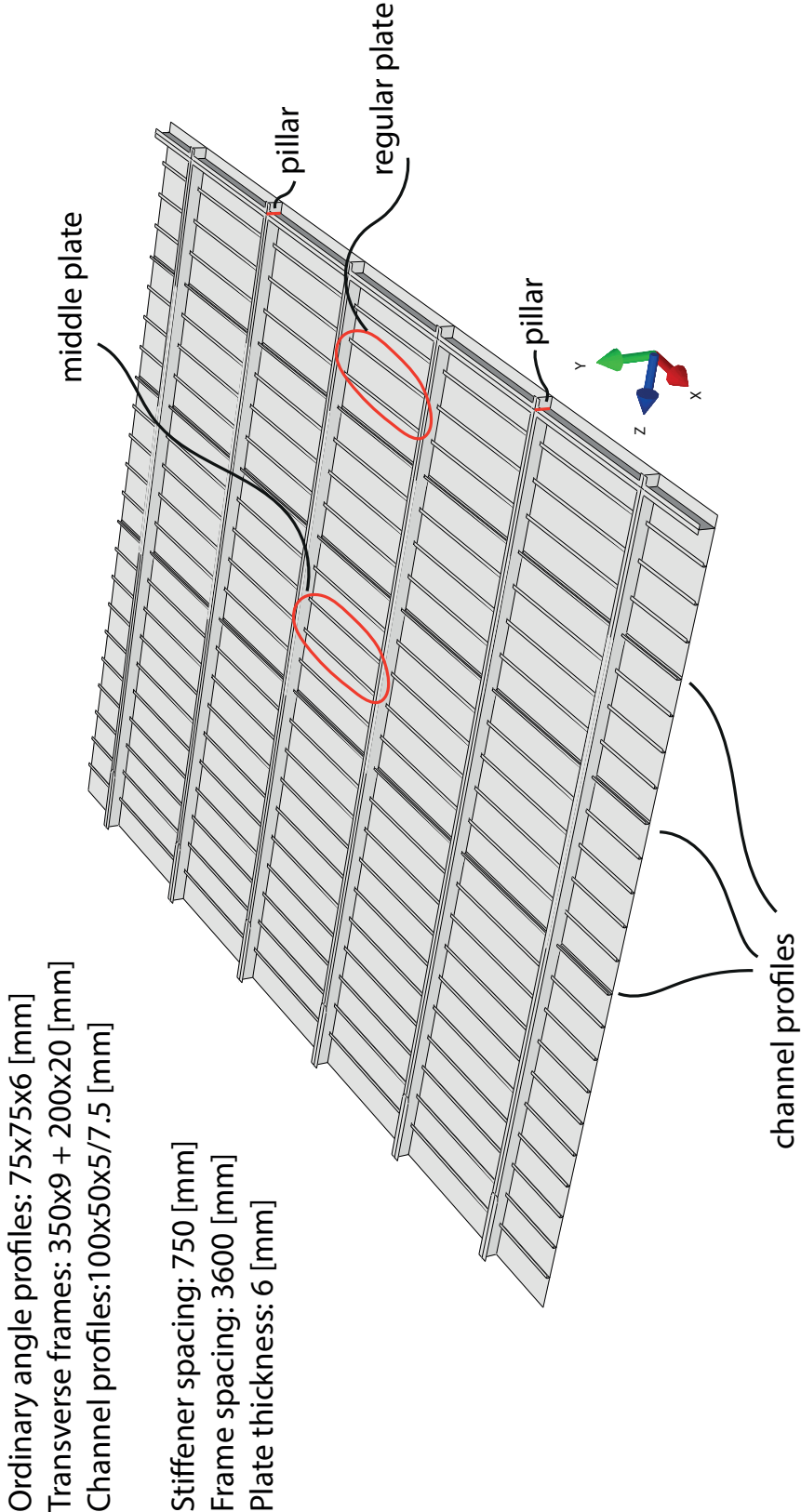


Figure 116: Transverse load-shortening relation, $w_0 = 9\text{mm HH}$

D Car-deck model



E Calculation Sheet - Initial stiffness

Reduced membrane stiffness C_{ij} (E_i, ν_{ij}) of plates due to geometrical imperfections/out-of-flatness (initial stiffness in $m=1, n=1$ mode)	
Author: Eivind Steen	
a	3600
b	750
t	6
E	206000
ν	0,3
sig f	235
x	0,025
δ	2,7
Geometry & Material (isotropic) plate length x-dir plate length y-dir (s) plate thickness (tp) E, Youngs modulus ν , Poisson ratio Yield stress x, Faulkner imperfection model Geometrical imperfection amplitude >0!	
$w_{max} (= \delta), q_{10} = w$ Faulkner imperfection model x = 0.025 slight imperfections x = 0.05 representative imperfections $q_{10} = x \left(\frac{s}{t}\right)^2 \frac{\sigma_f}{E} = x \beta^2$ x = 0.1 average imperfections x = 0.3 severe imperfections	
$a > b$ always required x-factor; tuning parameter towards non-linear FE mm	
$C_{11} = \frac{E}{1-\nu^2} \left[1 - 6 \frac{(k_1 + \nu k_2)^2}{A} \right]$ $C_{12} = \frac{E\nu}{1-\nu^2} \left[1 - \frac{6(k_1 + \nu k_2)(k_2 + \nu k_1)}{A} \right] = C_{21}$ $C_{22} = \frac{E}{1-\nu^2} \left[1 - 6 \frac{(k_2 + \nu k_1)^2}{A} \right]$ $A = \frac{2(k_1 + k_2)^2}{q_{10}^2} + 3(3 - \nu^2)(k_1^2 + k_2^2) + 12\nu k_1 k_2$ $k_1 = \left(\frac{t}{a}\right)^2, k_2 = \left(\frac{t}{b}\right)^2, q_{10} = \frac{\delta}{t}$	
Parameters in membrane stiffness model	
$k1 = (t/a)^2$	2,7778E-06
$k2 = (t/b)^2$	0,000064
A =	8,13785E-08
Stiffness coeff (membrane)	Initial stiffness (for zero load)
C11 =	218312
C12 = (C21)	44130
C22 =	156218
Initial stiffness E^* - pure transverse compression	147297
$E^* = C22 - C12^2/C11$ (pure transverse)	206000
C33 = $E/(2(1+\nu))$	79231
	Initial stiffness/Hooke's law (knock down %)
	96
	65
	69
	72

Reduced membrane stiffness C_{ij} (E_i, ν_{ij}) of plates due to geometrical imperfections/out-of-flatness (initial stiffness in $m=1, n=1$ mode)
 Author: Eivind Steen

$$\begin{bmatrix} \sigma_1 \\ \sigma_2 \\ \sigma_3 \end{bmatrix} = \begin{bmatrix} C_{11} & C_{12} & 0 \\ C_{21} & C_{22} & 0 \\ 0 & 0 & C_{33} \end{bmatrix} \begin{bmatrix} \epsilon_1 \\ \epsilon_2 \\ \epsilon_3 \end{bmatrix}$$



$$\begin{bmatrix} \epsilon_1 \\ \epsilon_2 \\ \gamma_{12} \end{bmatrix} = \begin{bmatrix} 1/E_1 & -\nu_{12}/E_1 & 0 \\ -\nu_{12}/E_1 & 1/E_2 & 0 \\ 0 & 0 & 1/G_{12} \end{bmatrix} \begin{bmatrix} \sigma_{11} \\ \sigma_{22} \\ \tau_{12} \end{bmatrix}$$

Output	Input to GenIE	Initial stiffness (for zero load)	linear Hook law (perfect geometry)	Initial stiffness/Hooke's law (knock down %)	NB! $\nu_{12} \neq \nu_{21}$ $\nu_{21} = C_{12}/C_{11}$	NB! $G_{12} = E/(2(1+\nu))$ isotrop $\nu_{21} = (E_2/E_1)\nu_{12}$
axial	E1 =	205845	206000	100		
transv	E2 =	147297	206000	72		
Poisson	$\nu_{12} =$	0.28	0.3	94	0,20	0,20
Shear	$G_{12} =$	79231	79231	100		

F Load-dependent Macro Material Input

S1/s _y	S2/s _y	e2/ey	E2	v12
0.001530	0.005431	0.007298	144758.484158	0.281771
0.002876	0.010276	0.014247	140669.463829	0.279837
0.004618	0.016686	0.024232	134789.923668	0.276758
0.006755	0.024866	0.038669	126534.486986	0.271670
0.009192	0.034969	0.060058	115390.715930	0.262857
0.011670	0.047255	0.093373	101219.230591	0.246949
0.013634	0.062623	0.149310	84778.803093	0.217722
0.013851	0.083548	0.251243	67912.262710	0.165787
0.009368	0.115611	0.449580	52889.194239	0.081028
-0.006963	0.170284	0.851433	41186.340089	-0.040891

Figure 117: Load-dependent macro material input, single plate model

S1/s _y	S2/s _y	e2/ey	E2	v12
0.001704	0.005820	0.007554	148814.053695	0.292726
0.003306	0.011296	0.015114	144663.015659	0.292686
0.005515	0.018854	0.026475	138266.241474	0.292514
0.008408	0.028797	0.043597	128839.222681	0.291975
0.011876	0.040999	0.069577	115725.295001	0.289654
0.015561	0.055109	0.109260	99959.248006	0.282364
0.018648	0.070841	0.170064	83473.394659	0.263233
0.019895	0.088677	0.262415	68495.165557	0.224355
0.017715	0.109957	0.400418	56188.025687	0.161106
0.010184	0.136962	0.604322	46632.184104	0.074359
0.000894	0.160046	0.793724	41537.584618	0.005585

Figure 118: Load-dependent macro material input, integrated plate